ABSTRACT

HARTON, SHANE EDWARD. Investigation of Polymer Phase Behavior at Heterogeneous Polymer-Polymer Interfaces using Secondary Ion Mass Spectrometry. (Under the supervision of Harald W. Ade)

Changes in the thermodynamic behavior of polymer blends from bulk to heterogeneous interfaces is investigated using secondary ion mass spectrometry (SIMS). The use of a magnetic sector spectrometer (CAMECA IMS-6f) is fully explored in order to determine the optimal conditions in which to probe polymer surfaces and heterogeneous interfaces using three bilayer film systems, namely polystyrene (PS) with poly(methyl methacrylate) (PMMA), poly(cyclohexyl methacrylate) (PCHMA) with PMMA, and PS with poly(2-vinylpyridine) (P2VP). Two primary ion beams have been employed, O_2^+ with detection of positive secondary ions, and Cs^+ with detection of negative secondary ions. It was found that each polymer thin film system must be closely investigated in order to determine the optimal conditions for depth profiling using SIMS. Three types of systems were further investigated using SIMS.

PCHMA and PS are miscible with each other, but each is highly immiscible with PMMA. Identifiable by the asymmetries in the binary mean-field interaction parameters χ, PS preferentially segregates to the PCHMA/PMMA interface. Secondary ion mass spectrometry was used to provide real-space depth profiles of dPS in a miscible blend with PCHMA. The initial dPS concentration was varied from 5-20% (v/v), and the blend film was annealed at 150 °C on a film of PMMA for 42 h. X-ray reflectometry was used

to determine the interfacial width between PCHMA and PMMA at 150 °C. Using self-consistent mean-field theory, good agreement was found between the experimental and theoretical interfacial excess Z^* of dPS at each concentration.

Isotopic labeling (deuteration) is known to affect the phase behavior of PS and PMMA blends, but little is known regarding the changes in the interfacial properties at the PS/PMMA interface due to deuteration of PS and/or PMMA. To investigate these potential changes, secondary ion mass spectrometry (SIMS) was used to measure real-space depth profiles of dPS in hPS:dPS/hPMMA bilayers, with the hPS:dPS blend being well within the single-phase region of the phase diagram. Profound changes in the thermodynamic behavior of this system at the polymer/polymer interface are observed in the form of significant segregation of dPS to the hPS:dPS/hPMMA interface. The observation of a depletion hole during the formation of an equilibrium excess of dPS implies that the energetic gain at the interface per dPS chain has to be > kT. These results cannot be described, even qualitatively, using previously reported changes in χ for PS/PMMA due to isotopic labeling. The previously reported values of χ for dPS/hPMMA and hPS/hPMMA actually predict a depletion of dPS at the hPS:dPS/hPMMA interface rather than the observed segregation. The observed interfacial excess is quantified by generating theoretical profiles, using self-consistent mean-field theory (SCMF), and fitting an effective interaction energy parameter $\Delta\chi_p$ as a function of temperature.

^{13}C labeling is introduced as a tracer for depth profiling of polymer films and multilayers using secondary ion mass spectrometry (SIMS). ^{13}C labeled PS (^{13}C-PS) and unlabeled PS (^{12}C-PS) and PMMA were synthesized using atom transfer radical

polymerization and assembled in several model thin film systems. Depth profiles were performed using a CAMECA IMS-6f magnetic sector mass spectrometer using both 6.0 keV Cs^+ and 5.5 keV impact energy O_2^+ primary ion bombardment with detection of negative and positive secondary ions, respectively. Although complete separation of $^{12}C^1H$ from ^{13}C is achieved using both primary ion species, 6.0 keV Cs^+ clearly shows improved detection sensitivity and signal-to-noise for detection of ^{12}C, $^{12}C^1H$, and ^{13}C secondary ions. The use of Cs^+ primary ion bombardment results in somewhat anomalous, non-monotonic changes in the ^{12}C, $^{12}C^1H$, and ^{13}C secondary ion yields through the PS/PMMA interface, however it is shown that this behavior is not due to sample charging. Through normalization of the ^{13}C secondary ion yield to the total C ($^{12}C + ^{13}C$) ion yield, the observed effects through the PS/PMMA interface can be greatly minimized, thereby significantly improving analysis of polymer films and multilayers using SIMS.

INVESTIGATION OF POLYMER PHASE BEHAVIOR AT HETEROGENEOUS POLYMER-POLYMER INTERFACES USING SECONDARY ION MASS SPECTROMETRY

by

Shane E. Harton

A dissertation submitted to the Graduate Faculty of
North Carolina State University
in partial fulfillment of the
requirements for the Degree of
Doctor of Philosophy

MATERIALS SCIENCE & ENGINEERING

Raleigh

2006

APPROVED BY

Dr. R. J. Nemanich	Dr. D. Griffis
Dr. B. M. Novak	
Dr. H. Ade Chair of Advisory Committee	Dr. P. E. Russell Co-Chair of Advisory Committee

BIOGRAPHY

Shane E. Harton was born on October 11, 1974 to Edward and Connie Harton, Mercer, Pennsylvania. He was graduated from Mercer Jr./Sr. High School in 1993. In May of 2001, he received his B.S. in chemical engineering from The Pennsylvania State University. In August of 2001, he began his graduate studies in the Department of Materials Science & Engineering at North Carolina State Unviversity.

ACKNOWLEDGEMENTS

The work presented in this dissertation could not have been accomplished without the knowledgeable staff at the Analytical Instrumentation Facility at North Carolina State University. Collaborations were also undertaken with the MRSEC Garcia Center, SUNY Stony Brook. Most of all, I would like to acknowledge the funding and support provided by my advisor, Harald W. Ade.

TABLE OF CONTENTS

LIST OF FIGURES

LIST OF TABLES

1. INTRODUCTION

1.1. Background and Motivation

Starting with the discoveries of Nylon, polystyrene, poly(vinyl chloride), poly(methyl methacrylate), polyethylene, and many others in the 1920's and 1930's,[1] synthetic polymers have invaded commercial markets as well as the scientific community. With their amazing weatherability and chemical resistance, as well as high strength-to-weight ratio, they have been extremely important in the improvement of paints and coatings, adhesives, and food packaging.[2] Developments of improved synthesis techniques, such as living anionic polymerization,[3,4] ring opening metathesis polymerization,[5] and controlled radical polymerization,[6] have led to nearly unlimited control of polymer chain architecture and chemical composition. Even with these advances, though, the exor bitant cost of commercializing new synthetic polymers has led to alternative strategies for the development of novel products through physical blending of two or more existing polymers.[1,2,7]

Polymer blend phase behavior is governed by the free energy of mixing,[8-11]

$$F_M = H_M - TS_M \,, \tag{1}$$

where F_M is the free energy of mixing, H_M is the enthalpy of mixing, T is the absolute temperature, and S_M is the entropy of mixing. For macromolecular chains, the entropy of mixing of a binary blend has been described by the expression[10]

$$\frac{S_M}{kT} = \frac{n_A}{N_A}\ln\varphi_A + \frac{n_B}{N_B}\ln\varphi_B \,, \tag{2}$$

where n is the number of segments of type A or B in the system, φ is the volume fraction of A or B, and N is the number of segments of A or B in a single chain. From this

expression, it is quite apparent that increasing the molecular weight of the polymer constituents in a polymer blend decreases the entropic driving force for mixing. Therefore, polymer phase behavior is often controlled by the enthalpic contribution to the free energy of mixing of a binary blend,[10,12]

$$\frac{H_M}{kT} = \chi n_A \varphi_B , \tag{3}$$

where χ is the mean-field interaction parameter. When $\chi < 0$, mixing will always occur, but when $\chi > 0.1$, mixing will only occur for very low molecular weight polymers (oligomers). Mixing two immiscible amorphous polymers as viscoelastic liquids at elevated temperatures consequently results in liquid-liquid phase separation commonly signified by the formation of dispersions (micrometer size or larger) of one polymer in a matrix of the other. These morphological features are frozen-in once the blend is cooled below the temperature at which one or both polymers vitrify.

Because of the inherent immiscibility of most polymer blend constituents, control of the interfacial thermodynamics is required in order to control the material properties, such as tensile and impact strength, of the blends.[13] Polymers at heterogeneous interfaces behave quite differently than in the bulk due to restrictions of the conformational entropy of the polymer chains.[14,15] Theoretically, these changes in chain conformations can be incorporated into free energy minimizations through the use of a self-consistent mean-field theory (SCMF).[12,15,16] The use of SCMF requires knowledge of the molecular weights of the polymer constituents, the bulk mean-field interaction parameters (χ),[9,10] and any other external fields present at a surface or interface.[17-24] For a one-dimensional binary polymer blend in the limit of very high molecular weights and infinite boundaries,

an analytical expression has been derived that results in the so-called hyperbolic tangent expression for the compositional profile,[12,25] as shown in Figure 1.1. This also allows the interfacial width (w) and interfacial tension (γ) to be related to χ ($w \propto \chi^{-1/2}$ and $\gamma \propto \chi^{1/2}$).[12,25] Finite molecular weights, multicomponent constituents, multiple dimensions, and end-effects (surfaces) can be incorporated into SCMF, although solution of the composition profile, interfacial width, and interfacial tension requires computational analysis.[26-29]

Increased understanding of the nature of polymer-polymer interfaces[2,13,30,31] has led to amazing advances in the emerging fields of bio- and nanotechnology.[32] These advances have been made possible due largely to significant improvements in characterization methods.[32] Many of these methods, including neutron reflectometry (NR), forward recoil spectrometry (FRES), nuclear reaction analysis (NRA), and secondary ion mass spectrometry (SIMS), utilize deuterium labeling in order to provide enhanced contrast for proper experimental characterization.[14] Deuterium labeling involves replacing the protium (^{1}H) in a compound (organic or inorganic) with their isotopic analog deuterium (^{2}H). Although this method of labeling seems simple and unobtrusive, it has been shown to have a small, albeit finite, impact on the polymer phase behavior, both at polymer surfaces[17,33] and in bulk (away from a surface or interface).[34,35] More recently, the effects of deuterium labeling have been shown to have profound effects at an interface between polystyrene (PS) and poly(methyl methacrylate) (PMMA), with the observation of segregation of deuterium labeled PS (dPS) to the heterogeneous

interface. This behavior cannot be explained within the context of the known bulk phase behavior of PS and PMMA.[35]

While the commonly used techniques NR, FRES, and NRA rely on deuterium substitution to provide contrast in polymer films, SIMS can utilize the contrast provided by various functional groups, chemical moieties, or isotopic labels.[36-38] This makes SIMS particularly versatile for depth profiling of polymer films and multilayers, although this versatility comes at a cost. Depth profiling using SIMS is particularly sensitive to matrix effects induced by changing densities or chemical environments,[39,40] which are encountered at polymer surfaces, polymer/polymer heterogeneous interfaces, and polymer/inorganic substrate interfaces. SIMS involves bombarding a target film with primary ions, such as O_2^+, O^-, Cs^+, Ar^+, Au^+, Ga^+, and C_{60}^+, and detecting positive or negative secondary ions that are sputtered from the surface.[38,41,42] When the primary ion fluence is below the so-called static limit (~ 10^{12}-10^{13} ions/cm^2),[43,44] detection is primarily from the top monolayer of the film. This is the static SIMS technique, which is useful for observing surface composition or two-dimensional surface imaging.[42] For one-dimensional depth profiling (dynamic SIMS), or even three-dimensional imaging,[45] analysis conditions must be implemented where the primary ion fluence is above the static limit, thereby causing erosion of the film at a controlled rate. This allows for information to be obtained regarding chemical composition as a function of depth through the sample. With dynamic SIMS, though, the chemical information obtainable is often quite different than with static SIMS analysis, as ion-induced mixing and chemical degradation can significantly alter the chemical structures below the surface.[42,46] This

often limits profiling of organic species to simple atomic or diatomic species, such as H, C, CH, O, CN, and Br.[36]

SIMS instruments have three types of mass analyzers, namely, quadrupole, magnetic sector, and time-of-flight (ToF).[47] Quadrupole mass spectrometers are commonly used for depth profiling of various types of samples, including metals, semiconductors, and organics. Because of the low primary ion impact energies possible with these instruments (< 1 keV), sub-nanometer depth resolutions are possible when depth profiling highly structured semiconductors,[47] and depth resolutions less than 10 nm have been reported for depth profiling of polymer films and multilayers.[17,48] These instruments are limited by low mass resolution (typical $m/\Delta m \sim 300$),[47] making it impossible to completely separate (mass resolve) secondary ions with identical nominal masses, such as ^{2}H (2.014 amu) from $^{1}H_2$ (2.01565 amu) and ^{13}C (13.00335 amu) from $^{12}C^{1}H$ (13.00782 amu).[38] Quadrupole instruments can, however, be used for depth profiling of deuterium labeled polymers, as there is negligible mass interference from $^{1}H_2^{-}$ when detecting negative ions.[36] In contrast to quadrupole instruments, magnetic sector mass spectrometers have relatively high mass resolving capabilities, with a maximum $m/\Delta m \sim 2 \times 10^4$, although $6\text{-}8 \times 10^3$ is somewhat of a practical upper limit for maintaining reasonable detection sensitivity.[47] These instruments can mass resolve secondary ion species such as ^{2}H from $^{1}H_2$ and ^{13}C from $^{12}C^{1}H$ with detection of positive or negative secondary ions.[38,49] Transmission of secondary ions into the detector is much greater for magnetic sector instruments than with quadrupole instruments,[47] but charging is often problematic for the analysis of insulators.[50] These problems can be overcome

with various active or passive charge neutralization measures that include a conductive coating, negative primary ions (e.g., O^-), and electron bombardment.[50,51] Time-of-flight mass spectrometers have seen significant growth in recent years, particularly with developments of the so-called cluster probes (e.g., Au_3^+, SF_5^+, and C_{60}^+).[42,44] Their mass range, mass resolution, and transmission exceed that for the other analyzers. Although their use has been restricted primarily to static SIMS (compositional analysis and two-dimensional imaging),[52] ToF SIMS have seen some use in depth profiling of tracer labeled polymers in polymer films,[53] and their use in depth profiling of somewhat high molecular weight species or fragments (~ 100 amu) has received considerable attention in recent years.[43,54-56]

1.2. Scope of Work

The work presented here details experimental and theoretical analyses of polymer phase behavior at heterogeneous polymer-polymer interfaces using SIMS. SCMF is used to provide quantitative explanations of the observed phenomena. Three different types of systems are investigated. The first involves a miscible blend composed of two different polymer species, dPS and poly(cyclohexyl methacrylate) (PCHMA), that is combined with a third polymer (hPMMA). hPMMA is completely immiscible with the miscible blend constituents, although asymmetric interactions are encountered for dPS/PMMA and PCHMA/PMMA, thereby driving dPS to the dPS:PCHMA/PMMA interface.[57] This system is used to demonstrate the effects of strong bulk interactions on the changes in phase behavior near interfaces. The second system demonstrates the strong effects of deuterium labeling on the phase behavior of polymers near polymer-polymer interfaces,

with strong segregation of dPS to an hPS:dPS/hPMMA interface.[58] Because deuterium labeling does not provide a true tracer for analysis of polymer systems, the use of a novel tracer, namely ^{13}C, was developed to overcome the artifacts created by deuterium labeling. It is clearly shown that ^{13}C labeled PS does indeed provide a true tracer for probing PS/PMMA polymer blends.

1.3. Organization of Dissertation

Chapter 2 describes the procedure for sample assembly and analysis using SIMS with a magnetic sector spectrometer. All SIMS depth profiles presented in this dissertation were performed by Mr. F. A. Stevie, who was assisted by Dr. C. Gu and Dr. Z. Zhu at the Analytical Instrumentation Facility, North Carolina State University, Raleigh, NC. All samples were prepared by S. E. Harton, and all reduction of SIMS data reported here was performed by S. E. Harton. Chapter 3 describes analysis of a dPS:PCHMA/PMMA system. This is a model system for demonstrating the interplay between bulk phase behavior and interfacial thermodynamics. Here, X-ray reflectometry was performed at beam line X10B at the National Synchrotron Light Source and analyzed by Dr. T. Koga, Department of Materials Science & Engineering, Stony Brook University, Stony Brook, NY. Samples for XR were prepared by S. E. Harton, and all SCMF calculations were performed by S. E. Harton. Chapter 4 describes the effects of deuterium labeling on an hPS:dPS/hPMMA interface. Somewhat anomalous segregation of dPS to the heterogeneous interface is observed, which is completely contradictory to the published bulk phase behavior,[35] which actually predicts a depletion of dPS at the hPS:dPS/hPMMA interface. Theoretical analysis using SCMF and numerical

convolution was performed by S. E. Harton. Chapter 5 details the use of ^{13}C labeling for improved SIMS analysis of polymer films and multilayers. The development of this novel tracer was essential for future investigations of polymer-polymer heterogeneous interfaces. ToF SIMS analyses were performed by Dr. Z. Zhu, and all samples were prepared by S. E. Harton. The polymer synthesis and regression of the convolution function parameters were performed by S. E. Harton.

1.4. References

1. Painter, P. C. & Coleman, M. M. *Fundamentals of Polymer Science: An Introductory Text* (Technomic Publishing Co., Inc., Lancaster, PA, 1997).
2. Ryan, A. J. Polymer science - designer polymer blends. *Nature Mater.* **1**, 8-10 (2002).
3. Szwarc, M. Living Polymers. *Nature* **178**, 1168-1169 (1956).
4. Szwarc, M., Levy, M. & Milkovich, R. Polymerization Initiated by Electron Transfer to Monomer - a New Method of Formation of Block Polymers. *J. Am. Chem. Soc.* **78**, 2656-2657 (1956).
5. Novak, B. M., Risse, W. & Grubbs, R. H. The Development of Well-Defined Catalysts for Ring-Opening Olefin Metathesis Polymerizations (Romp). *Adv. Polym. Sci.* **102**, 47-72 (1992).
6. Matyjaszewski, K. & Xia, J. Atom Transfer Radical Polymerization. *Chem. Rev.* **101**, 2921-2990 (2001).
7. Paul, D. R. & Bucknall, C. B. (eds.) *Polymer Blends, Vols. I and II* (Wiley, New York, 2000).
8. Prausnitz, J. M., Lichtenhaler, R. N. & de Azevedo, E. G. *Molecular Thermodynamics of Fluid-Phase Equilibria* (Prentice Hall, Englewood Cliffs, NJ, 1986).
9. Flory, P. J. Thermodynamics of High Polymer Solutions. *J. Chem. Phys.* **9**, 660 (1941).
10. Flory, P. J. *Principles of Polymer Chemistry* (Cornell University Press, Ithaca, NY, 1953).
11. Huggins, M. L. Solutions of Long Chain Compounds. *J. Chem. Phys.* **9**, 440 (1941).
12. Helfand, E. & Tagami, Y. Theory of the Interface Between Immiscible Polymers. *J. Polym. Sci., Part B: Polym. Phys.* **9**, 741 (1971).
13. Ruzette, A. V. & Leibler, L. Block copolymers in tomorrow's plastics. *Nature Mater.* **4**, 19-31 (2005).
14. Jones, R. A. L. *Polymers at Surfaces and Interfaces* (Cambridge University Press, New York, 1999).
15. Fleer, G. J., Stuart, M. A. C., Scheutjens, J. M. H. M., Cosgrove, T. & Vincent, B. *Polymers at Interfaces* (Chapman & Hall, New York, 1993).
16. Edwards, S. F. The statistical mechanics of polymers with excluded volume. *Proc. Phys. Soc. London* **85**, 613-624 (1965).
17. Hariharan, A. et al. The Effect of Finite Film Thickness on the Surface Segregation in Symmetrical Binary Polymer Mixtures. *J. Chem. Phys.* **99**, 656-663 (1993).
18. Hariharan, A., Kumar, S. K. & Russell, T. P. A Lattice Model for the Surface Segregation of Polymer-Chains Due to Molecular-Weight Effects. *Macromolecules* **23**, 3584-3592 (1990).
19. Hariharan, A., Kumar, S. K. & Russell, T. P. Surface Segregation in Binary Polymer Mixtures - a Lattice Model. *Macromolecules* **24**, 4909-4917 (1991).

20. Hariharan, A., Kumar, S. K. & Russell, T. P. Reversal of the Isotopic Effect in the Surface Behavior of Binary Polymer Blends. *J. Chem. Phys.* **98**, 4163-4173 (1993).
21. Hariharan, A., Kumar, S. K. & Russell, T. P. Free Surfaces of Polymer Blends .1. Theoretical Framework and Application to Symmetrical Polymer Blends. *J. Chem. Phys.* **98**, 6516-6525 (1993).
22. Hariharan, A., Kumar, S. K. & Russell, T. P. Free Surfaces of Polymer Blends .2. Effects of Molecular-Weight and Applications to Asymmetric Polymer Blends. *J. Chem. Phys.* **99**, 4041-4050 (1993).
23. Indrakanti, A., Jones, R. L. & Kumar, S. K. Do "nonequilibrium" effects control strong surface segregation from polymer blends? *Macromolecules* **37**, 9-12 (2004).
24. Indrakanti, A., Ramesh, N., Duda, J. L. & Kumar, S. K. Modeling diffusion in miscible polymer blend films. *J. Chem. Phys.* **121**, 546-553 (2004).
25. Broseta, D., Fredrickson, G. H., Helfand, E. & Leibler, L. Molecular Weight and Polydispersity Effects at Polymer-Polymer Interfaces. *Macromolecules* **23**, 132-139 (1990).
26. Genzer, J. Copolymer adsorption on planar substrates with a random distribution of chemical heterogeneities. *J. Chem. Phys.* **115**, 4873-4882 (2001).
27. Helfand, E. Theory of the Homopolymer/Binary-Polymer-Mixture Interface. *Macromolecules* **25**, 1676-1685 (1992).
28. Matsen, M. W. & Schick, M. Self-assembly of block copolymers. *Curr. Opin. Colloid Interface Sci.* **1**, 329-336 (1996).
29. Matsen, M. W. & Schick, M. Stable and Unstable Phases of a Diblock Copolymer Melt. *Phys. Rev. Lett.* **72**, 2660-2663 (1994).
30. Bates, F. S. & Fredrickson, G. H. Block copolymers - Designer soft materials. *Phys. Today* **52**, 32-38 (1999).
31. Mezzenga, R. et al. Templating Organic Semi-conductors via Self-Assembly of Polymer Colloids. *Science* **299**, 1872-1874 (2003).
32. Granick, S. et al. Macromolecules at surfaces: Research challenges and opportunities from tribology to biology. *J. Polym. Sci., Part B: Polym. Phys.* **41**, 2755-2793 (2003).
33. Jones, R. A. L., Kramer, E. J., Rafailovich, M. H., Sokolov, J. & Schwarz, S. A. Surface Enrichment in an Isotopic Polymer Blend. *Phys. Rev. Lett.* **62**, 280-283 (1989).
34. Bates, F. S. & Wignall, G. D. Isotope-Induced Quantum-Phase Transitions in the Liquid State. *Phys. Rev. Lett.* **57**, 1429-1432 (1986).
35. Russell, T. P. Changes in Polystyrene and Poly(methyl methacrylate) Interactions with Isotopic Substitution. *Macromolecules* **26**, 5819 (1993).
36. Schwarz, S. A. et al. Studies of Surface and Interface Segregation in Polymer Blends by Secondary ion Mass-Spectrometry. *Mol. Phys.* **76**, 937-950 (1992).
37. Harrison, C. et al. Layer by layer imaging of diblock copolymer films with a scanning electron microscope. *Polymer* **39**, 2733-2744 (1998).

38. Wilson, R. G., Stevie, F. A. & Magee, C. W. *Secondary Ion Mass Spectrometry: A Practical Handbook for Depth Profiling and Bulk Impurity Analysis* (John Wiley & Sons, New York, 1989).
39. Deline, V. R., Katz, W., Evans, C. A. & Williams, P. Mechanism of Sims Matrix Effect. *Appl. Phys. Lett.* **33**, 832-835 (1978).
40. Wilson, R. G., Lux, G. E. & Kirschbaum, C. L. Depth profiling and secondary ion mass spectrometry relative sensitivity factors and systematics for polymers/organics. *J. Appl. Phys.* **73**, 2524-2529 (1993).
41. Honig, R. E. Sputtering of Surfaces by Positive Ion Beams of Low Energy. *J. Appl. Phys.* **29**, 549-555 (1958).
42. Winograd, N. The Magic of Cluster SIMS. *Anal. Chem.* **77**, 142A-149A (2005).
43. Fuoco, E. R., Gillen, G., Wijesundara, M. B. J., Wallace, W. E. & Hanley, L. Surface Analysis Studies of Yield Enhancements in Secondary Ion Mass Spectrometry by Polyatomic Projectiles. *J. Phys. Chem. B* **105**, 3950-3956 (2001).
44. Weibel, D. et al. A C60 Primary Ion Beam System for Time of Flight Secondary Ion Mass Spectrometry: Its Development and Seconedary Ion Yield Characteristics. *Anal. Chem.* **75**, 1754-1764 (2003).
45. Jerome, J. et al. Phase segregation of thin film polymer blends on Au nanopatterned Si substrates. *Macromolecules* **37**, 6504-6510 (2004).
46. Postawa, Z., Czerwinski, B., Winograd, N. & Garrison, B. J. Microscopic insights into the sputtering of thin organic films on Ag{111} induced by C-60 and Ga bombardment. *J. Phys. Chem. B* **109**, 11973-11979 (2005).
47. Chia, V. K. F., Mount, G. R., Edgell, M. J. & Magee, C. W. Recent advances in secondary ion mass spectrometry to characterize ultralow energy ion implants. *J. Vac. Sci. Technol. B* **17**, 2345-2351 (1999).
48. Reynolds, B. J., Ruegg, M. L., Mates, T. E., Radke, C. J. & Balsara, N. P. Experimental and Theoretical Study of the Adsorption of a Diblock Copolymer to Interfaces between Two Homopolymers. *Macromolecules* **38**, 3872-3882 (2005).
49. Harton, S. E., Stevie, F. A. & Ade, H. SIMS Depth Profiling of Amorphous Polymer Multilayers using O2+ and Cs+ Ion Bombardment with a Magnetic Sector Instrument. *J. Vac. Sci. Technol., A*, (in press) (2006).
50. Pivovarov, A. L., Stevie, F. A. & Griffis, D. P. Improved charge neutralization method for depth profiling of bulk insulators using O2+ primary beam on a magnetic sector SIMS instrument. *Appl. Surf. Sci.* **231-232**, 786-790 (2004).
51. Migeon, H. N., Schuhmacher, M. & Slodzian, G. Analysis of Insulating Specimens with the Cameca Ims4f. *Surf. Interface Anal.* **16**, 9-13 (1990).
52. Castner, D. G. View from the edge. *Nature* **422**, 129-130 (2003).
53. Hu, X. et al. Dynamics of Polymers in Organosilicate Nanocomposites. *Macromolecules* **36**, 823-829 (2003).
54. Wagner, M. S. Molecular Depth Profiling of Multilayer Polymer Films Using Time-of-Flight Secondary Ion Mass Spectrometry. *Anal. Chem.* **77**, 911-922 (2005).
55. Szakal, C., Sun, S., Wucher, A. & Winograd, N. C60 molecular depth profiling of a model polymer. *Appl. Surf. Sci.* **231-231**, 183-185 (2004).

56. Mahoney, C. M., Yu, J. & Gardella, J. A. Depth Profiling of Poly(L-lactic acid)/Triblock Copolymer Blends with Time-of-Flight Secondary Ion Mass Spectrometry. *Anal. Chem.* **77**, 3570-3578 (2005).
57. Harton, S. E., Koga, T., Stevie, F. A., Araki, T. & Ade, H. Investigation of Blend Miscibility of a Ternary PS/PCHMA/PMMA System using SIMS and Mean-Field Theory. *Macromolecules* **38**, 10511-10515 (2005).
58. Harton, S. E., Stevie, F. A. & Ade, H. Investigation of the Effects of Isotopic Labeling at a PS/PMMA Interface using SIMS and Mean-Field Theory. *Macromolecules*, (in press) (2006).

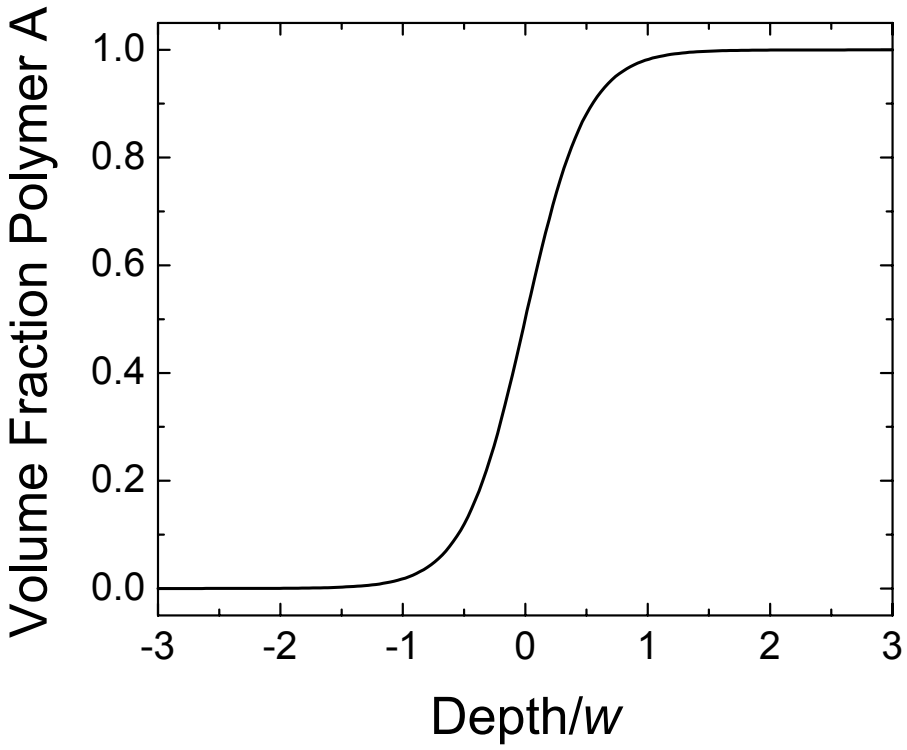

Figure 1.1. Theoretical composition profile for a one-dimensional A/B polymer blend as derived from SCMF.

2. SIMS DEPTH PROFILING OF AMORPHOUS POLYMER MULTILAYERS USING O2+ AND CS+ ION BOMBARDMENT WITH A MAGNETIC SECTOR INSTRUMENT

2.1. Introduction

Thin polymer films and multilayers are model systems for the investigation of phenomena related to physical confinement of polymer chains near surfaces and interfaces,[1-3] such as reaction mechanisms of functional polymers,[4,5] block copolymer segregation,[6,7] and block copolymer ordering.[8] These systems are ideally characterized using experimental techniques such as neutron or x-ray scattering and reflectometry (NR or XR),[9] scanning probe microscopy (SPM),[10] scanning transmission x-ray microscopy (STXM),[11-13] forward recoil spectrometry (FRES),[14] and secondary ion mass spectrometry (SIMS),[15] with the details depending on whether depth or lateral characteristics need to be probed. As the applications of these systems continually increase in a number of fields that include nano- and bio-technology, improvements in characterization methods and spatial resolution (depth and lateral) are essential, as the size scale of interest has become exceedingly small.[3]

Direct depth profiling techniques such as FRES and SIMS have undergone significant advances in recent years.[14,16] The relatively low depth resolution of ~ 80 nm[17] of conventional FRES (≈ 3.0 MeV $^4He^{++}$)[18] has been improved to a depth resolution of ~30 nm with the development of the low-energy (LE-FRES) (≈ 1.3 MeV $^4He^{++}$)[19] and time-of-flight (ToF-FRES) (≈ 2.0 MeV $^4He^{++}$)[20] techniques. Since the convolution

resulting from secondary scattering below the surface is an inherent limitation of FRES, further improvements are unlikely.[14]

Reciprocal space techniques such as NR and XR can have excellent depth resolution on the order of ~ 1 nm. In XR, the contrast depends on the relative electron density of the layers to be probed. In neutron scattering and NR depth profiling, deuterium (^{2}H) has a much higher scattering length density than protium (^{1}H) and is therefore frequently used as contrast agent for carbonaceous matter.[21] Although NR has superior depth resolution to FRES and SIMS, inversion of the reciprocal space information obtained with NR to composition profiles in real-space can be model dependent, requiring some *a priori* knowledge of the real-space profile.[15,22] This often necessitates a direct depth profiling technique such as FRES or SIMS to be used in conjunction with NR.[18]

Figure 2.1 shows a comparison of typical depth resolutions encountered using NR (1 nm), FRES (80 nm), LE- or ToF-FRES (30 nm), and SIMS (10 nm).[18] Because of its sensitivity, excellent depth resolution (~ 10 nm), and ability to provide real-space depth profiles directly, SIMS has become a prominent method for analysis of polymer thin films and multilayers.[4-6,23] There are three types of SIMS instruments, distinguished by the mass analyzer (i.e. quadrupole, time-of-flight (ToF), and magnetic sector) that can be utilized.[24,25] The quadrupole instrument has been extensively used in all areas of surface and interface science, including semiconductor[26] and polymer film[15] depth profiling. For depth profiling of deuterium-labeled polymers, quadrupole SIMS instruments provide excellent depth resolution of < 10 nm[6,27,28] due to the low impact energies (< 2 keV)

possible.[25] This high depth resolution comes at the cost of requiring low primary ion currents to minimize charging of the insulating polymer films, which can create long analysis times with somewhat poor signal/noise (S/N) ratios.[15,18] Furthermore, the quadrupole mass analyzer (mass resolution m/Δm typically about 300) cannot separate molecular hydrogen $^1H_2$ from ^2H (required mass resolution of m/Δm ~ 1250),[25] and as such, negative secondary ions must be detected when depth profiling deuterium-labeled polymers (negative $^1H_2$ is essentially nonexistent).[15]

ToF SIMS is a powerful technique for probing the surface composition of materials[29] and it can be used for depth profiling of various organic and inorganic films,[30] including polymer films and multilayers.[31-34] The mass resolution and mass range of these instruments is unmatched, making it particularly valuable for depth profiling of relatively high molecular weight (~ 100 Da) secondary ions.[33] Because of its lateral resolution of ~ 1 μm it can also be used for two- and three-dimensional imaging while providing detailed chemical information of the atomic and molecular species present.[16,35] Although its use for depth profiling of deuterium-labeled polymers has been limited,[36] the application of ToF SIMS for depth profiling of polymer films is currently an area of active investigation.[31-34] ToF SIMS technology is rapidly evolving with the availability of new primary ion species, such as C_{60}^+, Au^+, Au^+_2, Bi^+, and Bi_2^+, constantly emerging.[16,37]

Magnetic sector instruments have very high mass resolving capabilities (maximum m/Δm ~ 2×10^4),[25] which allows for complete separation of many ions possessing equal nominal mass numbers,[24] such as ^2H and $^1H_2$, ^{13}C and $^{12}C^1H$, and ^{28}Si and $^{12}C^{16}O$. They can also provide improved signal/noise ratios when compared to the

quadrupole instruments because of the high transmission of secondary ions into the detector.[25] However, charge build-up can be problematic for analysis of insulators (e.g. polymers) with magnetic sector SIMS.[24,38] These types of materials often require a conductive coating and/or other charge neutralization techniques, such as addition of an electron flood gun, to help reduce charge build-up.[39] Recent magnetic sector SIMS instruments can operate at impact energies reduced to < 1 keV, although initial investigations have shown significant charging during analysis of polymer films at these low energies. Depth resolutions ≈ 5-15 nm have been reported for depth profiling of deuterium-labeled polymers in polymer films using a magnetic sector SIMS at the higher impact energies of ~ 5 keV.[4,23,40]

SIMS can be used to quantify an interfacial excess,[4,6] surface excess,[15] and diffusion gradient[41] of a tracer polymer within a polymer film. At strongly segregated polymer/polymer (heterogeneous) interfaces, SIMS analysis can become difficult due to problems associated with changing matrix ion yields and varying sputtering rates for the two immiscible polymers. These problems exist due to complex molecular interactions during sputtering that are strongly dependent on the primary ion species and chemical environment.[42,43] By systematically investigating depth profiles through these polymer/polymer interfaces, one can better understand the parameters required to obtain accurate SIMS analysis of polymer films and multilayers.

Several model polymer bilayer systems have been characterized in order to delineate the utility of a magnetic sector SIMS instrument for soft matter depth analysis. The polymer systems included atactic polystyrene (PS) and syndiotactic poly(methyl

methacrylate) (PMMA), PS and atactic poly(2-vinylpyridine) (P2VP), and atactic poly(cyclohexyl methacrylate) (PCHMA) and PMMA. In all three cases, atactic deuterium-labeled polystyrene (dPS) was imbedded in PS or PCHMA at concentrations ranging from 5 to 20 % (v/v) as the tracer polymer. Using a CAMECA IMS-6f magnetic sector spectrometer, SIMS depth profiles have been obtained using Cs^+ and O_2^+ primary ion bombardment. Analysis conditions were varied to optimize S/N ratios and sensitivity, while preserving a high depth resolution of ~10 nm. Matrix ^{12}C ion yields (Y_M), which are the detected intensities (counts/s) of atomic ^{12}C, were measured for all three systems, with particular attention paid to the heterogeneous interface. Sputtering rates (S_R) for PS and PMMA films have been quantified for both Cs^+ and O_2^+ bombardment and referenced to S_R for intrinsic (100) silicon under identical conditions.

2.2. Experimental

2.2.1. Materials and Sample Preparation

The polymers used in this investigation were purchased from Polymer Source and Scientific Polymer Products. The PS, PMMA, and dPS were low polydispersity polymers ($M_w/M_n < 1.1$) with molecular weights ≈ 70-100 kDa, while PCHMA ($M_w \approx 70$ kDa) and P2VP ($M_w \approx 100$ kDa) had higher polydispersities ($M_w/M_n > 1.5$). Silicon (100) wafers (Wafer World) were cleaned using previously outlined procedures.[41] They were cut into 2 cm x 2 cm squares and soaked in a hydrogen peroxide/sulfuric acid solution at approximately 100 °C for 30 min and subsequently washed with deionized water (DI). They were then soaked in 10% (v/v) hydrofluoric acid for 1 min and again washed with DI. Some of the wafers were placed in a UV-ozone environment to

produce a thin (≈ 2 nm) native oxide layer (SiO_x), while others were used with the hydrogen passivation treatment (SiH).

All polymer solutions were allowed to fully dissolve for approximately 12 hours and were subsequently filtered with 0.45 μm pore PTFE syringe filters prior to spin casting. For bilayer film preparation, PMMA (T_g ≈ 125 °C) or P2VP (T_g ≈ 100 °C) was spun-cast onto the substrate using toluene or chlorobenzene, respectively, and annealed at 150 °C for approximately 30 min to remove residual solvent, allow the polymer chains to attain equilibrium conformations (relax), and reduce the surface roughness. The second layer, PS (T_g ≈ 100 °C) or PCHMA (T_g ≈ 100 °C), was cast from a selective solvent directly onto the first layer. It has been found that 1-chloropentane serves as a selective solvent for spin-casting of PS or PCHMA directly onto PMMA or P2VP, thereby providing sharp, uniform interfaces and smooth surfaces.[4] This is extremely important for measuring high-resolution depth profiles. Before the SIMS analysis was performed, a 50 nm PS sacrificial layer was added to the sample surface to ensure primary beam concentration uniformity was reached before the start of the second layer. This was done by casting PS onto SiO_x, scoring the film with a sharp tip, and floating it onto water. The floating film was then picked-up with the bilayer. A 20 nm Au coating was sputtered onto the sacrificial layer to minimize charge build-up. The analyzed film assembly is shown in Figure 2.2. For the sputtering rate (S_R) measurements, ≈ 100 kDa PS and PMMA single layer films were cast onto SiH from toluene with nominal thicknesses of 150 nm as determined by ellipsometery. The PMMA films were annealed for approximately 30 min at 150 °C, which is sufficient time for chain relaxation to occur,[44]

and both annealed (150 °C) and as-cast PS films were analyzed for comparison. No sacrificial layer or Au coating was used with these samples.

2.2.2. Secondary Ion Mass Spectrometry

Depth profiles were measured using a CAMECA IMS-6f magnetic sector secondary ion mass spectrometer. Typical analysis conditions for O_2^+ primary ion bombardment included a 25 nA primary current rastered over a 180 μm x 180 μm area at a 41° angle of incidence from normal, with 5.5 keV impact energy and a mass resolution m/Δm of 1250. Positive secondary ions were detected from a 60 μm diameter optically gated area positioned in the center of the raster. For Cs^+, typical analysis conditions included a 15 nA primary current rastered over a 200 μm x 200 μm area at a 27° angle of incidence, with 6.0 keV impact energy and similar mass resolution as with the O_2^+ bombardment. Negative secondary ions were detected from a 60 μm diameter optically gated area positioned in the center of the raster.

2.3. Results and Discussion

Most of the physically relevant information obtainable from a depth profile of a polymer film structure is gathered at or near the surface or a heterogeneous interface. These are the most important regions that require a detailed understanding of the conditions for optimal SIMS analysis. The chemical structures of the polymers used in the presented investigation are shown in Figure 2.3. Both Cs^+ and O_2^+ were used to evaluate Y_M for the three types of bilayers, as shown in Figure 2.4. For the profiles determined using Cs^+, a non-monotonic change in ion yield is observed through the heterogeneous interface for PS/PMMA and PCHMA/PMMA (Figure 2.4a-b). The

decrease in Y_M from PS to PMMA away from the interface (see Figure 2.4a) can be attributed partly to the decrease in number density of carbon atoms. The "anomalous", non-monotonic yield through the PS/PMMA interface, however, has been found to be nearly independent of primary ion current, as shown in Figure 2.5, which implies that it cannot be explained with sample charging. This same type of behavior was also observed through the PS/PMMA interface for the ion yields of other detected species, as shown in Figure 2.6. This non-monotonic change in ion yield was not observed with Cs^+ analysis of the PS/P2VP films (see Figure 2.4c), nor was it observable with any of the O_2^+ profiles (see Figure 2.4d-f). The underlying mechanism behind this behavior is unknown at this time and merits further investigation.

The constant Y_M through the PS/PMMA and PCHMA/PMMA interfaces using O_2^+ bombardment (see Figure 2.4d-e) with detection of positive secondary ions is an ideal situation for analysis of these bilayer systems. Because the separation of positive secondary ions of H_2 and ^2H is not possible with quadrupole SIMS,[15] these conditions could not be implemented with that type of instrument. The change in Y_M from PS to P2VP for Cs^+ bombardment (see Figure 2.4c) approximately scales with the number density of carbon atoms, as P2VP has a similar mass density to PS, yet there are 7/8 as many carbon atoms in a polymer segment (see Figure 2.3). For O_2^+ bombardment, however, there is a considerable increase in Y_M going from PS to P2VP (see Figure 2.4d). A similar increase in Y_M was also observed with O_2^+ bombardment at an interface between PS and a random copolymer of styrene and acrylonitrile (SAN), with 25 % (w/w) acrylonitrile segments (C_3H_3N). Nitrogen in the sample thus appears to have a

positive secondary ion yield enhancing effect for O_2^+ bombardment. At the interface between the substrate and the first polymer layer, there is an obvious increase in Y_M for all polymers with both Cs^+ and O_2^+ bombardment (see Figures 2.4-2.6). This is most likely due to the secondary ion enhancement resulting from a change in matrix species (i.e. going from a ^{12}C-based matrix to a ^{28}Si-based matrix).[24,45,46] The silicon matrix is oxidized more readily than the carbon based matrix and secondary ion yield for carbon is enhanced as we start to reach the silicon matrix.

A change in sputtering rates from one polymer to the next could have significant consequences for the interpretation of the depth profile near the heterogeneous interface. Hence, S_R was determined for PS and PMMA for 10 nA (6.0 keV impact energy) Cs^+ and 25 nA (5.5 keV impact energy) O_2^+ primary ion bombardment. Table 2.1 lists both the sputtering rates and the rates relative to intrinsic (100) Si ($S_R/S_{R,Si}$). There is a marked increase in sputtering rate from PS to PMMA for both Cs^+ and O_2^+ bombardment, with a two- to three-fold increase in S_R for PMMA relative to PS. As-cast PS was also analyzed to compare the effects of sample history on the sputtering rates. Previous O_2^+ SIMS analyses[4] have shown that the sputtering rate is much greater (nearly double) for PS as-cast from 1-chloropentane when compared to identical samples of annealed PS. Here, S_R for the PS as-cast from toluene is nominally identical to annealed PS, in stark contrast to the *increase* observed after casting from 1-chloropentane. It has also been found that both types of as-cast samples are far more susceptible to charging with both Cs^+ and O_2^+ bombardment than annealed PS. This means that the factors affecting the SIMS analysis, including sputtering rate, secondary ion yield, and sample charging, are strongly

dependent on sample preparation and history as well as chemical composition of the polymer constituents. These effects would be most significant for investigations involving as-cast films or measurements after relatively short annealing times (less than the terminal relaxation time).[44]

2.4. Conclusions

The utility of using magnetic sector SIMS for analyzing three different polymer/polymer bilayer systems (PS/PMMA, PCHMA/PMMA, and PS/P2VP) has been demonstrated. Excellent throughput, mass resolution, and S/N could be achieved at high depth resolution of ~10 nm with a CAMECA IMS-6f. The sputtering rates for PS and PMMA using 25 nA, 5.5 keV O_2^+ and 10 nA, 6.0 keV Cs^+ beams have been measured. The sputtering rates increased significantly (2-3 times) from PS to PMMA with Cs^+ and O_2^+ bombardment, and Cs^+ bombardment resulted in a non-monotonic change in matrix ion yield through the interface, which was shown to be nearly independent of primary ion current (see Figure 2.5). This non-monotonic change was also observed at the PCHMA/PMMA interface, but was not witnessed with the PS/P2VP system or in any of the systems when characterized with O_2^+ bombardment (see Figure 2.4). The use of O_2^+ bombardment with analysis of positive secondary ions showed constant matrix ^{12}C secondary ion yields through the PS/PMMA and PCHMA/PMMA interfaces. These ideal conditions could not be replicated with quadrupole SIMS because these types of instruments are not capable of mass resolving H_2 from ^2H. It has been established that there are profound effects due to sample preparation and history, chemical composition

of the samples, and type of primary ion bombardment, which result in changes in the sputtering rates and secondary ion yields.

2.5. References

1. Jones, R. A. L. *Polymers at Surfaces and Interfaces* (Cambridge University Press, New York, 1999).
2. Fleer, G. J., Stuart, M. A. C., Scheutjens, J. M. H. M., Cosgrove, T. & Vincent, B. *Polymers at Interfaces* (Chapman & Hall, New York, 1993).
3. Granick, S. et al. Macromolecules at surfaces: Research challenges and opportunities from tribology to biology. *J. Polym. Sci., Part B: Polym. Phys.* **41**, 2755-2793 (2003).
4. Harton, S. E., Stevie, F. A. & Ade, H. Diffusion-Controlled Reactive Coupling at Polymer-Polymer Interfaces. *Macromolecules* **38**, 3543-3546 (2005).
5. Kim, B. J. et al. Interfacial Roughening Induced by the Reaction of End-Functionalized Polymers at a PS/P2VP Interface: Quantitative Analysis by DSIMS. *Macromolecules* **38**, 6106-6114 (2005).
6. Reynolds, B. J., Ruegg, M. L., Mates, T. E., Radke, C. J. & Balsara, N. P. Experimental and Theoretical Study of the Adsorption of a Diblock Copolymer to Interfaces between Two Homopolymers. *Macromolecules* **38**, 3872-3882 (2005).
7. Zhu, S. et al. Confinement Induced Miscibility in Polymer Blends. *Nature* **400**, 49-51 (1999).
8. Mansky, P., Liu, Y., Huang, E., Russell, T. P. & Hawker, C. Controlling Polymer-Surface Interactions with Random Copolymer Brushes. *Science* **275**, 1458-1460 (1997).
9. Zhao, W. et al. Neutron and x-ray reflectivity measurements of polystyrene/poly(bromostyrene) (PS/PBrS) interfaces. *Physica B* **173**, 43-46 (1991).
10. Ge, S. et al. Shear Modulation Force Microscopy Study of Near Surface Glass Transition Temperatures. *Phys. Rev. Lett.* **85**, 2340-2343 (2000).
11. Ade, H. et al. Chemical Contrast in X-ray Microscopy and Spatially Resolved XANES Spectroscopy of Organic Specimens. *Science* **258**, 972 (1992).
12. Ade, H. & Hsiao, B. X-ray Linear Dichroism Microscopy. *Science* **262**, 1427-1429 (1993).
13. Kilcoyne, A. L. D. et al. Interferometer Controlled Scanning Transmission X-Ray Microscopes at the Advanced Light Source. *J. Synchr. Rad.* **10**, 125-136 part 2 (2003).
14. Composto, R. J., Walters, R. M. & Genzer, J. Application of ion scattering techniques to characterize polymer surfaces and interfaces. *Mater. Sci. Eng., R* **38**, 107-180 (2002).
15. Schwarz, S. A. et al. Studies of Surface and Interface Segregation in Polymer Blends by Secondary ion Mass-Spectrometry. *Mol. Phys.* **76**, 937-950 (1992).
16. Winograd, N. The Magic of Cluster SIMS. *Anal. Chem.* **77**, 142A-149A (2005).
17. *Depth resolution is defined as the full width at half maximum of a Gaussian convolution function.*
18. Kramer, E. J. Depth profiling methods that provide information complementary to neutron reflectivity. *Physica B* **173**, 189-198 (1991).

19. Genzer, J., Rothman, J. B. & Composto, R. J. Improved Hydrogen and Deuterium Depth Profiling in Polymers Using Low-Energy Forward Recoil Spectrometry. *Nucl. Instrum. Methods Phys. Res., B* **86**, 345-354 (1994).
20. Sokolov, J., Rafailovich, M. H., Jones, R. A. L. & Kramer, E. J. Enrichment Depth Profiles in Polymer Blends Measured by Forward Recoil Spectrometry. *Appl. Phys. Lett.* **54**, 590-592 (1989).
21. Roe, R.-J. *Methods of X-Ray and Neutron Scattering in Polymer Science* (Oxford University Press, New York, 2000).
22. Hariharan, A. et al. The Effect of Finite Film Thickness on the Surface Segregation in Symmetrical Binary Polymer Mixtures. *J. Chem. Phys.* **99**, 656-663 (1993).
23. Harton, S. E. et al. Low-Temperature Reactive Coupling at Polymer-Polymer Interfaces Facilitated by Supercritical CO2. *Polymer* **46**, 10173-10179 (2005).
24. Wilson, R. G., Stevie, F. A. & Magee, C. W. *Secondary Ion Mass Spectrometry: A Practical Handbook for Depth Profiling and Bulk Impurity Analysis* (John Wiley & Sons, New York, 1989).
25. Chia, V. K. F., Mount, G. R., Edgell, M. J. & Magee, C. W. Recent advances in secondary ion mass spectrometry to characterize ultralow energy ion implants. *J. Vac. Sci. Technol. B* **17**, 2345-2351 (1999).
26. Magee, C. W., Jacobson, D. & Gossmann, H.-J. Accuracy of secondary ion mass spectrometry in determining ion implanted B doses as confirmed by nuclear reaction analysis. *J. Vac. Sci. Technol. B* **18**, 489-492 (2000).
27. Zhao, X. et al. Determination of the Concentration Profile at the Surface of d-PS/ h-PS Blends Using High-Resolution Ion-Scattering. *Macromolecules* **24**, 5991-5996 (1991).
28. Strzhemechny, Y. M., Schwarz, S. A., Schacter, J., Rafailovich, M. H. & Sokolov, J. Secondary ion mass spectrometry study of silicon surface preparation and the polystyrene/silicon interface. *J. Vac. Sci. Technol. A* **15**, 894-898 (1997).
29. Castner, D. G. View from the edge. *Nature* **422**, 129-130 (2003).
30. Sostarecz, A. G., Sun, S., Szakal, C., Wucher, A. & Winograd, N. Depth profiling studies of multilayer films with a C60+ ion source. *Appl. Surf. Sci.* **231-232**, 179-182 (2004).
31. Fuoco, E. R., Gillen, G., Wijesundara, M. B. J., Wallace, W. E. & Hanley, L. Surface Analysis Studies of Yield Enhancements in Secondary Ion Mass Spectrometry by Polyatomic Projectiles. *J. Phys. Chem. B* **105**, 3950-3956 (2001).
32. Wagner, M. S. Molecular Depth Profiling of Multilayer Polymer Films Using Time-of-Flight Secondary Ion Mass Spectrometry. *Anal. Chem.* **77**, 911-922 (2005).
33. Szakal, C., Sun, S., Wucher, A. & Winograd, N. C60 molecular depth profiling of a model polymer. *Appl. Surf. Sci.* **231-231**, 183-185 (2004).
34. Mahoney, C. M., Yu, J. & Gardella, J. A. Depth Profiling of Poly(L-lactic acid)/Triblock Copolymer Blends with Time-of-Flight Secondary Ion Mass Spectrometry. *Anal. Chem.* **77**, 3570-3578 (2005).

35. Xu, J., Ostrowski, S., Szakal, C., Ewing, A. G. & Winograd, N. ToF-SIMS imaging with cluster ion beams. *Appl. Surf. Sci.* **231-232**, 159-163 (2004).
36. Hu, X. et al. Dynamics of Polymers in Organosilicate Nanocomposites. *Macromolecules* **36**, 823-829 (2003).
37. Weibel, D. et al. A C60 Primary Ion Beam System for Time of Flight Secondary Ion Mass Spectrometry: Its Development and Seconedary Ion Yield Characteristics. *Anal. Chem.* **75**, 1754-1764 (2003).
38. McKinley, J. M., Stevie, F. A., Granger, C. N. & Renard, D. Analysis of alkali elements in insulators using a CAMECA IMS-6f. *J. Vac. Sci. Technol. A* **18**, 273-277 (2000).
39. Pivovarov, A. L., Stevie, F. A. & Griffis, D. P. Improved charge neutralization method for depth profiling of bulk insulators using O2+ primary beam on a magnetic sector SIMS instrument. *Appl. Surf. Sci.* **231-232**, 786-790 (2004).
40. Coulon, G., Russell, T. P., Deline, V. R. & Green, P. F. Surface-Induced Orientation of Symmetric, Diblock Copolymers: A Secondary Ion Mass Spectrometry Study. *Macromolecules* **22**, 2581-2589 (1989).
41. Shin, K. et al. Silicon Oxide Surface as a Substrate of Polymer Thin Films. *Macromolecules* **34**, 4993-4998 (2001).
42. Postawa, Z., Czerwinski, B., Winograd, N. & Garrison, B. J. Microscopic insights into the sputtering of thin organic films on Ag{111} induced by C-60 and Ga bombardment. *J. Phys. Chem. B* **109**, 11973-11979 (2005).
43. Wilson, R. G., Lux, G. E. & Kirschbaum, C. L. Depth profiling and secondary ion mass spectrometry relative sensitivity factors and systematics for polymers/organics. *J. Appl. Phys.* **73**, 2524-2529 (1993).
44. Fuchs, K., Friedrich, C. & Weese, J. Viscoelastic Properties of Narrow-Distribution Poly(methyl methacrylates). *Macromolecules* **29**, 5893-5901 (1996).
45. Deline, V. R., Evans, C. A. & Williams, P. Unified Explanation for Secondary Ion Yields. *Appl. Phys. Lett.* **33**, 578-580 (1978).
46. Deline, V. R., Katz, W., Evans, C. A. & Williams, P. Mechanism of Sims Matrix Effect. *Appl. Phys. Lett.* **33**, 832-835 (1978).

Layer	O_2^+ S_R (nm/s)	O_2^+ $S_R/S_{R,Si}$	Cs^+ S_R (nm/s)	Cs^+ $S_R/S_{R,Si}$
(100) Si	0.16	1.00	0.19	1.00
PS Annealed	0.28	1.75	0.22	1.16
PS As-Cast	0.25	1.56	0.21	1.11
PMMA Annealed	0.57	3.56	0.62	3.26

Table 2.1 Sputtering rates (SR) in nm/s for 25 nA, 5.5 keV O2+ and 10 nA, 6.0 keV Cs+ SIMS, respectively. Values are normalized to SR for intrinsic Si (100) (SR/SR,Si). No sacrificial layer or Au coating was used with these measurements.

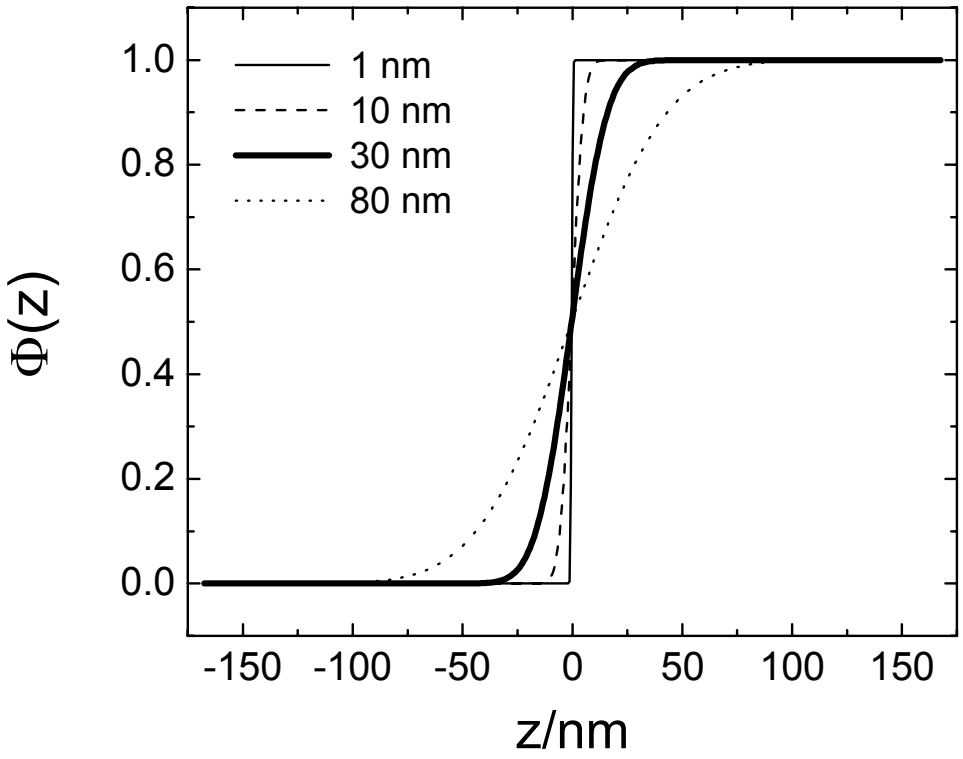

Figure 2.1. Gaussian convolution of a Heaviside (step) function Φ(z), where Φ(z) = 0 from -∞ to 0 and Φ(z) = 1 from 0 to ∞. Typical depth resolutions (FWHM) are represented for NR (solid line), SIMS (dashed line), LE- or ToF-FRES (bold line), and FRES (dotted line).

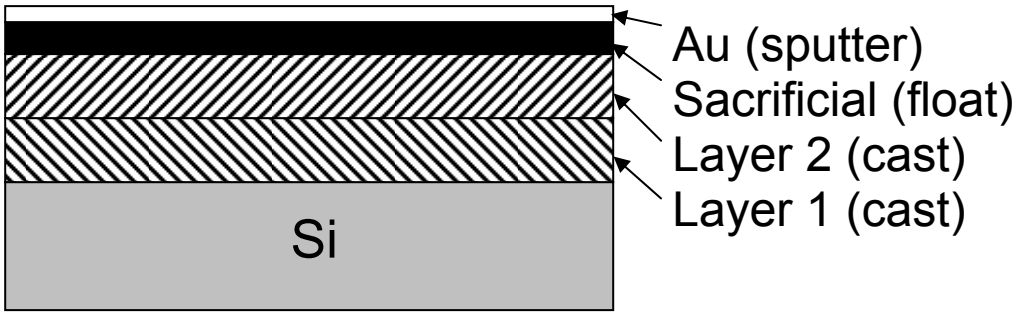

Figure 2.2. Schematic of thin film assembly used for SIMS analysis. From the bottom up: Si substrate (with SiO_x or SiH at the surface), first polymer layer (~ 100-200 nm PMMA or P2VP), second polymer layer (~ 100-200 nm PS or PCHMA) 'doped' with dPS, 50 nm PS sacrificial layer, and 20 nm Au coating.

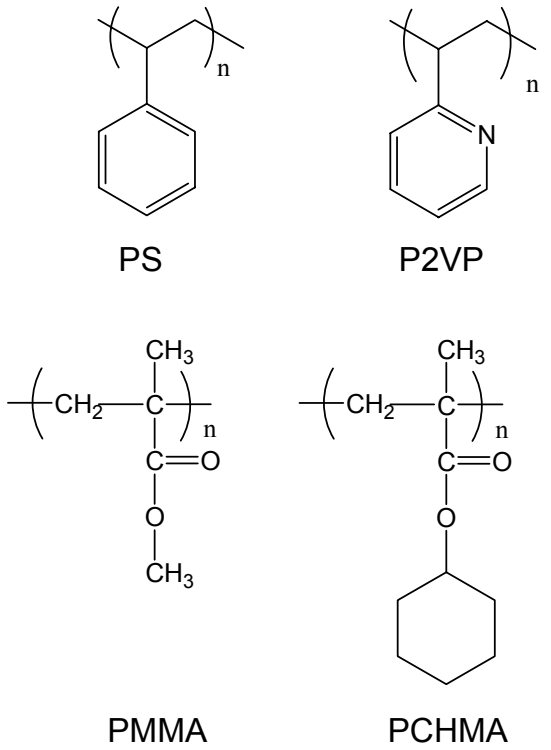

Figure 2.3. Chemical structures of polystyrene (PS), poly(2-vinylpyridine) (P2VP), poly(methyl methacrylate) (PMMA), and poly(cyclohexyl methacrylate) (PCHMA). Deuterium-labeled polystyrene (dPS) is identical to PS, except a percentage of hydrogen sites are occupied with deuterium. For the dPS used here, ≈ 100% of the hydrogen sites are occupied with deuterium.

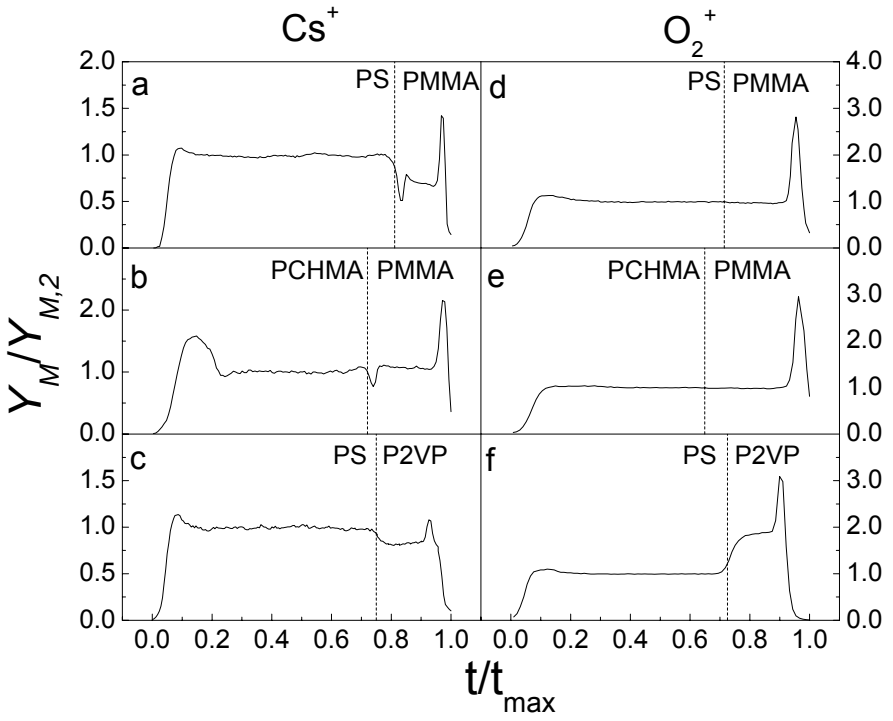

Figure 2.4. Matrix ^{12}C ion yields (Y_M), which are the detected intensities (counts/s) of atomic ^{12}C, normalized to the nominal value for the second layer (PS or PCHMA) for Cs^+ with a) PS/PMMA, b) PCHMA/PMMA, and c) PS/P2VP and O_2^+ with d) PS/PMMA, e) PCHMA/PMMA, and f) PS/P2VP. The x-axis is the sputtering time (t) normalized to the maximum time of analysis (t_{max}). The location of the heterogeneous polymer-polymer interface is indicated by the vertical dashed line, as determined by the deuterium profiles (not shown). All bilayers had a 50 nm PS sacrificial layer and a 20 nm Au coating at the surface (see Figure 2.2).

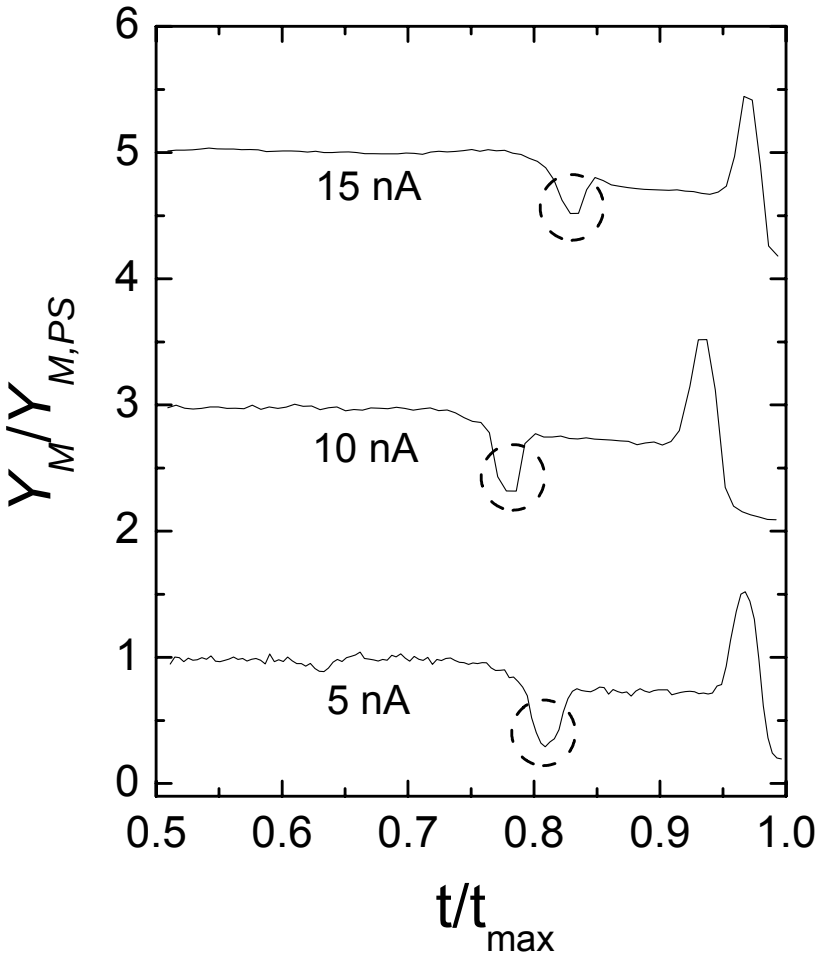

Figure 2.5. Matrix ^{12}C ion yields (YM) for PS/PMMA normalized to the nominal value for the PS layer for 6.0 keV (impact energy) Cs^+ with 5 (bottom), 10 (middle), and 15 (top) nA primary ion currents. The 10 and 15 nA profiles have been offset by an arbitrary amount for clarity. The x-axis is the sputtering time (t) normalized to the maximum time of analysis (t_{max}). The location of the PS/PMMA interface (circled) is obvious from the non-monotonic change in Y_M. This change in Y_M at the PS/PMMA interface is nearly independent of the primary ion current.

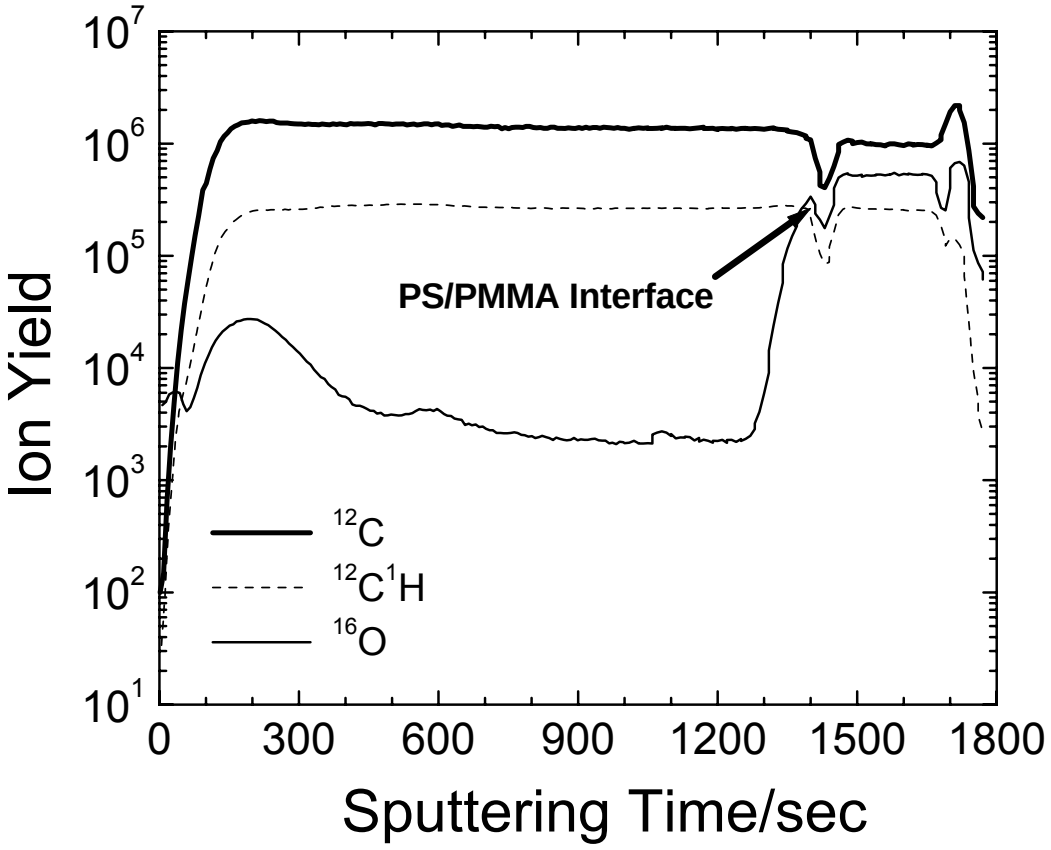

Figure 2.6. Secondary ion yields for ^{12}C (bold line), $^{12}C^{1}H$ (dashed line), and ^{16}O (solid line) for 5 nA (6.0 keV impact energy) Cs^{+} primary ion bombardment of a PS/PMMA bilayer as a function of sputtering time (t).

3. INVESTIGATION OF BLEND MISCIBILITY OF A TERNARY PS:PCHMA/PMMA SYSTEM

3.1. Introduction

Miscible polymer blends have been model systems for investigation of polymer dynamics[1-6] and equilibrium segregation at polymer surfaces[7-9] and polymer/polymer interfaces.[10,11] They are often composed of polymer pairs that have an apparent exothermic enthalpy of mixing.[1,7,12-14] Characterized by a lower critical solution temperature (LCST) type phase behavior, these systems are miscible at low temperatures when $\chi_{AB} < 0$, where χ_{AB} is the mean-field enthalpic interaction parameter between homopolymers *A* and *B*,[15] and tend to phase separate as they are heated above the critical temperature (T_c). This type of phase behavior can often be attributed to specific interactions, such as hydrogen bonding,[16] or large differences in polymer free-volume.[17] Previously investigated binary LCST blends have included polystyrene (PS) in combination with poly(xylenyl ether) (PXE),[1,14] poly(vinylmethyl ether) (PVME),[7,18] or tetramethylbisphenol-A polycarbonate (TMPC).[12,13] Although these systems have been employed for investigations of such phenomena as surface segregation[7] and mutual or self diffusion,[1,12-14] they suffer from highly asymmetric glass transition temperatures (T_g's). These asymmetries can led to spatially varying T_g's and polymer chains possessing significantly different monomeric friction coefficients,[13,14] making accurate decoupling of various phenomena extremely difficult.[4-6] The need for a model LCST

system involving polymers with similar T_g's and well defined thermodynamic parameters has motivated the present investigation.

Polymer blend phase behavior changes dramatically near surfaces and interfaces due to a reduction in conformational entropy,[19] and asymmetries in χ_{AC} and χ_{BC} can led to segregation of an *A* polymer to an *A*:*B*/*C* interface,[10,11,20,21] where *A* and *B* are miscible with each other, yet each is immiscible with *C*. An extremely powerful theoretical method for analyzing these types of systems is self-consistent mean-field theory (SCMF).[19] Even though it is computationally much less costly than detailed numerical simulations,[22] SCMF has been found to produce accurate representation of polymer interfaces within the mean-field limit.[23] Due to its accuracy and low computational cost, it can be used to determine χ from such experimental measurements as interfacial width *w*[24] and interfacial segregation.[25]

Secondary ion mass spectrometry (SIMS) is a widely used experimental technique for obtaining depth profiles of tracer-labeled polymers.[26] With its high depth resolution, it can be used to quantify an interfacial excess,[27,28] surface excess,[29] and diffusion gradient[30] of a labeled polymer in a polymer film. Even with the superb depth resolution attainable using SIMS, it is extremely difficult to measure *w* for systems where *w* is smaller than the instrumental resolution.[31] For this situation, x-ray or neutron reflectometry[32,33] (XR or NR, respectively) can complement SIMS.[26] In this article, we present direct measurements of the interfacial excess *Z** of deuterated polystyrene (dPS) at the interface between poly(cyclohexyl methacrylate) (PCHMA) and poly(methyl methacrylate) (PMMA) as a function of dPS concentration in PCHMA using SIMS. XR

is used to determine *w* between PCHMA and PMMA. SCMF is used to theoretically analyze *Z** and the changes in *w* and interfacial tension γ as a function of dPS concentration in PCHMA. The potential applications of the PS/PCHMA and PS/PCHMA/PMMA systems for model investigations of polymer diffusion and dynamics are outlined.

3.2. Experimental

3.2.1. Materials and Sample Preparation

Atactic dPS (polymer *A*) (M_w = 76.6 kDa; M_w/M_n = 1.05) was purchased from Polymer Source. Atactic PCHMA (polymer *B*) and syndiotactic PMMA (polymer *C*) (M_w = 101.0 kDa; M_w/M_n = 1.09) were purchased from Scientific Polymer Products. For PCHMA, the viscosity average molecular weight M_v was determined to be 74 kDa using dilute solution viscometry in 1-butanol at 22.5 °C (T_θ).[34] The inflection-point T_g's of dPS, PCHMA, and PMMA were determined to be 97, 102, and 127 °C, respectively, using differential scanning calorimetry (cooling cycle of 10 °C/min).

Silicon (100) wafers were cut into 2.5 cm x 2.5 cm squares and cleaned according to established procedures.[30] Immediately prior to spin casting, they were soaked in hydrofluoric acid (~ 10 % v/v in water) for 1 min and washed with deionized water. PMMA was cast onto the H-passivated Si from toluene and annealed for 1 h at 150 °C to remove residual solvent and create smooth surfaces. For SIMS analysis dPS/PCHMA films were cast from 1-chloropentane directly onto the PMMA layer and annealed at 150 °C for 42 h. The dPS concentration in the film was varied from 5 to 20 % (v/v). These samples had a PMMA layer thickness of 95 nm, and a dPS/PCHMA layer thickness of

125 nm as measured using ellipsometry. Films of the dPS/PCHMA blend were also cast onto Si wafers possessing a native oxide layer (~ 2 nm) and floated onto TEM grids from deionized water. Scanning transmission x-ray microscopy (STXM) at beamline 5.3.2 at the Advanced Light Source in Berkeley[35,36] confirms that no phase separated domains larger than ~ 25 nm (minimum resolvable domain size) were present in the as-cast dPS/PCHMA layers. Two characteristic photon energies, the PS phenyl ring $\pi^*_{C=C}$ peak energy (≈ 285.2 eV) and PCHMA carbonyl $\pi^*_{C=O}$ peak energy (≈ 288.4 eV), were used in the STXM analyses. Due to absence of an observable morphology, the STXM results are not included here explicitly. For XR analysis, PCHMA was cast onto PMMA from 1-chloropentane and annealed for 24 h at 150 °C. Single layer PMMA and PCHMA films were also prepared to determine the x-ray dispersions δ of the two polymers.

3.2.2. Secondary Ion Mass Spectrometry

The deuterium depth profiles were acquired using a CAMECA IMS-6f magnetic sector spectrometer using a 15 nA Cs^+ primary beam (6.0 keV impact energy) rastered over a 200 μm x 200 μm area with detection of negative secondary ions from a 60 μm diameter circle at the center. A sacrificial PS top layer (50 nm) was added after the 42 h anneal to ensure that the pre-equilibrium distance (range of bombarding species) was sputtered away before the layer of interest was reached, and a 20 nm gold coating was deposited on top of the sacrificial layer to minimize sample charging. The analysis conditions used provide a nominal depth resolution of ~ 8-10 nm. Some analyses were also made using O_2^+ at 5.5 keV impact energy, but the results showed poorer depth resolution than the Cs^+ data for the structure analyzed.

3.2.3. X-ray Reflectometry

The XR measurements have been carried out at beam line X10B at the National Synchrotron Light Source (NSLS), Brookhaven National Laboratory (BNL) using a photon energy of 14 keV (i.e. x-ray wavelength λ=0.87Å). The specularly reflected intensity was measured by varying α_i and α_f while maintaining $\alpha_i = \alpha_f$ (α_i and α_f are the incident and reflected angles, respectively). Because the specular reflectivity, presented as scattered intensity versus scattering vector $q_z = (4\pi/\lambda)\sin\alpha_i$, detects the variation of the electron density in the direction normal to the surface, it is sensitive to film thickness h, density ρ, interfacial width w, and surface roughness σ. However, in the case of XR analysis of polymer bilayer systems, difficulties often arise in obtaining details regarding polymer-polymer interfaces due to the small x-ray contrast $\Delta\delta/\delta$ between the individual polymers,[32] which is typically less than 10% for most polymer pairs.[33] In order to overcome this difficulty, we used a Fourier transformation (FT) analysis method developed previously.[32] A four-layer model (i.e., Si substrate, native oxide layer, PMMA layer, and PCHMA layer) was used to fit the XR data.

3.3. Results and Discussion

Table 3.1 shows the χ-values for the three binary interactions at 150 °C. Note the two different values that have been reported for PS/PCHMA.[37,38] To analyze the PCHMA/PMMA bilayers with XR, single layers of PCHMA and PMMA were used to measure the dispersion δ of the two polymers individually. Those values, along with the statistical segment lengths a,[34,39] h, and σ are listed in Table 3.2. Using the measured values for δ, the PCHMA/PMMA bilayers were analyzed using the FT method[32] as

shown in Figure 3.1, and w_{BC} was determined to be 1.6 nm. It should be noted that the x-ray contrast between PCHMA and PMMA is quite small (< 3%), and the value for w_{BC} is considered a lower limit. From the analytical solution of SCMF for w_{BC},[40]

$$w_{BC} = \left(\frac{a_B^2 + a_C^2}{3\chi_{BC}} \right)^{1/2}, \quad (1)$$

χ_{BC} was approximated to be 0.1, in agreement with prior results (see Table 3.1).[38]

Using SIMS, the interfacial excess of dPS at the PCHMA/PMMA interface was determined for initial dPS concentrations of 5, 10, and 20% (v/v) in PCHMA, as shown in Figure 3.2. The convoluted dPS profiles were fit to a Gaussian error function for the surface and equilibrium dPS in the PCHMA layer and a Gaussian peak for the segregated dPS at the interface.[27] The interfacial excess is determined from the expression

$$Z^* \equiv \left(\frac{\pi}{4 \ln 2} \right)^{1/2} \varphi_p \Delta \quad (2)$$

where φ_p is the height and Δ is the full width at half maximum of the Gaussian peak. The full width at half maximum of the error function is used as a measure of the instrumental resolution, which is ~ 8-10 nm for this system under these analysis conditions. As shown in Figure 3.3, the use of Cs^+ primary ions provides improved depth resolution when compared with bombardment using 5.5 keV impact energy O_2^+ primary ions for this system. Using Equation 2 Z^*/R was determined to be 0.053, 0.055, and 0.068 for initial concentrations of dPS of 5, 10, and 20%, respectively, where R is the RMS end-to-end distance[15] of a dPS chain ($R \approx 18$ nm). The RMS error for each measurement is ~ 5-10%.

The χ parameters for PS/PCHMA,[37,38] PCHMA/PMMA,[38] and dPS/PMMA[41] (χ_{AB}, χ_{BC}, and χ_{AC}, respectively) have been reported previously as a function of temperature. The χ for PCHMA/PMMA determined using XR ($\chi_{BC} \approx 0.1$) is almost identical to the reported value at 150 °C.[38] The measured χ_{BC} and the reported value of χ for dPS/PMMA at 150 °C ($\chi_{AC} = 0.038$)[41] are used in the SCMF calculations. The corresponding highly incompatible interaction should drive the PCHMA away from the PMMA interface and led to dPS segregation. Two significantly different values of χ for PS/PCHMA at 150 °C have been reported (χ_{AB} = -0.0034[37] and -0.015[38] as shown in Table 3.1), and the compatibility of each with the experimental measurements will be examined. Details of the equations and computational methods used in the SCMF calculations have been outlined elsewhere.[11,20,21] Only the results are presented here for this ternary system of dPS/PCHMA on PMMA. A constant effective segment length (a_e = 0.69 nm)[40] was used, where

$$a_e = \left(\frac{a_B^2 + a_C^2}{2} \right)^{1/2} . \quad (3)$$

The effective segment length is almost identical to the segment length of PS (a = 0.67 nm),[39] and the PS segmental volume (0.174 nm^3)[42] is used as the reference volume. For simplicity, it was assumed that the number of segments was identical to that of dPS for all polymers (N = 700), and the polydispersity of PCHMA was neglected. Although polydispersity has been shown to have significant effects on polymer profiles at polymer/polymer interfaces,[43] the depth profiles for dPS, PCHMA, and PMMA should be dominated by enthalpic rather than entropic contributions,[44] because $\chi_{BC}N \sim 40$ (based on

M_v of PCHMA) and there is a highly favorable interaction between dPS and PCHMA ($\chi_{AB}N << 0$).

Figure 3.4a shows an example of a simulated depth profile using χ_{AB} = -0.015. The zero-point for the z-axis is set by the inflection point in the depth profile for *C*. To compare the SCMF calculations to the experimental data, the SCMF *Z** was calculated from

$$Z^* \equiv \int_{-\infty}^{\infty} \left[\varphi_A - \varphi_A^{\infty}(1-\varphi_C)\right] dz\,, \tag{4}$$

where φ_A^{∞} is the value of φ_A far from the interface (the depleted value for dPS), as demonstrated in Figure 3.4b. As shown in Figure 3.5, the value of χ_{AB} = -0.015 provides much better agreement with the experimental measurements than χ_{AB} = -0.0034, indicating that PS/PCHMA is indeed a highly miscible system at 150 °C, with $T_c \approx 225$ °C.[38] Using χ_{AB} = -0.015, the interfacial tensions γ_{ABC} and interfacial widths w_{ABC} have been calculated (see Figure 3.6) using[11,20,21]

$$w_{ABC} = 4\int_{-\infty}^{\infty} \varphi_C(1-\varphi_C)dz \tag{4}$$

$$\gamma_{ABC} = kT\rho_o\zeta \int_{-\infty}^{\infty} (1-\varphi_A-\varphi_B-\varphi_C)dz\,, \tag{6}$$

where kT is the thermal energy, ρ_o is the lattice density, and ζ is a compressibility factor.[19] For all of the calculations performed in this investigation, ζ was set to 8.0, which maintains high degree of incompressibility (i.e. $1-\varphi_A-\varphi_B-\varphi_C \sim 10^{-3}$).[45] These

values are scaled to w_{BC} (Equation 1) and γ_{BC} in the limit of infinite molecular weight,[40] where

$$\gamma_{BC} = kT\rho_o a_e \left(\frac{\chi_{BC}}{6} \right)^{1/2} . \quad (7)$$

The seemingly low interfacial excess observed for dPS initial concentrations of 5-20% is due to the highly favorable interaction between dPS and PCHMA. This creates a powerful driving force to keep the dPS in the bulk.[21] Although compatibilization does occur due to dPS segregation, from Figure 3.6 we see that the changes in γ_{ABC} and w_{ABC} are very small over this concentration range.

Because PS and PCHMA are so highly miscible over a large temperature range (< 225 °C),[38] and the polymers have nearly identical T_g's, this is indeed a model system for investigation of chain dynamics in miscible blends.[4-6,37] We can also infer that, with known thermodynamic constants[38] and good agreement with SCMF (see Figure 3.5), the PS/PCHMA/PMMA ternary system would be ideal for investigation of potential driven diffusion near a bounding interface.[46,47] Many of the polymers previously used for such investigations, such as PXE,[1,14] PVME,[7,18] and TMPC,[12,13] are extremely difficult to controllably synthesize,[48] often resulting in somewhat high polydispersities ($M_w/M_n > 2$). Future investigations would be greatly improved through the use of a polymer system with each of the polymers having a low polydispersity ($M_w/M_n < 1.2$). PS and PMMA are well known for their ability to be controllably synthesized with a low polydispersity,[49] but PCHMA has also been synthesized with techniques such as anionic[37] and controlled-radical[50,51] polymerizations. These polymerization techniques have resulted in $M_w/M_n <$

1.2,[49] but unlike the synthesis of PMMA, the choice of method (radical or anionic) does not strongly influence the T_g of PCHMA.[37,51,52]

3.4. Conclusions

We have presented an investigation of the segregation of dPS to an interface between highly immiscible PCHMA and PMMA. With SIMS, we have measured Z^*/R of 0.053, 0.055, and 0.068 for 5, 10, and 20% initial concentrations, respectively, of dPS in the PCHMA layer after 42 h at 150 °C. Using XR, the interfacial width between PCHMA and PMMA has been determined to be 1.6 nm at 150 °C. Calculated values of Z^*/R from SCMF calculations have shown good agreement with the experimental values of Z^*/R at all three concentrations using the reported value of χ for PS/PCHMA of -0.015[38] rather than -0.0034.[37] SCMF calculations also show that, because PS and PCHMA are so highly miscible, there is little change in w_{ABC} and γ_{ABC} over the concentration range employed here due to relatively low dPS segregation. We anticipate PS/PCHMA and PS/PCHMA/PMMA to be model systems for future investigations of such phenomena as diffusion in miscible blends[13,14] and diffusion near interfaces[46,47] by minimizing problems associated with asymmetric T_g's of the polymer constituents.[4-6]

3.5. References

1. Composto, R. J., Mayer, J. W., Kramer, E. J. & White, D. M. Fast Mutual Diffusion in Polymer Blends. *Phys. Rev. Lett.* **57**, 1312-1315 (1986).
2. Brochard, F., Jouffroy, J. & Levinson, P. Polymer-Polymer Diffusion in Melts. *Macromolecules* **16**, 1638-1641 (1983).
3. Brochard, F., Jouffroy, J. & Levinson, P. Polymer Diffusion in Blends: Effects of Mutual Friction. *Macromolecules* **17**, 2925-2927 (1984).
4. Lodge, T. P. & McLeish, T. C. B. Self-concentrations and effective glass transition temperatures in polymer blends. *Macromolecules* **33**, 5278-5284 (2000).
5. Haley, J. C. & Lodge, T. P. Failure of time-temperature superposition in dilute miscible polymer blends. *Colloid Polym. Sci.* **282**, 793-801 (2004).
6. Haley, J. C. & Lodge, T. P. A framework for predicting the viscosity of miscible polymer blends. *J. Rheol.* **48**, 463-486 (2004).
7. Forrey, C., Koberstein, J. T. & Pan, D. H. Surface segregation in miscible blends of polystyrene and poly(vinylmethyl ether): Comparison of theory and experiment. *Interface Sci.* **11**, 211-223 (2003).
8. Jones, R. A. L., Kramer, E. J., Rafailovich, M. H., Sokolov, J. & Schwarz, S. A. Surface Enrichment in an Isotopic Polymer Blend. *Phys. Rev. Lett.* **62**, 280-283 (1989).
9. Kim, E., Kramer, E. J., Garrett, P. D., Mendelson, R. A. & Wu, W. C. Surface Segregation in Blends of Styrene-Acrylonitrile Copolymers. *Polymer* **36**, 2427-2433 (1995).
10. Faldi, A., Genzer, J., Composto, R. J. & Dozier, W. D. Segregation at the Interface between a Homopolymer and a Binary Polymer Blend. *Phys. Rev. Lett.* **74**, 3388-3391 (1995).
11. Genzer, J. & Composto, R. Effect of Molecular Weight on the Interfacial Excess, Tension, and Width in a Homopolymer Binary Polymer Blend System. *Macromolecules* **31**, 870-878 (1998).
12. Kim, E., Kramer, E. J., Osby, J. O. & Walsh, D. J. Mutual Diffusion and Thermodynamics in the Blends of Polystyrene and Tetramethylbisphenol-a Polycarbonate. *J. Polym. Sci., Part B: Polym. Phys.* **33**, 467-478 (1995).
13. Kim, E., Kramer, E. J. & Osby, J. O. Tracer Diffusion in the Blends of Polystyrene and Tetramethylbisphenol-a Polycarbonate. *Macromolecules* **28**, 1979-1989 (1995).
14. Composto, R. J., Kramer, E. J. & White, D. M. Reptation in Polymer Blends. *Polymer* **31**, 2320-2328 (1990).
15. Flory, P. J. *Principles of Polymer Chemistry* (Cornell University Press, Ithaca, NY, 1953).
16. Coleman, M. M., Graf, J. F. & Painter, P. C. *Specific Interactions and the Miscibility of Polymer Blends* (Technomic, Lancaster, PA, 1991).

17. Hino, T., Song, Y. H. & Prausnitz, J. M. Equation-of-State Analysis of Binary Copolymer Systems .2. Homopolymer and Copolymer Mixtures. *Macromolecules* **28**, 5717-5724 (1995).
18. Sferrazza, M., Jones, R. A. L. & Bucknall, D. G. Thermally driven collapse of a polymer brush in a polymer matrix. *Phys. Rev. E* **59**, 4434-4440 (1999).
19. Helfand, E. & Tagami, Y. Theory of the Interface between Immiscible Polymers. II. *J. Chem. Phys.* **56**, 3592-3601 (1972).
20. Genzer, J., Faldi, A. & Composto, R. J. Mean-field theory of the interface between a homopolymer and a binary-polymer mixture. *J. Chem. Phys.* **105**, 10134-10144 (1996).
21. Helfand, E. Theory of the Homopolymer/Binary-Polymer-Mixture Interface. *Macromolecules* **25**, 1676-1685 (1992).
22. Binder, K. *Monte Carlo and Moecular Dynamics Simulations in Polymer Science* (Oxford University Press, Oxford, 1995).
23. Werner, A., Schmid, F. & Müller, M. Monte Carlo simulations of copolymers at homopolymer interfaces: Interfacial structure as a function of the copolymer density. *J. Chem. Phys.* **110**, 5370-5379 (1999).
24. Clarke, C. J. et al. Measurements of the Flory-Huggins interaction parameter for polystyrene-poly(4-vinylpyridine) blends. *Macromolecules* **30**, 4184-4188 (1997).
25. Dai, K. H. & Kramer, E. J. Determining the Temperature-dependent Flory Interaction Parameter for Strongly Immiscible Polymers from Block-Copolymer Segregation Measurements. *Polymer* **35**, 157-161 (1994).
26. Kramer, E. J. Depth profiling methods that provide information complementary to neutron reflectivity. *Physica B* **173**, 189-198 (1991).
27. Harton, S. E., Stevie, F. A. & Ade, H. Diffusion-Controlled Reactive Coupling at Polymer-Polymer Interfaces. *Macromolecules* **38**, 3543-3546 (2005).
28. Reynolds, B. J., Ruegg, M. L., Mates, T. E., Radke, C. J. & Balsara, N. P. Experimental and Theoretical Study of the Adsorption of a Diblock Copolymer to Interfaces between Two Homopolymers. *Macromolecules* **38**, 3872-3882 (2005).
29. Schwarz, S. A. et al. Studies of Surface and Interface Segregation in Polymer Blends by Secondary ion Mass-Spectrometry. *Mol. Phys.* **76**, 937-950 (1992).
30. Shin, K. et al. Silicon Oxide Surface as a Substrate of Polymer Thin Films. *Macromolecules* **34**, 4993-4998 (2001).
31. Genzer, J. & Composto, R. J. The Interface Between Immiscible Polymers Studied by Low-Energy Forward Recoil Spectrometry and Neutron Reflectivity. *Polymer* **40**, 4223-4228 (1999).
32. Seeck, O. H. et al. Analysis of X-Ray Reflectivity Data from Low-Contrast Polymer Bilayer Systems using a Fourier Method. *Appl. Phys. Lett.* **76**, 2713-2715 (2000).
33. Stamm, M., Reiter, G. & Kunz, K. The use of X-Ray and Neutron Reflectometry for the Investigation of Polymeric Thin-Films. *Physica B* **173**, 35-42 (1991).
34. Amashta, I. A. K. & Sanchez, G. Estimation of Unperturbed Dimensions of Poly(cyclohexyl methacrylate) from light scattering, osmometry and viscosity data. *Eur. Polym. J.* **11**, 223-223 (1975).

35. Ade, H. et al. Scanning Transmission X-Ray Microscopy at a Bending Magnet Beamline at the Advanced Light Source. *J. Phys. IV* **104**, 3-8 (2003).
36. Kilcoyne, A. L. D. et al. Interferometer Controlled Scanning Transmission X-Ray Microscopes at the Advanced Light Source. *J. Synchr. Rad.* **10**, 125-136 part 2 (2003).
37. Friedrich, C., Schwarzwaelder, C. & Riemann, R.-E. Rheological and thermodynamic study of the miscible blend polystyrene/poly(cyclohexyl methacrylate). *Polymer* **37**, 2499-2507 (1996).
38. Pomposo, J. A., Mugica, A., Areizaga, J. & Cortazar, M. Modeling of phase behavior of binary and ternary blends involving copolymers of styrene, methyl methacrylate, and cyclohexyl methacrylate. *Acta Polym.* **49**, 301-311 (1998).
39. Fetters, L. J., Lohse, D. J., Milner, S. T. & Graessley, W. W. Packing length influence in linear polymer melts on the entanglement, critical, and reptation molecular weights. *Macromolecules* **32**, 6847-6851 (1999).
40. Helfand, E. & Sapse, A. M. Theory of Unsymmetric Polymer-Polymer Interfaces. *J. Chem. Phys.* **62**, 1327-1331 (1975).
41. Russell, T. P. Changes in Polystyrene and Poly(methyl methacrylate) Interactions with Isotopic Substitution. *Macromolecules* **26**, 5819 (1993).
42. Sferrazza, M. et al. Evidence for Capillary Waves at Immiscible Polymer/Polymer Interfaces. *Phys. Rev. Lett.* **78**, 3693-3696 (1997).
43. Fredrickson, G. H. & Sides, S. W. Theory of polydisperse inhomogeneous polymers. *Macromolecules* **36**, 5415-5423 (2003).
44. Broseta, D., Fredrickson, G. H., Helfand, E. & Leibler, L. Molecular Weight and Polydispersity Effects at Polymer-Polymer Interfaces. *Macromolecules* **23**, 132-139 (1990).
45. Shull, K. R. & Kramer, E. J. Mean-Field Theory of Polymer Interfaces in the Presence of Block Copolymers. *Macromolecules* **23**, 4769-4779 (1990).
46. Zheng, X. et al. Long-Range Effects on Polymer Diffusion Induced by a Bounding Interface. *Phys. Rev. Lett.* **79**, 241 (1997).
47. Zheng, X. et al. Reptation Dynamics of a Polymer Melt near an Attractive Solid Interface. *Phys. Rev. Lett.* **74**, 407-410 (1995).
48. White, D. M. & Nye, S. A. Preparation of Deuterated Poly(2,6-Dimethyl-1,4-Phenylene Oxide). *Macromolecules* **17**, 2643-2645 (1984).
49. Odian, G. *Principles of Polymerization* (John Wiley & Sons, Inc., Hoboken, NJ, 2004).
50. Munoz-Bonilla, A., Madruga, E. L. & Fernandez-Garcia, M. Atom transfer radical polymerization of cyclohexyl methacrylate at a low temperature. *J. Polym. Sci., Part A: Polym. Chem.* **43**, 71-77 (2005).
51. Miwa, Y. et al. Segmental dynamics and self-concentration around chain ends in miscible blend of poly(cyclohexyl methacrylate) and poly(cyclohexyl acrylate) as studied by the spin-label technique. *Macromolecules* **37**, 8612-8617 (2004).
52. Fuchs, K., Friedrich, C. & Weese, J. Viscoelastic Properties of Narrow-Distribution Poly(methyl methacrylates). *Macromolecules* **29**, 5893-5901 (1996).

Polymer Pair	χ (150 °C)
dPS/PMMA[41]	0.038
PS/PCHMA (1)[37]	-0.0034
PS/PCHMA (2)[38]	-0.015
PCHMA/PMMA[38]	0.097

Table 3.1. Reported values of χ for dPS/PMMA, PS/PCHMA, and PCHMA/PMMA at 150 °C.

	***h*/nm**	**σ/nm**	***a*/nm**	**δ x10^6**
PCHMA	72.5	0.28	0.73[34]	1.24
PMMA	61.7	0.43	0.65[39]	1.21

Table 3.2. XR analysis of PCHMA and PMMA single layer films.

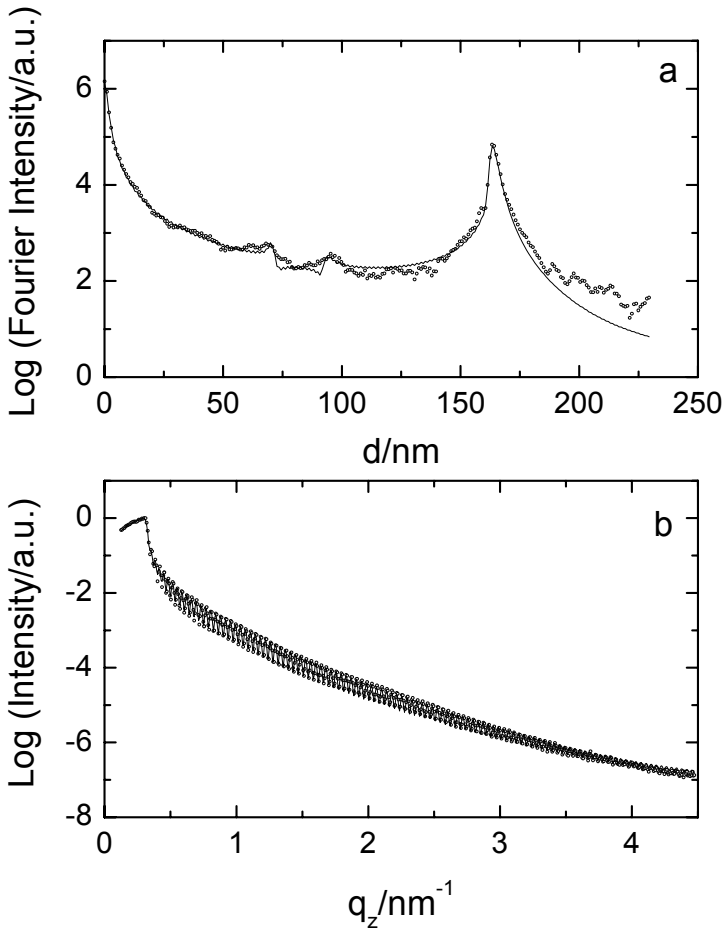

Figure 3.1. XR of PCHMA/PMMA (*B*/*C*) bilayers. The Fourier method (a) was used to determine the interfacial width of this low contrast system (see Table 2). The low contrast is observed in the reflectivity profile (b). Using Equation 1, χ_{BC} was approximated to be 0.1.

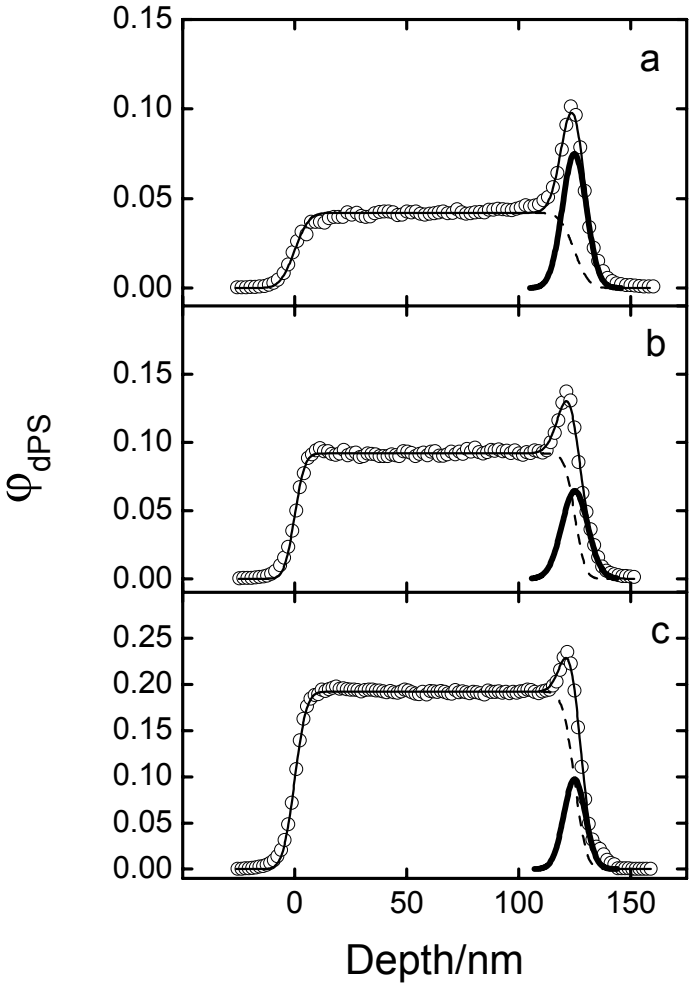

Figure 3.2. SIMS profiles for bilayers of dPS in PCHMA on PMMA (*A*:*B*/*C*) with (a) 5, (b) 10, and (c) 20% (v/v) initial concentrations of dPS. After depletion of dPS due to segregation to the interface during the 42 h anneal at 150 °C, the bulk concentration away from the interface (φ_A^{∞}) was reduced to (a) 4.3, (b) 9.2, and (c) 19.2%. The interfacial excess (*Z**) was determined from Equation 2 after fitting the SIMS profiles to a Gaussian error function (dotted line) and a Gaussian peak (bold line) which superimpose to represent the convoluted dPS profile (solid line).

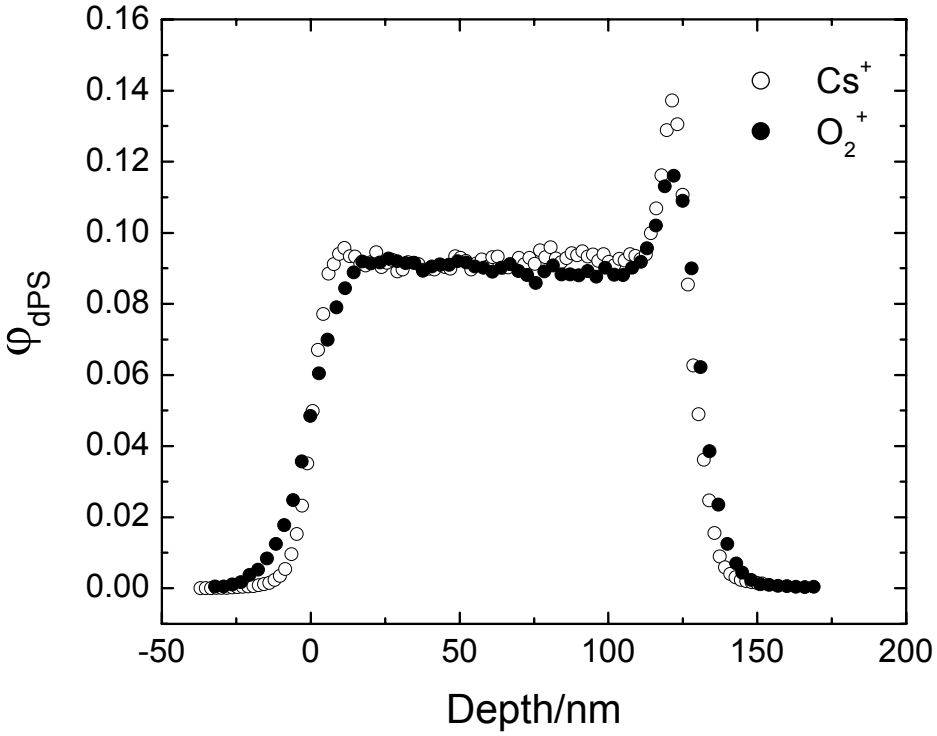

Figure 3.3. Comparison of Cs+ (○) and O_2+ (●) primary ion bombardment with 6.0 and 5.5 keV impact energies, respectively. For this system, Cs^+ clearly provides improved depth resolution.

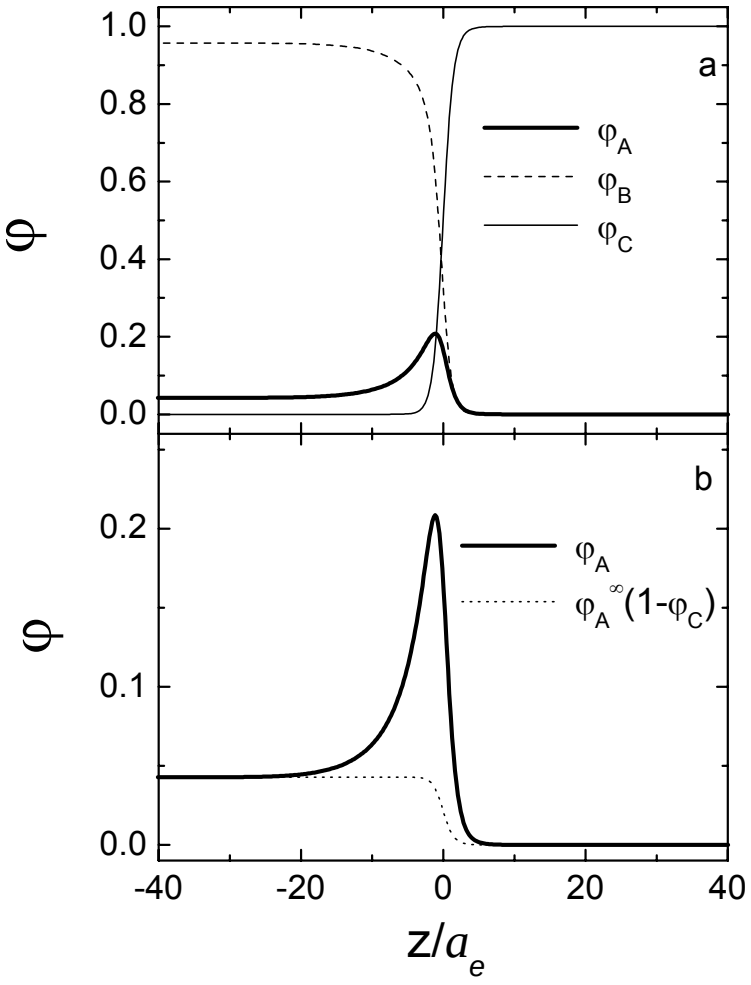

Figure 3.4. SCMF simulated profile for $\varphi_A^{\infty} = 0.043$ (depleted dPS concentration for 5% initial concentration) using $\chi_{AB} = -0.015$, $\chi_{AC} = 0.038$, and $\chi_{BC} = 0.1$. Polymer *A* (dPS) is the bold line, *B* (PCHMA) is the dotted line, and *C* (PMMA) is the solid line in (a). Z^*/R was determined to be 0.044 from Equation 4, and is the area between the bold and dotted lines in (b). Here, a_e is the effective segment length for *B* and *C* segments from Equation 3. The zero-point for the z-axis is set by the inflection point in the depth profile for *C*.

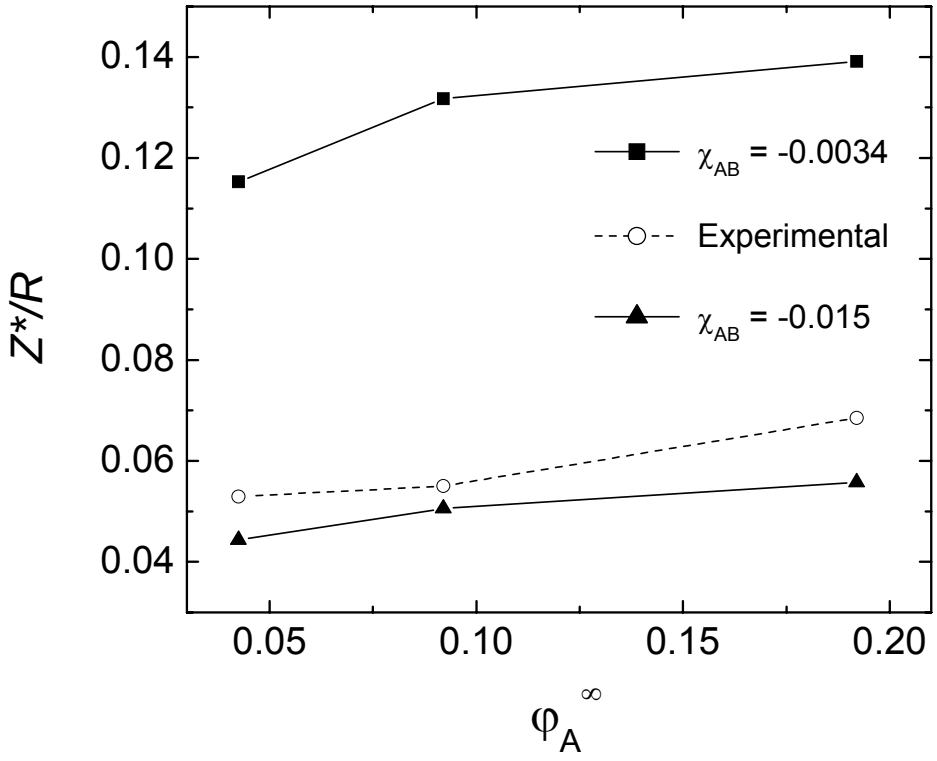

Figure 3.5. Interfacial excess (Z^*/R) measured from the SIMS profiles using Equation 2 (○) as compared to SCMF calculations using $\chi_{AC} = 0.038$, $\chi_{BC} = 0.1$ and $\chi_{AB} =$ -0.0034 (■) or -0.015 (▲). Lines are a guide for the eye. The theoretical values of Z^*/R were determined using Equation 4. It is clear that $\chi_{AB} = -0.015$ provides far better representation of the experimental values than $\chi_{AB} = -0.0034$.

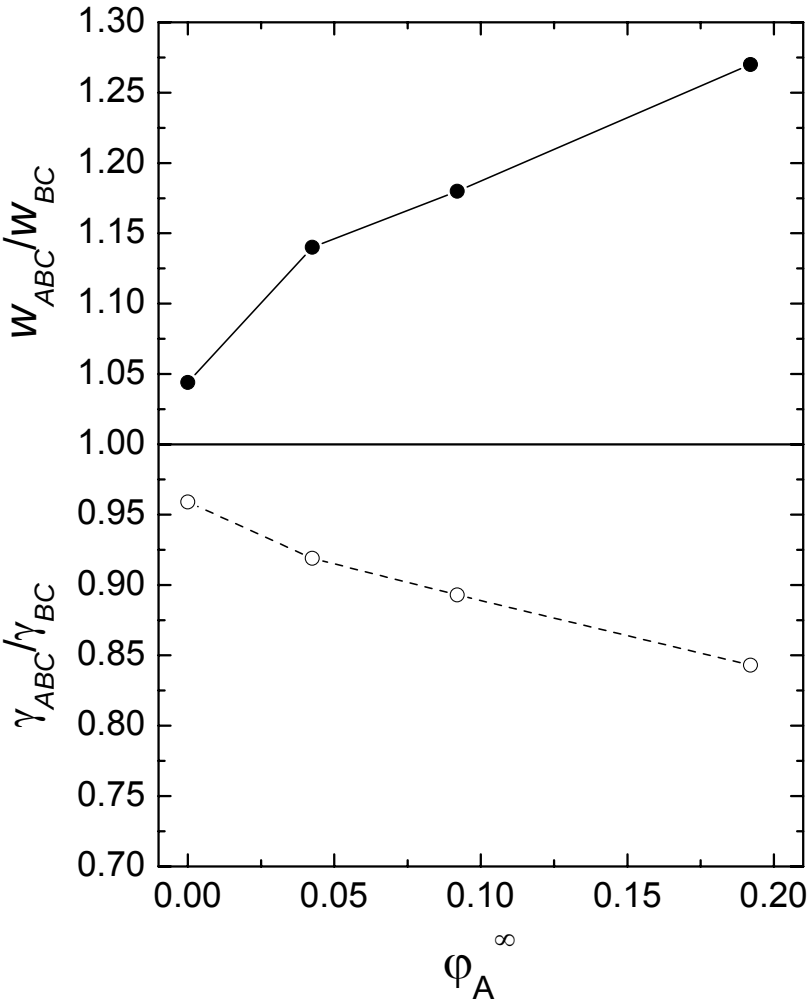

Figure 3.6. Interfacial width w_{ABC} (●) and interfacial tension γ_{ABC} (○) as determined using SCMF and Equations 5 and 6 with χ_{AB} = -0.015, χ_{AC} = 0.038, and χ_{BC} = 0.1. Lines are a guide for the eye. Values are scaled to the infinite molecular weight w_{BC} and γ_{BC} from Equations 1 and 7, respectively. Results are also shown for a numerical solution of a PCHMA/PMMA bilayer, where $\varphi_A^{\infty} = 0$ (N = 700).

4. INVESTIGATION OF THE EFFECTS OF ISOTOPIC LABELING AT A PS/PMMA INTERFACE

4.1. Introduction

Isotopic labeling of polymers is a well-established method for providing a tracer component or creating enhanced contrast for characterization using experimental techniques such as small angle neutron scattering (SANS),[1] neutron specular reflectivity (NR),[2] forward recoil spectrometry (FRES),[3] and secondary ion mass spectrometry (SIMS).[4,5] Although labeling is often necessary for experimental characterization, it is well-known that deuterium labeling (deuteration) can alter the thermodynamic properties of the polymer constituents.[6-8] In fact, many simple mixtures involving a polymer species and its deuterated analog are known to have a small, but finite mean-field interaction parameter χ, and are characterized by upper-critical solution-type phase behavior (UCST).[7,9,10] Therefore, a polymer mixture of h*A* and d*A*, where h*A* is unlabeled polymer *A* and d*A* is deuterium-substituted polymer *A*, can exhibit classical phase changes such as spinodal decomposition.[11]

The effects of deuteration can also influence the surface and interfacial interactions of polymers. Deuterium-substituted polystyrene (dPS) is known to have a lower surface tension than simple hydrogen-containing PS (hPS),[12] and it has an enthalpic preference for a silicon oxide (SiOx) surface.[13] These types of interactions have been shown to be significant at conditions well within the single-phase region of the phase diagram. Even with the enormous amount of existing information on the effects of isotopic labeling, investigations involving the effects of deuteration at polymer/polymer

interfaces have been limited.[14] Here, we probe the effects of deuteration at a polymer/polymer interface using secondary ion mass spectrometry (SIMS) and a highly-investigated polymer pair, PS and poly(methyl methacrylate) (PMMA).[15-17] Results show significant changes in the thermodynamic behavior of this system at the polymer/polymer interface, namely significant segregation of dPS to the hPS:dPS/hPMMA interface. Control experiments with end-functionalized polymers eliminated segregation due to endgroups as a possible reason for the observed segregation. A mean-field theory[18,19] that was previously implemented to describe surface segregation of dPS and segregation of dPS to an hPS:dPS/SiOx interface[13,20] is used to quantify the results presented here for segregation of dPS to an hPS:dPS/hPMMA interface as a function of temperature, dPS concentration, and dPS molecular weight. An energetic parameter $\Delta\chi_p$, which is related to the difference in χ for dPS/hPMMA and hPS/hPMMA, was determined as a function of temperature. It is clearly shown that the results presented here cannot be described, even qualitatively, using the reported changes in χ for PS/PMMA due to isotopic labeling.[6]

4.2. Experimental

4.2.1. Materials and Sample Preparation

Atactic PS (hPS and dPS), syndiotactic hPMMA, and atactic poly(2-vinyl pyridine) (hP2VP) were purchased from Polymer Source (PolS) or Scientific Polymer Products (SPP). Their molecular weight and polydispersity properties are listed in Table 4.1. All dPS have ≈ 100% deuterium substitution (perdeuterated). The inflection-point glass transition temperatures (T_g's) of the respective polymers, as determined using DSC

(10°C/min cooling cycle), are also listed in Table 4.1. Silicon (100) substrates were cut to 2.5 cm x 2.5 cm squares and cleaned according to established procedures.[21] First, the substrates were soaked in a sulfuric acid/hydrogen peroxide/water (1:1:3) bath at 100 °C for 30 min to remove organic and inorganic contaminants, and then washed with deionized water. Then, they were soaked in aqueous HF (~ 10% v/v) for 1 min, washed with deionized water, and blown dry with nitrogen leaving a hydrogen-passivated substrate (SiH). hPMMA and hP2VP were spun-cast from chlorobenzene onto SiH to a thickness ≈ 200 nm and annealed at 150 °C for 3 h. PS (hPS + dPS) was cast directly onto hPMMA or hP2VP from 1-chloropentane, a selective solvent for PS over PMMA or P2VP.[17] For segregation measurements, the PS thickness ranged from ≈ 200-250 nm, and the dPS concentration was varied from 5 to 30% (v/v) relative to the total PS. Samples were annealed under vacuum at temperatures ranging from 128 to 166 °C. A bilayer consisting of 100 nm 100% dPS-130 on 100 nm hPMMA was also prepared to quantify sputtering rates and the depth resolution during SIMS analysis. All systems are listed in Table 4.2.

4.2.2. Secondary Ion Mass Spectrometry

The deuterium depth profiles were acquired using a CAMECA IMS-6f magnetic sector spectrometer. Typical conditions implemented for the PS/PMMA system involved a 25-30 nA O_2^+ primary beam with 5.5 keV impact energy that was rastered over a 180 μm x 180 μm area. Positive secondary ions were detected from a 60 μm diameter optically gated area at the center of the raster crater. A mass resolution (m/Δm) of 1250 was used to completely separate D^+ from H_2^+ while maintaining high detection

sensitivity.[17,22] For the hPS:dPS-OH/hP2VP system, identical conditions were used with the exception of a 50 nA O_2^+ primary ion beam. Before the bilayers were analyzed, a 50 nm hPS sacrificial layer was added to the sample surface to ensure uniform sputtering rates and secondary ion yields before the start of the hPS:dPS layer. A 20 nm Au coating was deposited on top of the sacrificial layer to prevent charge build-up. Three to four spots on each sample were analyzed.

4.3. Results and Discussion

From Figure 4.1, it is clearly evident that dPS preferentially segregates to the hPS:dPS/hPMMA interface at 128 °C. The depletion hole at the hPS:dPS surface and hPS:dPS/hPMMA interfaces (Figure 4.1b) after 4 h (System *B*) indicates that this is a diffusion-controlled event. Diffusion-controlled segregation of dPS to an hPS:dPS surface has been quantified previously, although without direct observation of a depletion hole.[12,23] However, this phenomenon has not been observed for homopolymer segregation to a polymer/polymer interface. The observation of the depletion hole implies that the energetic gain at the interface per dPS chain has to be > kT, which is surprisingly large. At longer times (Figure 4.1c) there is a considerable amount of dPS at the hPS:dPS/hPMMA interface (System *A*). Figure 4.2 shows the raw SIMS profiles for D^+ and the $^{12}C^+$ matrix after 4 h at 128 °C (System *B*). The use of O_2^+ primary ion bombardment with detection of positive primary ions, under the conditions implemented here, provides a constant $^{12}C^+$ secondary ion yield through the hPS:dPS/hPMMA interface, which has been observed previously.[24] This is an optimal situation for analysis of a heterogeneous interface, and it should be noted that these analysis conditions (i.e.,

detection of positive secondary ions) could not be implemented with the commonly used quadrupole SIMS instrument, with its inferior mass resolution (typical $m/\Delta m \sim 300$) and, hence, inability to mass resolve D^+ from H_2^+.[4,25] Therefore, the phenomena observed at the hPS:dPS/hPMMA interface in Figures 4.1b and 4.1c are not artifacts of the SIMS analysis. This is also evidenced in Figure 4.1a with the absence of any discernible features near the hPS:dPS/hPMMA interface for $t = 0$.

To ensure that the observed segregation of dPS is not driven by chemical bonding or specific interactions due to unwanted functional groups created on the dPS by improper synthesis,[26] a control experiment was performed with a system containing highly end-functionalized dPS (dPS-OH; > 95% -OH end-functionalized) and P2VP as bottom layer. P2VP was chosen because it does not show strong isotopically driven segregation. It has the added benefit of having an enhanced attractive enthalpic interaction of the –OH end group at the interface, as it was previously determined that an –OH moiety will hydrogen bond much more strongly with the tertiary amine groups in the P2VP than the carbonyl groups in PMMA.[27] After 96 h at 130 °C, there is clearly negligible interfacial segregation of dPS-OH to the hPS:dPS-OH/hP2VP interface, as shown in Figure 4.3. Another common end-functional group such as –COOH (carboxy) would be expected to behave in a similar manner. Therefore, end groups that might have been unintentionally introduced to the dPS-130 (primarily –COOH from carbon dioxide contamination[28]) would not play a significant role in the interfacial segregation of dPS at a hPS:dPS/hPMMA interface. A functional group such as a primary amine, which is

highly unlikely to be unintentionally introduced, would be required to irreversibly react with the ester groups along the PMMA chain to cause an interfacial excess.[29]

For quantitative analysis of the interfacial segregation, we have employed a self-consistent mean-field lattice model (SCMF-L)[18] as derived previously for polymer segregation to polymer surfaces and polymer/substrate interfaces.[19] A cubic lattice was used for all calculations. Because the relaxed chain diameter of dPS-130 ($R_o = aN^{1/2} \approx 23$ nm, where R_o is the RMS end-to-end distance, a is the statistical segment length, and N is the number of segments in a dPS-130 chain) is much greater than the overlap of PS and PMMA at the interface ($w_{1/2} = a/(6\chi)^{1/2} \approx 1.4$ nm for $\chi = 0.038$),[16,30] the PMMA layer is treated as an infinitely flat (rigid) substrate. The free energy of mixing (F_M) in the hPS:dPS layer can be described using the Flory-Huggins expression:[31]

$$\frac{F_M}{kT} = \frac{n_{dPS}}{N_{dPS}} \ln \varphi_{dPS} + \frac{n_{hPS}}{N_{hPS}} \ln \varphi_{hPS} + \chi_{dPS,hPS} n_{dPS} \varphi_{hPS}, \quad (1)$$

where n_{dPS} and n_{hPS} are the number of segments of dPS and hPS, respectively. When the constraints of a surface are imposed, an excess energy is incorporated:

$$\frac{F_s}{kT} = -\Delta\chi_s n'_{dPS} \quad (2)$$

where n'_{dPS} is the number of dPS segments in contact with the surface, and $kT\Delta\chi_s$ is the net energetic preference for dPS over hPS at a surface.[13,19,20] Similarly,

$$\frac{F_p}{kT} \equiv -\Delta\chi_p n'_{dPS} = \lambda_1(\chi_{dPS,hPMMA} - \chi_{hPS,hPMMA}) n'_{dPS} \quad (3)$$

where $kT\Delta\chi_p$ is the net energetic preference per segment for dPS over hPS at an hPMMA 'substrate,' and λ_1 is a lattice weighting factor (1/6 for cubic).[18] As shown in Equation 3,

$\Delta\chi_p$ should be proportional to a simple difference in χ-values for dPS/hPMMA and hPS/hPMMA. Realistically, we would expect the number of contacts between PS (hPS or dPS) and hPMMA to be greater than one per segment, as there is indeed finite overlap at the interface. Therefore, $\Delta\chi_p$ can be considered an effective fitting parameter with physical limits

$$1 \geq \frac{\Delta\chi_p}{\chi_{hPS,hPMMA} - \chi_{dPS,hPMMA}} \geq \lambda_1 . \quad (4)$$

The use of this model helps to minimize computational cost, and it allows for direct comparison to parameters that have been previously determined for dPS segregation to hPS:dPS surfaces and hPS:dPS/SiOx interfaces.[13,20]

The reported χ-values for hPS:dPS are nominally 2.0×10^{-4} over the range of temperatures employed in this investigation (128 – 166 °C).[10,32] Figure 4.4 shows a theoretical comparison of dPS segregation using $\chi = 0.0$ and $\chi = 2.0 \times 10^{-4}$ for $N_{hPS} = N_{dPS} = 1200$ and $\Delta\chi_p = 0.01$. For the molecular weights used here, the interaction between hPS and dPS is negligible, as the system is deep inside the single-phase region of the phase diagram ($\chi N << 2$). Therefore, segregation of dPS-130 to the interface is driven exclusively by the $-kT\Delta\chi_p$ energy gain, and as such, it can be assumed that $\chi \approx 0.0$ for the hPS:dPS blends used here.

PS and PMMA are known to have a weak enthalpic interaction with each other, with or without isotopic labeling (see Table 4.3).[6,33] The temperature dependency of the dPS segregation was tested for System *B* at temperatures ranging from 138 to 166 °C by fitting convoluted theoretical profiles to SIMS depth profiles. A constant value of $\Delta\chi_s =$

0.005, as reported previously for dPS surface segregation at 160 °C,[20] was used to account for dPS segregation to the hPS:dPS surface. To determine the effective depth resolution, System *H* was fit to a Gaussian convoluted step function (error function) with a measured full width at half maximum (FWHM) of 15 nm as shown in Figure 4.5. Besides the inherent instrumental convolution for a given system and analysis conditions,[22,34] any convolution due to interfacial roughness[35] is also included in this value.[36] This line shape represents the profile quite well, both at the sacrificial layer/dPS and dPS/hPMMA interfaces, and as such, Gaussian convolution with a constant FWHM = 15 nm was used to convolute the theoretical depth profiles.

Figure 4.6 shows the depth profiles and convoluted SCMF-L profiles for System *B*. Three to four different profiles at each condition were analyzed. For System *A* no change in the dPS profile was found after annealing for times greater than 94 h at 138 °C. Tracer diffusion coefficients (D^o)[37] and characteristic diffusion times[38] ($\tau_D = L^2/4D^o$, where L is the PS layer thickness) for dPS-130 are shown in Table 4.4. According to the relative diffusion times ($\tau_D/\tau_{D,138}$) shown in Table 4.4, all annealing times used here were sufficient to reach equilibrium segregation, with the exception of the profiles shown in Figure 4.1. Qualitatively, one can see a clear decrease in the interfacial segregation of dPS from 138 to 166 °C. The quantitative changes in the interfacial interactions from 138 to 166 °C are shown in Figure 4.7, with a comparison to the values of $\Delta\chi_p$ measured here and the reported values of χ for hPS/hPMMA, dPS/dPMMA, dPS/hPMMA, and hPS/dPMMA (see Table 4.3).[6,33] The values for hPS/hPMMA had been determined using cloud-point measurements with homopolymer mixtures,[33] while the values for the

dPS/dPMMA, dPS/hPMMA, and hPS/dPMMA had been determined using SANS with block copolymers.[6,39] The RMS error for the $\Delta\chi_p$ measurements is approximately 2-3% for all values shown in Figure 4.7a. According to the linear fit of $\Delta\chi_p$ vs. $1/T$ (see Figure 4.7a),

$$\Delta\chi_p = \frac{14.8}{T} - 0.022 \tag{5}$$

the reported values of χ for dPS/hPMMA and hPS/hPMMA actually predict a *depletion* of dPS at the hPS:dPS/hPMMA interface ($\Delta\chi_p < 0$) rather than the observed *segregation*, and the temperature dependency of $\Delta\chi_p$ in Equation 5 is a factor of 3-4 greater than any of the values shown in Table 4.3. In fact, the reported change in χ for PS/PMMA over the temperature range used here (128 – 166 °C) is very small for all the values shown in Figure 4.7b, and the temperature dependence of $\Delta\chi_p$ using reported values would be completely negligible. This type of discrepancy can also be observed with interfacial tension (γ) measurements for hPS/hPMMA[40,41] when compared to γ predicted by the mean-field expression[30]

$$\gamma = a\rho_o kT\left(\frac{\chi}{6}\right)^{1/2} , \tag{6}$$

where ρ_o is the segmental density[16] (5.75 nm^{-3}). As shown in Figure 4.8, mean-field theory does not even qualitatively describe γ for hPS/hPMMA when the values for χ determined from bulk systems are used. The mechanism behind this apparent change in the phase behavior of PS/PMMA from bulk miscible systems to heterogeneous systems (interface) is not understood at this time.

The $\Delta\chi_s$ reported for dPS segregation to a hPS:dPS/SiOx interface at 170 °C ($\Delta\chi_s$ = 0.0098)[13] is also shown in Figure 4.7a. Clearly, the effects of isotopic labeling are more pronounced at an hPS:dPS/hPMMA than the hPS:dPS/SiOx interface, which is further demonstrated with a comparison of the theoretical dPS excess (Z*) for segregation of dPS to a hPS:dPS/SiOx interface, hPS:dPS/hPMMA interface, and an hPS:dPS surface ($\Delta\chi_s$ = 0.005)[20] for $N_{dPS} = N_{hPS} = 1200$ as shown in Figure 4.9. The excess was calculated from

$$\frac{Z^*}{a} \equiv \int_{M_1}^{M_2} (\varphi_{dPS} - \varphi_{dPS,b}) dz', \tag{7}$$

where z' is the depth scaled to the statistical segment length (a), M_1 is the (scaled) depth where φ_{dPS} becomes $\varphi_{dPS,b}$ (bulk concentration of dPS) and M_2 is the location of the interface (or surface), and scaled to the dPS radius of gyration ($R_g = a(N/6)^{1/2} \approx 9.5$ nm). Because the SCMF-L model is inherently discrete,[18] Equation 7 becomes a simple summation.

Next, the ability of the SCMF-L model to describe the dPS segregation as a function of dPS concentration and dPS molecular weight is evaluated. All of the systems employed for this (Systems *C* to *F*) were brought to equilibrium at 138 °C, and constant values of $\Delta\chi_p$ = 0.0134 and $\Delta\chi_s$ = 0.005 were used for all calculations. Clearly the SCMF-L model provides excellent representation of the dPS-130 segregation at 138 °C for 10 – 30% (v/v) dPS using the constant value of $\Delta\chi_p$. The excellent agreement of the concentration dependence indicates that the model does indeed provide some physical interpretation of the isotopically-driven segregation for Systems *A* – *E*. Values for Z^*/R_g

as a function of dPS concentration at 138 °C are shown in Figure 4.10. To determine if the model is truly universal for dPS segregation to an hPS:dPS/hPMMA interface, System *F* (10% dPS-70 + 90% hPS-70) was analyzed after equilibration at 138 °C. After comparison to the SCMF-L model (see Figure 4.11), it is evident that the model does not quantitatively describe the molecular weight dependency. A value of $\Delta\chi_p \approx 0.016$ provides much better theoretical agreement with the experimental results for dPS-70 segregation at 138 °C.

An apparent change in the energetic interaction with molecular weight has been observed previously with surface segregation of dPS.[20] The value of $\Delta\chi_s$ for an hPS:dPS surface was shown to deviate by as much as 50% from the nominal value of 0.005 over a range of dPS molecular weights of ~ 30 - 500 kDa.[20] This is also evidenced in Figure 4.11 with the surface excess of dPS-70, which is clearly much larger for the measured profile when compared to the simulated profile using $\Delta\chi_s = 0.005$. Therefore, there is an apparent increase in $\Delta\chi_p$ and $\Delta\chi_s$ from dPS-130 to dPS-70. Finite overlapping of PS and PMMA at the interface may be the reason behind the change in $\Delta\chi_p$. This could also be the result of an inability of the Flory-Huggins theory to accurately describe the entropic changes in the system. Modifications have been made to this theory through incorporation of equation-of-state effects.[42] These effects were shown to be particularly important for dPS segregation to an hPS:dPS surface when dPS and hPS have significantly different chain lengths (molecular weights).[43,44] Because χ for PS/PMMA (bulk) is nearly independent of temperature, owing primarily to entropic contributions,[6,33]

incorporation of equation-of-state effects may be necessary for a more complete theoretical description of this system.

4.4. Conclusions

The effects of isotopic labeling have been shown experimentally to have profound effects at a PS/PMMA interface. dPS was observed to strongly segregate to an hPS:dPS/hPMMA interface from a symmetric dPS:hPS blend with dPS concentrations ranging from 5 – 30 % (v/v) and temperatures ranging from 128 – 166 °C. At 128 °C, diffusion-controlled segregation was observed (see Figure 4.1), implying an energetic gain $>kT$ per dPS chain. Using a self-consistent mean-field lattice model,[18,19] the enthalpic preference for dPS over hPS at the hPS:dPS/hPMMA interface was interpreted using an energetic parameter $\Delta\chi_p$. This is in complete disagreement with previously reported χ values for PS/PMMA as a function of isotopic labeling (see Figure 4.7b),[6] which predict a depletion of dPS at a hPS:dPS/hPMMA interface. The temperature dependency is much greater for $\Delta\chi_p$ (see Figure 4.7a) than for any of the reported values of χ for PS/PMMA (see Table 4.3 and Figure 4.7b). Analogously, the reported values for the interfacial tension γ of PS/PMMA show a strong decrease with increasing temperature, however, the reported values of χ predict an increase in γ with increasing temperature (see Figure 4.8). This indicates an apparent change in the phase behavior of PS/PMMA from bulk miscible systems to heterogeneous systems (interface). Although SCMF-L could accurately describe the concentration dependence for dPS-130

segregation at 138 °C using a single value of $\Delta\chi_p = 0.0134$, universal behavior was not found when the molecular weight was varied.

4.5. References

1. Roe, R.-J. *Methods of X-Ray and Neutron Scattering in Polymer Science* (Oxford University Press, New York, 2000).
2. Zhao, W. et al. Neutron and x-ray reflectivity measurements of polystyrene/poly(bromostyrene) (PS/PBrS) interfaces. *Physica B* **173**, 43-46 (1991).
3. Composto, R. J., Walters, R. M. & Genzer, J. Application of ion scattering techniques to characterize polymer surfaces and interfaces. *Mater. Sci. Eng., R* **38**, 107-180 (2002).
4. Schwarz, S. A. et al. Studies of Surface and Interface Segregation in Polymer Blends by Secondary ion Mass-Spectrometry. *Mol. Phys.* **76**, 937-950 (1992).
5. Harton, S. E., Stevie, F. A. & Ade, H. SIMS Depth Profiling of Amorphous Polymer Multilayers using O2+ and Cs+ Ion Bombardment with a Magnetic Sector Instrument. *J. Vac. Sci. Technol., B* **(in submission)** (2005).
6. Russell, T. P. Changes in Polystyrene and Poly(methyl methacrylate) Interactions with Isotopic Substitution. *Macromolecules* **26**, 5819 (1993).
7. Bates, F. S., Muthukumar, M., Wignall, G. D. & Fetters, L. J. Thermodynamics of Isotopic Polymer Mixtures - Significance of Local Structural Symmetry. *J. Chem. Phys.* **89**, 535-544 (1988).
8. Dudowicz, J., Freed, K. F. & Lifschitz, M. Towards a Molecular-Basis for Understanding the Behavior of Isotopic Polymer Blends - Lattice Cluster Theory Computations for Psd Psh Blends. *Macromolecules* **27**, 5387-5398 (1994).
9. Bates, F. S., Wignall, G. D. & Koehler, W. C. Critical-Behavior of Binary-Liquid Mixtures of Deuterated and Protonated Polymers. *Phys. Rev. Lett.* **55**, 2425-2428 (1985).
10. Bates, F. S. & Wignall, G. D. Nonideal Mixing in Binary Blends of Perdeuterated and Protonated Polystyrenes. *Macromolecules* **19**, 932-934 (1986).
11. Jones, R. A. L., Norton, L. J., Kramer, E. J., Bates, F. S. & Wiltzius, P. Surface-Directed Spinodal Decompositon. *Phys. Rev. Lett.* **66**, 1326-1329 (1991).
12. Jones, R. A. L., Kramer, E. J., Rafailovich, M. H., Sokolov, J. & Schwarz, S. A. Surface Enrichment in an Isotopic Polymer Blend. *Phys. Rev. Lett.* **62**, 280-283 (1989).
13. Hariharan, A. et al. The Effect of Finite Film Thickness on the Surface Segregation in Symmetrical Binary Polymer Mixtures. *J. Chem. Phys.* **99**, 656-663 (1993).
14. Genzer, J. & Composto, R. J. The Interface Between Immiscible Polymers Studied by Low-Energy Forward Recoil Spectrometry and Neutron Reflectivity. *Polymer* **40**, 4223-4228 (1999).
15. Coulon, G., Russell, T. P., Deline, V. R. & Green, P. F. Surface-Induced Orientation of Symmetric, Diblock Copolymers: A Secondary Ion Mass Spectrometry Study. *Macromolecules* **22**, 2581-2589 (1989).
16. Sferrazza, M. et al. Evidence for Capillary Waves at Immiscible Polymer/Polymer Interfaces. *Phys. Rev. Lett.* **78**, 3693-3696 (1997).

17. Harton, S. E., Stevie, F. A. & Ade, H. Diffusion-Controlled Reactive Coupling at Polymer-Polymer Interfaces. *Macromolecules* **38**, 3543-3546 (2005).
18. Fleer, G. J., Stuart, M. A. C., Scheutjens, J. M. H. M., Cosgrove, T. & Vincent, B. *Polymers at Interfaces* (Chapman & Hall, New York, 1993).
19. Hariharan, A., Kumar, S. K. & Russell, T. P. Surface Segregation in Binary Polymer Mixtures - a Lattice Model. *Macromolecules* **24**, 4909-4917 (1991).
20. Hariharan, A., Kumar, S. K. & Russell, T. P. Reversal of the Isotopic Effect in the Surface Behavior of Binary Polymer Blends. *J. Chem. Phys.* **98**, 4163-4173 (1993).
21. Shin, K. et al. Silicon Oxide Surface as a Substrate of Polymer Thin Films. *Macromolecules* **34**, 4993-4998 (2001).
22. Wilson, R. G., Stevie, F. A. & Magee, C. W. *Secondary Ion Mass Spectrometry: A Practical Handbook for Depth Profiling and Bulk Impurity Analysis* (John Wiley & Sons, New York, 1989).
23. Zhao, X. et al. Determination of the Concentration Profile at the Surface of d-PS/ h-PS Blends Using High-Resolution Ion-Scattering. *Macromolecules* **24**, 5991-5996 (1991).
24. Harton, S. E., Stevie, F. A. & Ade, H. SIMS Depth Profiling of Deuterium Labeled Polymers in Polymer Multilayers. *Appl. Surf. Sci.*, (in press) (2006).
25. Chia, V. K. F., Mount, G. R., Edgell, M. J. & Magee, C. W. Recent advances in secondary ion mass spectrometry to characterize ultralow energy ion implants. *J. Vac. Sci. Technol. B* **17**, 2345-2351 (1999).
26. Kramer, E. J. Depth profiling methods that provide information complementary to neutron reflectivity. *Physica B* **173**, 189-198 (1991).
27. Coleman, M. M., Narvett, L. A. & Painter, P. C. A counterintuitive observation concerning hydrogen bonding in polymer blends. *Polymer* **39**, 5867-5869 (1998).
28. Quirk, R. P., Yin, J. & Fetters, L. J. Carbonation and Related Reactions of Poly(Styryl)Lithium. *Macromolecules* **22**, 85-90 (1989).
29. Pavlinec, J. & Lazar, M. Cross-linking of poly(methyl methacrylate) by aminolysis of ester functions with diamines. *J. Appl. Polym. Sci.* **55**, 39-45 (1995).
30. Helfand, E. & Tagami, Y. Theory of the Interface Between Immiscible Polymers. *J. Polym. Sci., Part B: Polym. Phys.* **9**, 741 (1971).
31. Flory, P. J. *Principles of Polymer Chemistry* (Cornell University Press, Ithaca, NY, 1953).
32. Geoghegan, M., Nicolai, T., Penfold, J. & Jones, R. A. L. Kinetics of Surface Segregation and the Approach to Wetting in an Isotopic Polymer Blend. *Macromolecules* **30**, 4220-4227 (1997).
33. Callaghan, T. A. & Paul, D. R. Interaction Energies for Blends of Poly(methyl methacrylate), Polystyrene, and Poly(a-methylstyrene) by the Critical Molecular Weight Method. *Macromolecules* **26**, 2439-2450 (1993).
34. Postawa, Z., Czerwinski, B., Winograd, N. & Garrison, B. J. Microscopic insights into the sputtering of thin organic films on Ag{111} induced by C-60 and Ga bombardment. *J. Phys. Chem. B* **109**, 11973-11979 (2005).

35. Russell, T. P., Karim, A., Mansour, A. & Felcher, G. P. Specular Reflectivity of Neutrons by Thin Polymer-Films. *Macromolecules* **21**, 1890-1893 (1988).
36. Reynolds, B. J., Ruegg, M. L., Mates, T. E., Radke, C. J. & Balsara, N. P. Experimental and Theoretical Study of the Adsorption of a Diblock Copolymer to Interfaces between Two Homopolymers. *Macromolecules* **38**, 3872-3882 (2005).
37. Antonietti, M., Coutandin, J. & Sillescu, H. Chainlength and temperature dependence of self-diffusion coefficients in polystyrene. *Makromol. Chem., Rapid Commun.* **5**, 525-528 (1984).
38. Crank, J. *The Mathematics of Diffusion* (Oxford University Press, New York, 1975).
39. Russell, T. P., Hjelm, R. P. & Seeger, P. A. Temperature-Dependence of the Interaction Parameter of Polystyrene and Poly(Methyl Methacrylate). *Macromolecules* **23**, 890-893 (1990).
40. Wu, S. Surface and Interfacial Tensions of Polymer Melts. II. Poly(methyl methacrylate), Poly(n-butyl methacrylate), and Polystyrene. *J. Phys. Chem* **74**, 632-638 (1970).
41. Carriere, C. J., Biresaw, G. & Sammler, R. L. Temperature dependence of the interfacial tension of PS/PMMA, PS/PE, and PMMA/PE blends. *Rheol. Acta* **39**, 476-482 (2000).
42. Sanchez, I. C. & Lacombe, R. H. Statistical Thermodynamics of Polymer Solutions. *Macromolecules* **11**, 1145-1156 (1978).
43. Hariharan, A., Kumar, S. K. & Russell, T. P. Free Surfaces of Polymer Blends .1. Theoretical Framework and Application to Symmetrical Polymer Blends. *J. Chem. Phys.* **98**, 6516-6525 (1993).
44. Hariharan, A., Kumar, S. K. & Russell, T. P. Free Surfaces of Polymer Blends .2. Effects of Molecular-Weight and Applications to Asymmetric Polymer Blends. *J. Chem. Phys.* **99**, 4041-4050 (1993).

Polymer	T_g/°C	Supplier	M_w/kDa	M_w/M_n
dPS-130	97	PolS	140	1.07
dPS-70	97	PolS	82.8	1.15
hPS-130	96	PolS	138	1.05
hPS-70	96	PolS	73.0	1.04
hPMMA	127	PolS	155	1.05
hP2VP	98	SPP	514	1.08
dPS-OH	97	PolS	76.6	1.05

Table 4.1. Polymers used in this investigation.

System	PS Layer	h_{PS}/nm	Bottom Layer
A	5 % dPS-130 + 95 % hPS-130	255	hPMMA
B	5 % dPS-130 + 95 % hPS-130	230	hPMMA
C	10 % dPS-130 + 90 % hPS-130	250	hPMMA
D	20 % dPS-130 + 80 % hPS-130	240	hPMMA
E	30 % dPS-130 + 70 % hPS-130	225	hPMMA
F	10 % dPS-70 + 90 % hPS-70	210	hPMMA
G	10 % dPS-OH + 90 % hPS-70	170	hP2VP
H	100 % dPS-130	100	hPMMA

Table 4.2. Sample properties for various systems employed. For Systems *A*-*G* the bottom layer (hPMMA or hP2VP) was ≈ 200 nm, while the hPMMA layer thickness was 100 nm for System *H*. Concentrations (% v/v) are based on volume fraction at t = 0.

Polymer Pair	χ (T)
hPS/hPMMA	$3.20/T + 0.021$
dPS/hPMMA	$3.902/T + 0.0284$
hPS/dPMMA	$3.188/T + 0.0292$
dPS/dPMMA	$3.199/T + 0.0251$

Table 4.3. Values of χ for PS/PMMA as a function of isotopic labeling as previously reported in Ref (6). Note that χ for dPS/hPMMA, hPS/dPMMA, and dPS/dPMMA were measured with block copolymers using SANS in Refs (6) and (39), and χ for hPS/hPMMA originated from cloud point measurements of homopolymers in Ref (33).

T/°C	$D^o/(nm^2/s)$	τ_D/h	$\tau_D/\tau_{D,138}$
138	0.26	16.7	1.00
148	1.22	3.5	0.21
158	4.86	0.89	0.05
166	13.3	0.33	0.02

Table 4.4. Tracer diffusion coefficients (D^o) for dPS-130 from Ref (37) and characteristic diffusion times ($\tau_D = L^2/4D^o$, where L is the PS layer thickness) for dPS-130. A constant L = 250 nm was assumed.

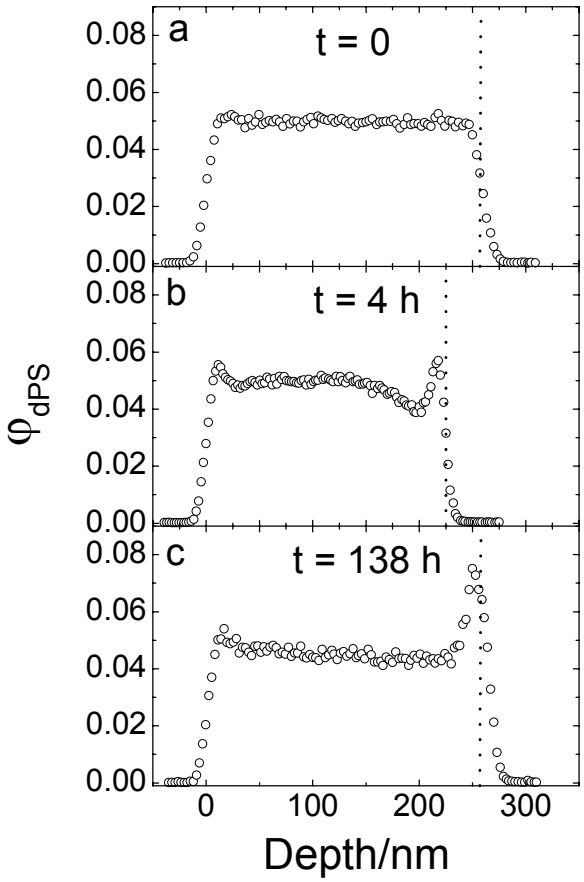

Figure 4.1. SIMS profiles for the dPS-130 volume fraction (φ_{dPS}) as a function of depth after annealing at 128 °C for (a) 0 (System *A,* 255 nm thick), (b) 4 h (System *B,* 230 nm thick), and (c) 138 h (System *A,* 255 nm thick). A clear depletion hole with a corresponding interfacial excess is apparent near the dPS:hPS/PMMA interface after 4 h (b). A large segregated amount of dPS-130 is present after 138 h (c). The interfaces are marked here and in similar subsequent figures by a line as a quide to where the (dPS:hPS)/PMMA interface is. Due to the depletion hole in (b), the exact location can not be established readily.

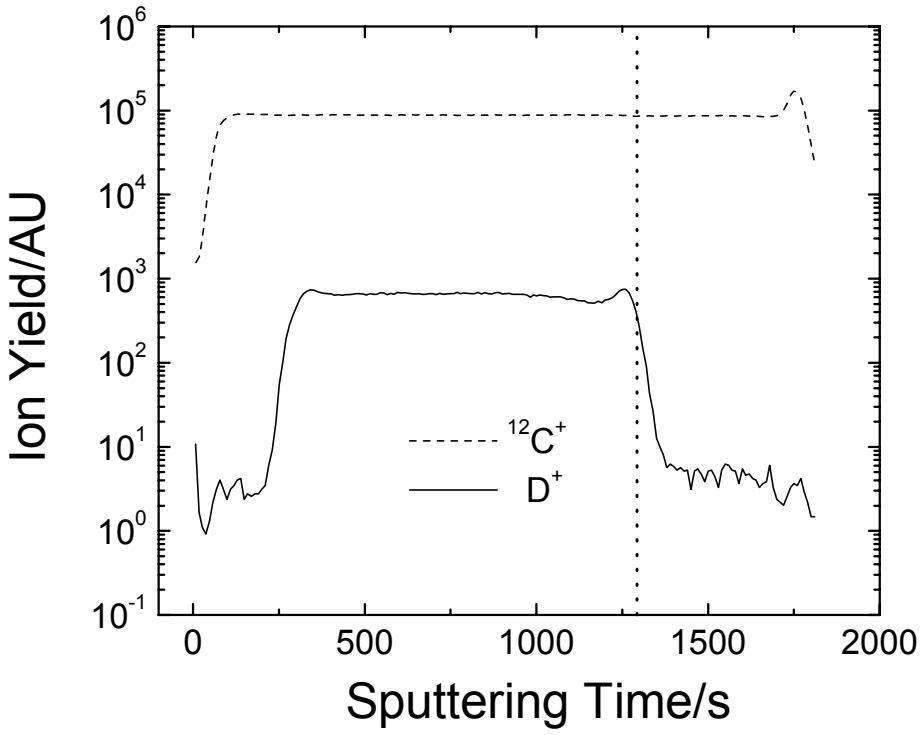

Figure 4.2. Raw SIMS profiles (i.e., secondary ion yield as a function of sputtering time) for D^+ and the $^{12}C^+$ matrix after 4 h at 128 °C (System *B*). A constant $^{12}C^+$ secondary ion yield is observed through the hPS:dPS/hPMMA interface (vertical line), clearly demonstrating that the profiles shown in Figure 4.1 are not analysis artifacts.

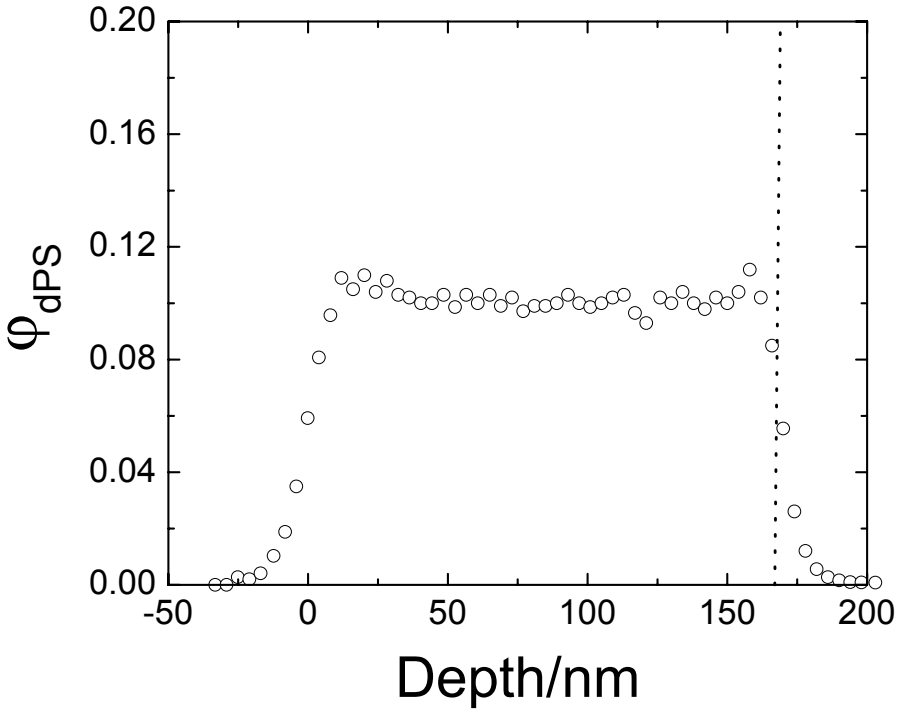

Figure 4.3. SIMS depth profile of System *G* after 96 h at 130 °C. Because an –OH group, such as that at the end of the dPS-OH is known to hydrogen bond with P2VP much more strongly than with PMMA the negligible dPS-OH excess at the hPS:dPS-OH/P2VP interface (vertical line) further supports that unwanted end-functional groups on the dPS-130 are not the underlying cause of the dPS segregation shown in Figure 1.

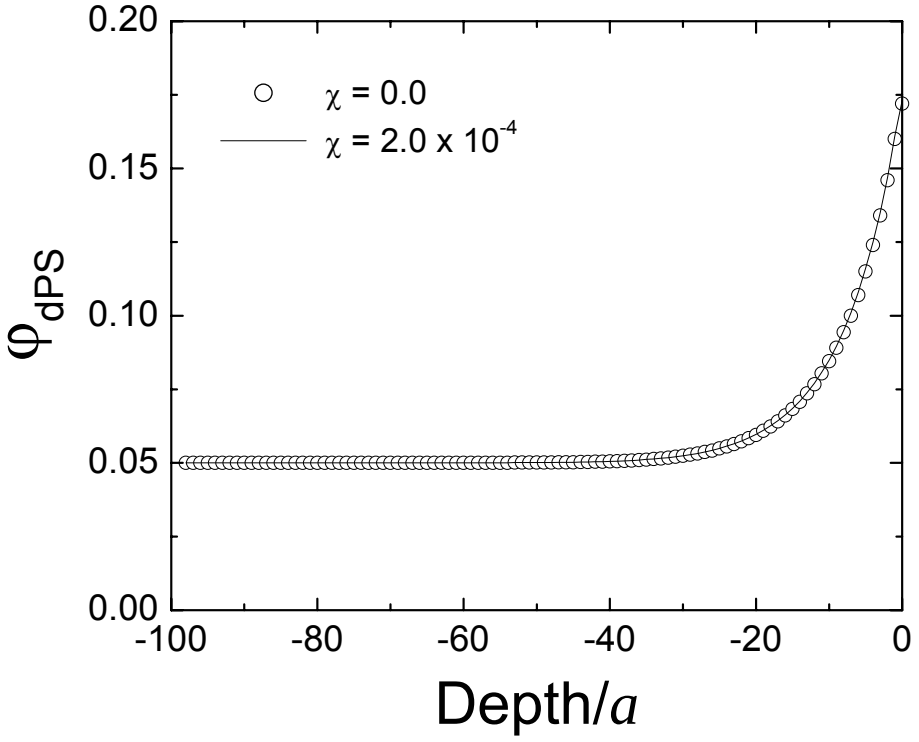

Figure 4.4. SCMF-L results for $N_{dPS} = N_{hPS} = 1200$, $\Delta\chi_p = 0.01$, and χ for hPS:dPS = 0.0 (○), and 2.0 x 10^{-4} (solid line). The interface is set to 0, and the depth is scaled to the statistical segment length (a) of hPS and dPS. At these molecular weights, the hPS:dPS interaction is completely negligible.

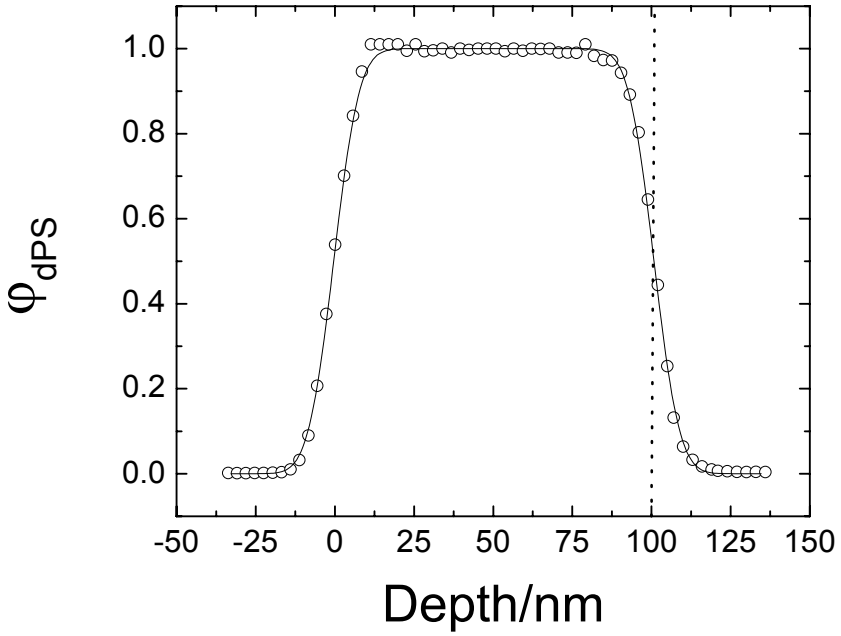

Figure 4.5. SIMS depth profile of System *H* (100 % dPS-130), which was used to quantify the depth resolution. From a Gaussian convoluted step function (error function) the effective depth resolution was determined to be 15 nm (FWHM).

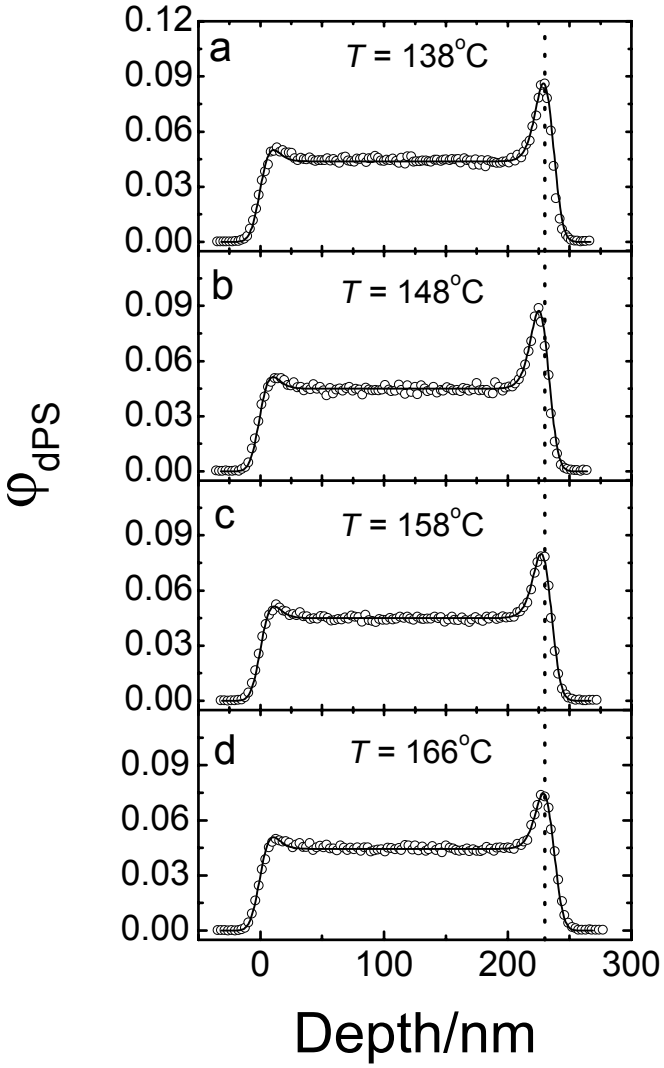

Figure 4.6. SIMS depth profiles for 5% (v/v) initial dPS-130 concentration (○) compared to convoluted theoretical profiles generated using SCMF-L (solid lines) for System *B* after (a) 160 h at 138 °C, (b) 73 h at 148 °C, (c) 53 h at 158 °C, and (d) 41 h at 166 °C. The values of $\Delta\chi_p$ were determined by fitting theoretical profiles to the experimental profiles at each temperature. The PS/PMMA interface is shown with the vertical line.

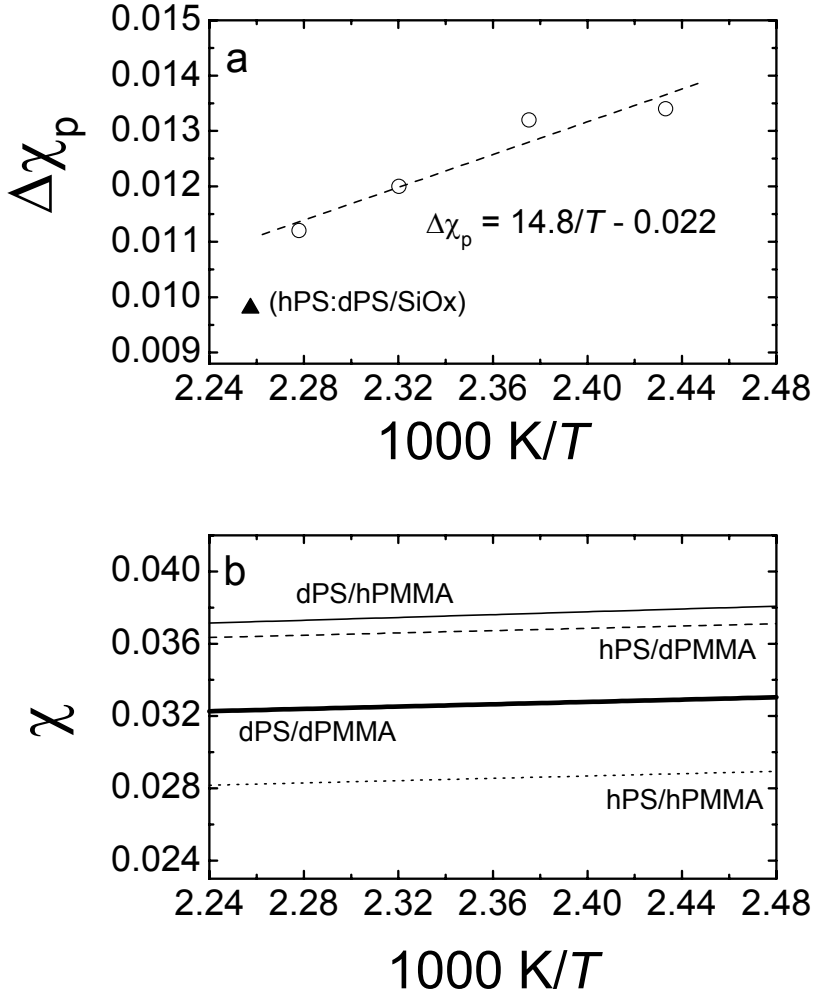

Figure 4.7. A comparison of (a) values of $\Delta\chi_p$ determined from Figure 6 (○) with the linear regression (dashed line), and (b) χ reported in Ref (6) for dPS/hPMMA (solid line), hPS/dPMMA (dashed line), dPS/dPMMA (bold line), and hPS/hPMMA (dotted line) (see Table 3). The temperature dependency for (a) $\Delta\chi_p$ is a factor of 3-4 greater than those for (b) χ. Also shown in (a) is the value for $\Delta\chi_s$ for hPS:dPS/SiOx at 170 °C (▲) from ref 13.

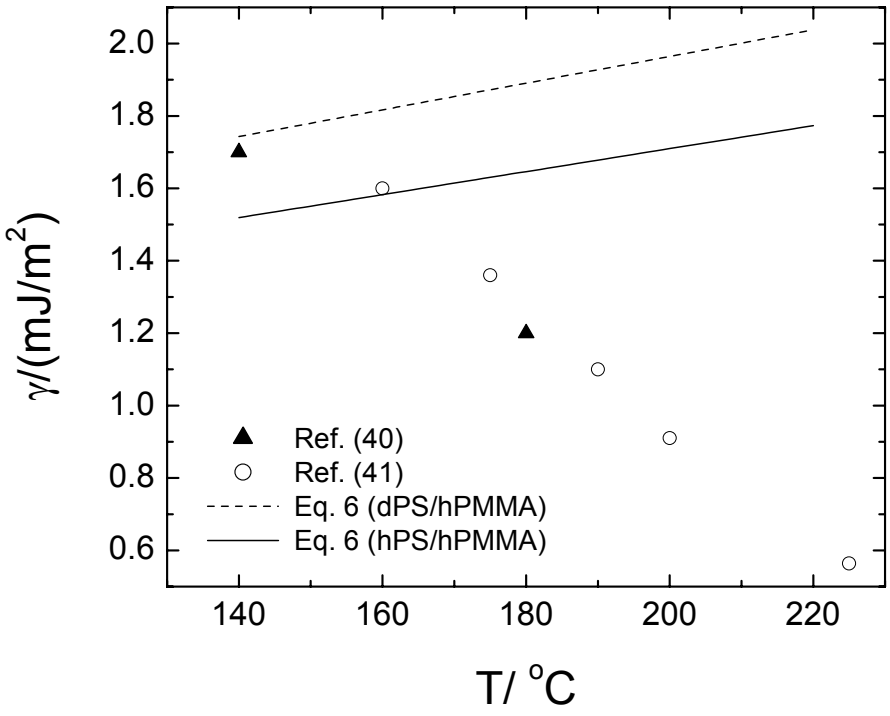

Figure 4.8. Interfacial tension (γ) measurements for hPS/hPMMA from Refs (▲) (40) and (○) (41) as compared to values predicted by mean-field theory (eq 6) using values of χ for (dashed line) dPS/hPMMA and (solid line) hPS/hPMMA from ref 6.

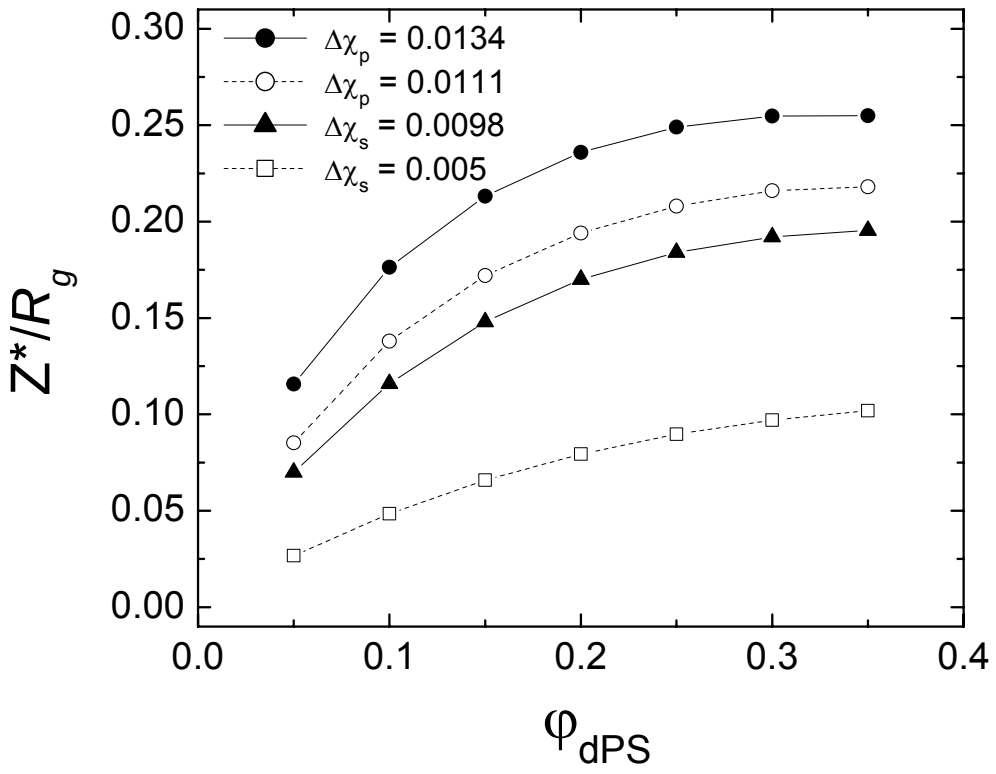

Figure 4.9. A comparison of normalized interfacial excess (Z^*/R_g), calculated from SCMF-L and Equation 7 and scaled to the dPS-130 R_g (≈ 9.5 nm), as a function of dPS concentration for (●) $\Delta\chi_p$ = 0.0134 (hPS:dPS/hPMMA interface at 138 °C), (○) $\Delta\chi_p$ = 0.0111 (extrapolation from Figure 7) (hPS:dPS/hPMMA interface at 170 °C), (▲) $\Delta\chi_s$ = 0.0098 (hPS:dPS/SiOx interface at 170 °C), and (□) $\Delta\chi_s$ = 0.005 (hPS:dPS surface at 160 °C). Lines are a guide for the eye. Clearly, dPS segregates much more strongly to an hPS:dPS/hPMMA interface than an hPS:dPS/SiOx interface or an hPS:dPS surface.

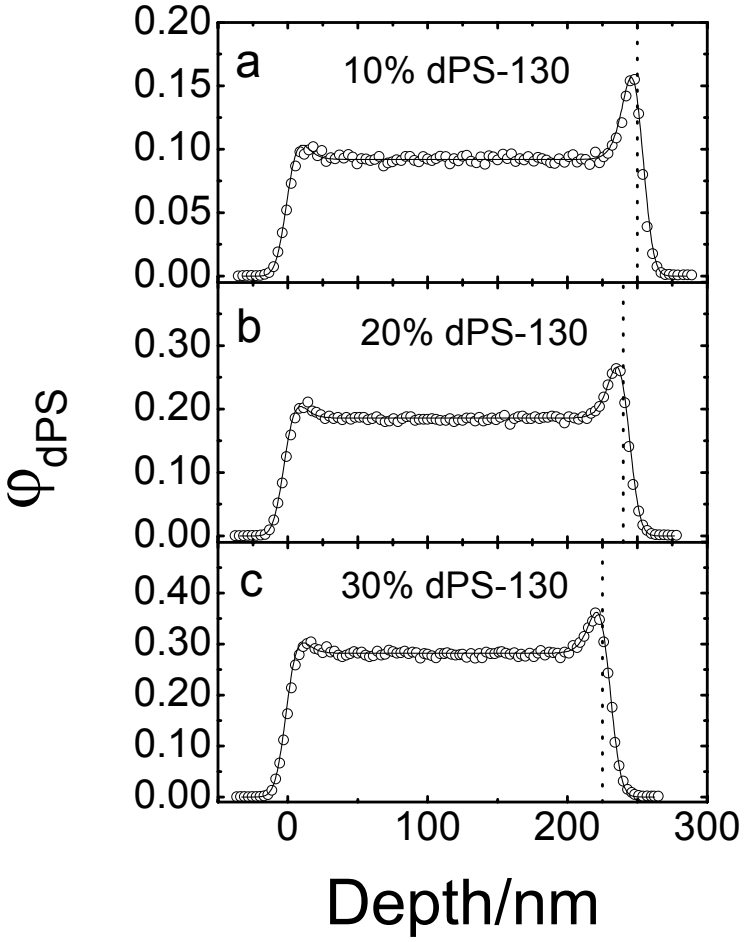

Figure 4.10. SIMS depth profiles (○) for dPS-130 segregation after 94 h at 138 °C for initial concentrations of (a) 10% dPS (System *C*) (b) 20% dPS (System *D*), and (c) 30% dPS (System *E*). The PS/PMMA interface is shown with the vertical line. The convoluted theoretical profiles (solid line) were generated using a constant value of $\Delta\chi_p$ = 0.0134. Excellent agreement is found with a constant $\Delta\chi_p$ over this concentration range for dPS-130 segregation at 138 °C.

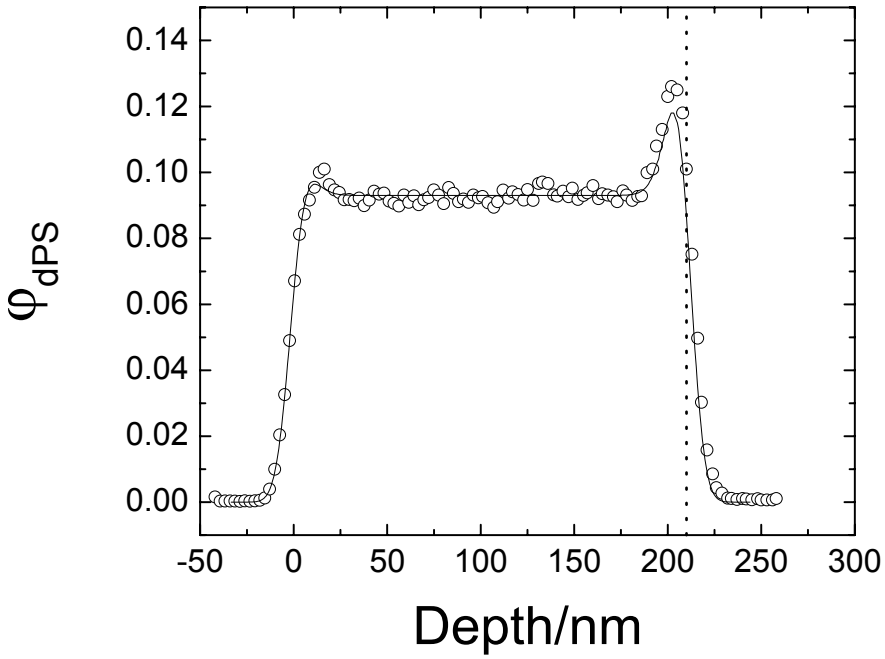

Figure 4.11. SIMS depth profile (○) for dPS-70 segregation after 94 h at 138 °C for an initial concentration of 10% dPS (System *F*). The PS/PMMA interface is shown with the vertical line. The convoluted theoretical profile (solid line) was generated using a value of $\Delta\chi_p = 0.0134$, which was measured with System *B* (dPS-130) at this temperature. The SCMF-L theory does not appear to accurately predict the changes in dPS segregation as a function of molecular weight with a constant $\Delta\chi_p$. A $\Delta\chi_p \approx 0.016$ would be required to represent the profile shown here.

5. CARBON-13 LABELED POLYMERS FOR DEPTH PROFILING OF POLYMER FILMS AND MULTILAYERS USING SIMS

5.1. Introduction

Advances in one-dimensional depth profiling of polymer films have provided a significant driving force for growth in experimental and theoretical polymer physics over the past 20 years.[1] Particularly useful for investigations involving thin films (< 1 μm), these measurements generally focus on probing various physical phenomena related to two-dimensional confinement of polymer chains, including segregation phenomena[2] and diffusion properties near surfaces and heterogeneous interfaces.[3] Several experimental techniques have been used for depth profiling of polymer films and multilayers,[1] including neutron, X-ray, or resonant X-ray reflectometry (NR, XR, or RXR, respectively),[4,5] Rutherford backscattering (RBS),[6] forward recoil spectrometry (FRES),[7] nuclear reaction analysis (NRA),[8] and secondary ion mass spectrometry (SIMS).[9,10] These techniques are frequently used to probe the concentration of a labeled polymer, often deuterium (^{2}H) substituted,[1] as a function of depth to observe various phenomena, including reactive coupling at polymer interfaces,[11,12] polymer chain mobility near surfaces and interfaces,[13,14] surface or interfacial segregation,[15,16] and block copolymer ordering.[17,18] Even though deuterium substitution has led to many advances, it can affect the phase behavior of the polymer constituents with reported changes in both bulk phase behavior (see Figure 5.1)[19,20] and surface and interfacial interactions.[2,15] More recently, it was found that deuterium substitution can have a profound effect on the properties of a polymer/polymer heterogeneous interface, with the observation of diffusion-controlled

segregation of deuterium labeled polystyrene (dPS) to an hPS:dPS/poly(methyl methacrylate) (hPMMA) interface.[21,22] Because deuterium labeling can introduce changes in the properties being measured, alternative methods of tracer labeling are desired for optimal analysis.

Here, the use of ^{13}C labeling for depth profiling of polymer films and multilayers is demonstrated. Polystyrene (PS) was synthesized with ^{13}C labeled styrene monomer (^{13}C-PS) and analyzed in multilayers containing films of ^{13}C-PS or ^{13}C-PS/unlabeled PS (^{12}C-PS) blends. Using a CAMECA IMS-6f magnetic sector mass spectrometer, we were able to mass resolve $^{12}C^{1}H$ from ^{13}C with $m/\Delta m \approx 3000$. Two primary ions were investigated, O_2^+ and Cs^+, with detection of positive and negative secondary ions, respectively. It was found that Cs^+ provides considerably higher ^{12}C, ^{13}C, and $^{12}C^{1}H$ detection sensitivity than O_2^+ for the conditions implemented, but the interface between PS and poly(methyl methacrylate) (PMMA) is more susceptible to matrix effects with Cs^+ primary ion bombardment. Because a submatrix (^{13}C) is analyzed and can be normalized to the total carbon secondary ion yield ($^{12}C + {}^{13}C$) to convert the secondary ion yield to ^{13}C-PS concentration, a reduction in matrix effects encountered at the PS/PMMA interface can be realized. Mass spectra of ^{13}C-PS and ^{12}C-PS were measured using a PHI TRIFT I ToF mass spectrometer (static SIMS) with Ga^+ primary ion bombardment and detection of positive secondary ions. These results demonstrate the potential for future use of ToF SIMS for depth profiling high molecular weight (~ 100 amu) fragments of ^{13}C labeled polymers. ^{13}C labeling of polymers should thus be a very beneficial approach for analysis using ToF or magnetic sector SIMS, and the ^{13}C labeling

method presented here should be applicable for analysis of various soft condensed matter systems in fields ranging from polymer science to biology.

5.2. Experimental

5.2.1. Polymer Synthesis

^{13}C-PS, ^{12}C-PS, and PMMA were synthesized using atom transfer radical polymerization (ATRP).[23] The chemical structures of PS and PMMA are shown in Figure 5.2. The polymerization mechanisms and procedures have been described in detail previously,[24] and will only be briefly outlined here. Before the synthesis was performed, copper(I) bromide (98% CuBr, Sigma-Aldrich) was purified according to established procedures.[25] Initiator, ligand, and solvent were used as received. For synthesis of atactic ^{13}C-PS, 2 mL unlabeled styrene (99%, Sigma-Aldrich) and 1 mL α,β-^{13}C labeled styrene monomer (99%, Isotec) were put through a neutral activated alumina column. Into a 10 mL Schlenk flask, 10.5 mg CuBr, 16 μL *N,N,N',N'',N''*-pentamethyldiethylenetriamine (99% PMDETA, Sigma-Aldrich), and monomer were added. The flask was sealed with a rubber septum, and the solution was bubbled with N_2 for 20 min. to remove O_2. Next, 4.2 μL of 1-bromoethylbenzene (97% BrEb, Sigma-Aldrich) was injected into the solution, and the flask was immersed in an oil bath held at 110 °C and its content continuously stirred using a magnetic stir bar. After 7.5 h, the reaction was stopped (~ 75% monomer conversion), and the solution was diluted with tetrahydrofuran (THF, Acros) and run through a neutral activated alumina column to remove the CuBr. This solution was precipitated into 1 L of methanol (MeOH, Fisher), filtered, and dried overnight at 70 °C. For atactic ^{12}C-PS synthesis, 50 mL styrene, which

had been put through a neutral activated alumina column, 144 mg CuBr, and 210 mL PMDETA were added to a 100 mL round-bottom flask. The flask was sealed with a rubber septum, bubbled with N_2 for 25 min, and 70 μL BrEb was injected into the solution. The solution and flask was immersed in an oil bath held at 110 °C with continuous stirring. After 6.5 h, the reaction was stopped and the solution was diluted with THF and run through a neutral activated alumina column. This solution was precipitated into 2 L of MeOH, filtered, and dried overnight at 70 °C. The molecular weights and polydispersities of ^{12}C-PS and ^{13}C-PS were measured using gel permeation chromatography (GPC) with a chloroform ($CHCl_3$) diluent at 30 °C, after calibration with atactic PS standards (Polymer Laboratories). Using differential scanning calorimetry (DSC), with a cooling cycle of 10 °C/min, the inflection-point glass transition temperatures (T_g's) were determined to be 100 °C for both ^{12}C-PS and ^{13}C-PS.

For synthesis of PMMA, methyl methacrylate (> 99%, Fluka) was put through a basic activated alumina column. To a 125 mL round-bottom flask, 30 mL monomer, 30 mL phenyl ether (99%, Acros), 43 mg CuBr, and 63 μL PMDETA were added. The flask was sealed with a rubber septum and bubbled with N_2 for 30 min. The flask was then immersed in an oil bath held at 90 °C, its content continuously stirred using a magnetic stir bar, and 42 μL of ethyl 2-bromoisobutyrate (98%, Sigma-Aldrich) was injected. The reaction was stopped after 4 h, and the solution was diluted with THF and run through an activated neutral alumina column. The solution was then precipitated into 2 L of hexanes (Fisher), filtered, and dried overnight at 70 °C. Using DSC, the T_g was determined to be 100 °C (10 °C/min cooling cycle), implying a somewhat random

monomeric sequence distribution (atactic PMMA).[26] This was further confirmed using proton nuclear magnetic resonance spectroscopy[27,28] (^{1}H NMR, Varian Mercury 400 MHz) in deuterium labeled chloroform (99.8%, Aldrich) which shows 4 % isotactic, 38 % heterotactic, and 58 % syndiotactic triad distributions (*mm*, *mr*, and *rr*, respectively). PMMA tacticity is highly sensitive to the choice of polymerization technique (i.e., radical or anionic) and conditions (i.e., temperature, solvent, and initiator).[28] The molecular weight and polydispersity were measured using GPC with a $CHCl_3$ diluent at 30 °C, after calibration with atactic PS standards, and converted to corrected values for atactic PMMA using the universal calibration principle[29] with known Mark-Houwink parameters for atactic PS ($K = 4.9 \times 10^{-3}$ mL/g; $a = 0.794$) and atactic PMMA ($K = 4.3 \times 10^{-3}$ mL/g; $a = 0.80$).[30] The characteristics of the polymers utilized are summarized in Table 5.1.

5.2.2. Sample Preparation

Six solutions (summarized in Table 5.2) were prepared for six different sample types. First, HPLC grade benzene (Aldrich) was distilled over calcium hydride and stored under N_2. Toluene (Fisher), 1-chloropentane (Sigma-Aldrich), and HPLC grade n-heptane (Aldrich) were used as received. Silicon (100) wafers were cut to 2.5 cm x 2.5 cm squares and soaked in BakerClean JTB-111 (J.T. Baker) for 30 min and subsequently washed with deionized (DI) water. They were then etched in 10 % (v/v) aqueous hydrofluoric acid, washed with DI water, and placed in a UV-ozone oven for 30 min to build a SiO_x layer (≈ 2 nm) on the hydrogen-passivated Si surface. Samples prepared for dynamic SIMS (depth profiling) were all spin-cast at 3000 rpm (samples A-D). For samples C and D, solution 4 was cast and annealed for 30 min at 125 °C. Solution 3 was

then cast directly onto the PMMA layer, as 1-chloropentane is a selective solvent for PS over PMMA. For samples A-C the bottom layer(s) were annealed at 125 °C for 24 h, and then the top ^{12}C-PS layer was cast onto the Si + SiO_x substrates, scored with a sharp tip, floated into DI water, and picked-up with the bottom layer(s). These polymer film assemblies were then annealed at 80 °C for 12 h to remove residual solvent while preventing interdiffusion.[31] For sample D the bottom layers were annealed at 125 °C for 24 h, and the top PMMA layer was cast onto a microscope cover glass, scored with a sharp tip, floated into water, and picked-up with the bottom layers. This polymer film assembly was annealed at 125 °C for 3 h. Samples for ToF SIMS analysis (samples E and F) were prepared using a procedure that was outlined previously.[32] ^{13}C-PS (solution 5) and ^{12}C-PS (solution 6) were spin-cast at 5000 rpm onto individual substrates and annealed on a hot plate, which had been cleaned with n-heptane, for 5 min at 100 °C to remove residual solvent. The samples were then washed with n-heptane to remove any potential surface contaminants, such as poly(dimethyl siloxane). All layer thicknesses were measured individually using single wavelength ellipsometry (Rudolph Auto El III). Properties of all six sample types (samples A-F) are summarized in Table 5.3.

5.2.3. Secondary Ion Mass Spectrometry

All depth profiles were performed using a CAMECA IMS-6f magnetic sector mass spectrometer. A 20 nm Au coating was sputtered onto samples A-D before the SIMS analysis to help minimize charging (passive charge neutralization). Typical analysis conditions for O_2^+ primary ion bombardment included a 30 nA primary current rastered over a 180 μm x 180 μm area, with 5.5 keV impact energy (10 kV primary with

4.5 kV sample bias) and m/Δm = 3000. The angle of incidence for the primary ions was 41°. Transport of ions in matter (TRIM) simulations,[33] using the SRIM-2003 commercial software package, show a penetration depth $R_p \approx 10$ nm with a straggle $\Delta R_p \approx 5$ nm for O_2^+ implantation into PS and PMMA under these conditions. Positive secondary ions were detected from a 60 μm diameter optically gated area positioned in the center of the raster. For Cs^+, typical analysis conditions included a 10 nA primary current rastered over a 180 μm x 180 μm area, with 6.0 keV impact energy (5 kV primary with -1 kV sample bias) and m/Δm = 2910. The angle of incidence for the primary ions was 27°. TRIM simulations show $R_p \approx 17$ nm with $\Delta R_p \approx 3$ nm for Cs^+ implantation into PS and PMMA under these conditions. Negative secondary ions were detected from a 60 μm diameter optically gated area positioned in the center of the raster. For sample C, charge neutralization for Cs^+ bombardment with detection of negative secondary ions was evaluated using the so-called "electron cloud" method.[34] Electrons at normal incidence to the sample are provided with a potential just below that of the sample and are present just above the surface. In this self-compensating method, any charging due to ion bombardment of the surface of the sample is compensated by electrons that are drawn from the electron cloud. For 5 kV primary ions with a -1 kV sample bias, the typical electron coverage area is approximately 125 μm in diameter and an ion beam raster 110 μm x 110 μm was used for the analysis. At least two spots per sample were analyzed for samples A-D. ToF SIMS analyses (static SIMS) were performed using a PHI TRIFT I ToF mass spectrometer with 15 keV Ga^+ primary ion bombardment and detection of positive secondary ions. A 600 pA primary ion current was used over a 100 μm x 100

μm detection area with a 7.2 kV extraction voltage. Data acquisition time was set to 7 min, resulting in a total ion fluence of *ca*. 5 x 10^{11} ions/cm^2 per analysis. Mass spectra collected for three different spots for Samples E and F were analyzed using WinCadence software.

5.3. Results and Discussion

The sputtering rates S_R for PS and PMMA were determined for both 5.5 keV O_2^+ and 6.0 keV Cs^+ bombardment from the known thicknesses of the various layers for systems A-C as determined using ellipsometry. The rate approximations and averages are summarized in Table 5.4. The real space depth profiles of sample A, using the typical analysis conditions for Cs^+ and O_2^+ primary ion bombardment as described above, are shown in Figure 5.3. In Figures 5.3a and 5.3b, the $^{12}C^1H$ profile clearly traces the ^{12}C profile but not that of ^{13}C. This clearly establishes that $^{12}C^1H$ and ^{13}C have been completely mass resolved. High ^{13}C detection sensitivity for Cs^+ and O_2^+ bombardment is also revealed via the efficient detection of the ^{13}C background (natural abundance) in the top ^{12}C-PS layer. Figures 5.3c and 5.3d show the normalized profiles for the experimental volume fraction of ^{13}C-PS (φ) as a function of effective depth (z), based on the PS sputtering rates, as determined by:

$$\varphi(z) = \frac{Y_{13}(z) - Y_{NA}}{Y_P - Y_{NA}}, \qquad (1)$$

where $Y_{13}(z)$ is the ^{13}C ion yield, normalized to the total atomic C (^{12}C + ^{13}C) ion yield, at depth z, Y_{NA} is the normalized ^{13}C ion yield of pure ^{12}C-PS (natural abundance), and Y_P is the normalized ^{13}C ion yield of pure ^{13}C-PS. Under the conditions implemented here for

both O_2^+ and Cs^+ bombardment, excellent signal-to-noise (S/N) is observed in the profiles in Figures 5.3c and 5.3d, even though there is only 10.3 % ^{13}C in the ^{13}C-PS (relative to $^{12}C + {}^{13}C$), as determined using ToF SIMS (see below).

The experimental profiles shown in Figures 5.3c and 5.3d for 6.0 keV Cs^+ and 5.5 keV O_2^+ reveal asymmetric profiles through the ^{12}C-PS/^{13}C-PS interface for both ion probes. The experimental widths corresponding to 84/16 ($\Delta_{84/16}$), 50/16 ($\delta_{50/16}$), and 84/50 ($\delta_{84/50}$) intensity changes are tabulated in Table 5.5. The differences between the $\delta_{50/16}$ and $\delta_{84/50}$ values are a measure of the asymmetry. Furthermore, the 84/16 depth resolution for 6.0 keV Cs^+ is better than that with 5.5 keV O_2^+ primary ion bombardment ($\Delta_{84/16}$ = 14 and 19 nm, respectively), which is consistent with previous observations.[35,36]

The profile lineshapes and nearly a factor of two difference between $\delta_{50/16}$ and $\delta_{84/50}$ observed through the ^{12}C-PS/^{13}C-PS interface clearly demonstrate that these profiles cannot be accurately represented by a symmetric Gaussian instrument resolution convoluted with a sharp intrinsic profile. The observed convolution-type arises primarily from ion-induced mixing of the ^{13}C and ^{12}C matrix and implantation of the ^{13}C further into the film (tailing).[37] Analogous behavior has been observed for ^{30}Si implants in a ^{28}Si matrix.[37] A physically meaningful convolution function is required in order to compare SIMS depth profiles to various theoretical models when probing physical phenomena at polymer surfaces and heterogeneous interfaces.[16,21] Here we employ a simplified version of a convolution scheme that has been outlined previously.[37,38] It combines a Gaussian with a FWHM Δ_{eff} that accounts for ion-induced mixing and other sources of uncorrelated convolution, such as sample roughness and intrinsic interfacial width,[16,17]

and an exponential for the observed tailing, which has a characteristic decay length λ_d. The Gaussian convolution function is

$$G(z) = \frac{2}{\Delta_{eff}}\left(\frac{\ln 2}{\pi}\right)^{1/2} \exp\left[-4\ln 2\left(\frac{z}{\Delta_{eff}}\right)^2\right]; z \rightarrow (-\infty,\infty), \quad (2)$$

and the exponential decay is described by

$$F(z) = \frac{1}{\lambda_d}\exp\left(-\frac{z}{\lambda_d}\right); z \rightarrow (0,\infty). \quad (3)$$

$G(z)$ and $F(z)$ are numerically convoluted, using the Fourier transform method,[39] with a Heaviside step function $\theta(z)$,[16] where

$$\theta(z) = 0\ (-\infty\ ,\ z_I) \text{ and } \theta(z) = 1\ (z_I\ ,\ \infty), \quad (4)$$

to approximate the experimental profiles. These convoluted profiles are fit to the data with Δ_{eff} and λ_d as regression parameters. Results for 6.0 keV Cs^+ and 5.5 keV O_2^+ primary ion bombardment are summarized in Table 5.5. The best fit lineshapes are also plotted as solid lines in the graphs shown in Figures 5.3c and 5.3d, clearly indicating that the combination of a Gaussian and exponential decay function yields excellent results. The effective location of the interface z_I was determined by the fit. Although an attempt has been made to put physical meaning into the functionalization of the profiles shown in Figures 5.3c and 5.3d, molecular level complexities inherent to SIMS analysis of polymer films[40,41] make further interpretation of the regressed parameters Δ_{eff} and λ_d extremely difficult.

The detection sensitivity and S/N were further evaluated using sample B, which contains a layer of 5% (v/v) ^{13}C-PS + ^{12}C-PS and a top layer of 100 % ^{12}C-PS. Here, the

^{13}C-PS doped film only contains *ca.* 40% ^{13}C above the natural abundance background. Figure 5.4 shows the depth profiles analyzed using both 6.0 keV Cs^+ and 5.5 keV O_2^+ primary ion bombardment. Figures 5.4a and 5.4b show complete mass resolution of $^{12}C^1H$ from ^{13}C, and a marginal increase in ^{13}C secondary ion yield from the ^{12}C-PS top layer to the ^{13}C-PS doped layer. The normalized profiles in Figures 5.4c and 5.4c show decreased S/N compared to the profiles in Figures 5.3c and 5.3d. Furthermore, 6.0 keV (10 nA) Cs^+ provides higher detection sensitivity and S/N than 5.5 keV (30 nA) O_2^+ for ^{12}C, ^{13}C, and $^{12}C^1H$. It is well known that Cs^+ primary ion bombardment often provides improved detection sensitivity, depth resolution, and sputtering efficiency (see Table 5.4), all of which are observed here, for a variety of detected species and matrices when compared to O_2^+ under similar conditions.[35,40] Unfortunately, the use of Cs^+ has also been observed to produce somewhat anomalous secondary ion yields through a heterogeneous polymer/polymer interface, particularly with the PS/PMMA interface.[10] As shown in Figure 5.5 (sample C), there is quite a difference in secondary ion yields through the ^{13}C-PS:^{12}C-PS/PMMA interface for 6.0 keV Cs^+ (Figure 5.5a) that is absent for 5.5 keV O_2^+ (Figure 5.5b) primary ion bombardment.

Even though the anomalous ^{12}C secondary ion yield at the ^{13}C-PS:^{12}C-PS/PMMA interface is nearly independent of Cs^+ primary ion current (Figure 5.6), implying that sample charging is not the underlying cause of these non-monotonic changes in secondary ion yields through the interface, sample charging was explicitly ruled-out by evaluating ^{12}C secondary ion energy spectra at various locations through the film and through the use of active charge neutralization with the so-called "electron cloud"

method.[34] These energy spectra of a 3 nA Cs^+ primary ion beam rastered over a 110 μm x 110 μm area are shown in Figure 5.7 along with the approximate depth at which each spectrum was recorded (inset). No significant shift in the location of the ^{12}C yield maximum is observed, and a shift would be expected if sample charging occurred. Using Cs^+ primary beam and charge neutralization with the "electron cloud" method, depth profiles were generated and are shown in Figure 5.8. Again, similar to Fig. 5 and 6, the secondary ion yield through the PS/PMMA interface was non-monotonic, even though the sample has now been adequately charge compensated. This is significant for two very important reasons. First, the anomalous behavior observed with the secondary ion yields at the PS/PMMA interface (see Figure 5.5a) is clearly not due to sample charging. Second, this confirms that the "electron cloud" method of charge neutralization, which is completely unique to a magnetic sector SIMS instrument,[34] can be implemented during analysis of systems involving organic species without causing excess sample degradation, thereby permitting these types of analyses to include a broad range of polymer systems and sample thicknesses.

In an attempt to gain insight into the underlying mechanism behind the changes in secondary ion yields at the PS/PMMA interface, a trilayer consisting of PMMA as the top and bottom layer, with 5% (v/v) ^{13}C-PS + ^{12}C-PS in the middle layer (sample D), was assembled to look at the interface while sputtering through an interface from PMMA to PS and PS to PMMA. SIMS analysis was performed with a 3 nA (6.0 keV) Cs^+ primary ion bombardment rastered over a 180 μm x 180 μm area. Figure 5.9 clearly shows somewhat erratic changes in secondary ion yields through both interfaces, although the

behavior is quite different at each interface, almost the inverse of each other. A plot on a linear scale has also been provided in Figure 5.9b in order to highlight the changes in secondary ion yields at both PS/PMMA interfaces. A possible mechanism may be a loss of constant equilibrium primary ion concentration (transient sputtering) when sputtering through the heterogeneous PS/PMMA interfaces. This always occurs at the onset of dynamic SIMS analysis,[42] necessitating the addition of a sacrificial layer to the film or multilayer before the analysis, which is composed of a polymer identical to the top layer, if accurate profiling of the surface region is required.[9,10]

Further investigation into yield changes across interfaces will be necessary for a better understanding of this intriguing system. Fortunately, the method delineated here that relies on ^{13}C labeling might greatly help to alleviate nonmonotonic yield changes as ^{13}C secondary ion yields should be affected nearly identically to ^{12}C matrix ion yields through heterogeneous interfaces. Through normalization of the ^{13}C secondary ion yield to the total C (^{12}C + ^{13}C) ion yield (see Equation 1), changes such as those that occur through the PS/PMMA interface can be greatly minimized. The ^{13}C SIMS depth profile from Figure 5.5a is normalized is this way and shown in Figure 5.10. There is no readily observable artifact or segregation of ^{13}C-PS to the ^{13}C-PS:^{12}C-PS/PMMA interface. In contrast, prior results using an analogous hPS:dPS/PMMA system have shown strong segregation of 83 kDa dPS (^{13}C-PS used here is 79.4 kDa) to the heterogeneous interface at 138 °C[21,22] (Note: there is less than a 15 % change in the hPS:dPS phase diagram shown in Figure 5.1 from 125 to 138 °C[20]). Therefore, the use of ^{13}C labeling can greatly improve the characterization of polymer films and multilayers using SIMS and improve

the physical and theoretical interpretation of various experimentally observed phenomena at polymer/polymer heterogeneous interfaces, such as reactive coupling[11,12] and polymer chain mobility,[13,14] because the effects of tracer labeling on the properties of the system are greatly reduced.[22]

Finally, with the recent advances in the use of high molecular weight cluster probes for ToF SIMS analysis,[43,44] depth profiling of high molecular weight fragments (~ 100 amu) has become possible.[45-48] This may led to future use of ToF SIMS for high resolution depth profiling of ^{13}C labeled polymers. To evaluate this possibility, we have looked at the mass spectra of ^{13}C-PS and ^{12}C-PS (samples E and F, respectively) using a PHI TRIFT I ToF mass spectrometer with 15 keV Ga^+ primary ion bombardment and detection of positive secondary ions, as shown in Figure 5.11. Subtle differences can be found between the spectra of ^{12}C- PS (Figure 5.11a) and ^{13}C-PS (Figure 5.11b), but particular attention is paid to the intense peak for $^{12}C_7{}^1H_7$ (91.05474 amu) and its isotopically labeled analogs (Figures 5.11c and 5.11d). From Figure 5.11c, natural abundance of ^{13}C is determined from the peaks at 91 and 92 amu (nominal) for ^{12}C-PS, thereby demonstrating that there are no significant mass interferences for this fragment. This is quite significant, as every ^{13}C labeled monomer contains this fragment (see Figure 5.11d). This analysis also provides invaluable insight into the isotopic composition of the ^{13}C-PS used here, as the peak at 93 amu (nominal) in Figure 5.11d shows that the ^{13}C labeled monomer used in synthesis of the ^{13}C-PS has a slight enrichment of ^{13}C in the aromatic ring (see Figure 5.2), with approximately 50% over natural abundance. Depth profiling of high molecular weight fragments, such as C_7H_7, may be possible under

highly optimized conditions,[45,47] requiring low primary ion implant depths and efficient removal of damaged molecular layers.[49]

5.4. Conclusions

The use of ^{13}C labeling as an alternative to deuterium labeling for depth profiling of polymer films and multilayers using SIMS has been introduced. By minimizing the changes in bulk[19,20] and surface properties[2,15] of polymers and polymer blends due to isotopic labeling, significant improvements can now be obtained when probing various physical phenomena at polymer surfaces and heterogeneous interfaces.[21] In order to mass resolve $^{12}C^{1}H$ (13.00782 amu) from ^{13}C (13.00335 amu), which requires $m/\Delta m \approx 3000$, a magnetic sector mass spectrometer (CAMECA IMS-6f) was used with both 6.0 keV impact energy Cs^+ and 5.5 keV impact energy O_2^+ primary ions, with detection of negative and positive secondary ions, respectively. Complete mass resolution of $^{12}C^{1}H$ from ^{13}C was achieved for 6.0 keV Cs^+ and 5.5 keV O_2^+ primary ion bombardment in a ^{12}C-PS/^{13}C-PS bilayer film. This type of analysis cannot be performed with a quadrupole mass spectrometer, with a typical $m/\Delta m \sim 300$.[50] It was shown that the convolution of the depth profiles analyzed here have to be described by a combination of a Gaussian and an exponential function. The parameters derived from a fit to this combined convolution function have been summarized in Table 5.5 for both 6.0 keV Cs^+ and 5.5 keV O_2^+, thereby permitting future analyses to involve comparison of the SIMS profiles to various theoretical models.[16,21] It has also been shown that 6.0 keV Cs^+ provides improved detection sensitivity and signal-to-noise over 5.5 keV O_2^+ primary ion bombardment when depth profiling ^{13}C labeled polymers, although analysis using Cs^+ appears to be

much more susceptible to changes in secondary ion yields through a heterogeneous polymer/polymer interface such as the PS/PMMA interface.[10] Sample charging was conclusively ruled-out as the underlying cause of this behavior at the PS/PMMA interface. By using ^{13}C as a tracer, these matrix effects could be greatly reduced when depth profiling ^{12}C-PS:^{13}C-PS/PMMA multilayers, thereby proving that the use of this novel technique provides a true tracer for analysis of polymer systems. Finally, mass spectra of ^{13}C-PS and ^{12}C-PS were analyzed using ToF SIMS (15 keV Ga^+ with detection of positive secondary ions) with a PHI TRIFT I mass spectrometer to evaluate the potential use of ToF SIMS for depth profiling of relatively high molecular weight fragments (~ 100 amu) of ^{13}C-labeled polymers. The C_7H_7 secondary ions were found to have significant detection intensities with negligible mass interferences.

5.5. References

1. Kramer, E. J. Depth profiling methods that provide information complementary to neutron reflectivity. *Physica B* **173**, 189-198 (1991).
2. Jones, R. A. L., Kramer, E. J., Rafailovich, M. H., Sokolov, J. & Schwarz, S. A. Surface Enrichment in an Isotopic Polymer Blend. *Phys. Rev. Lett.* **62**, 280-283 (1989).
3. Zheng, X. et al. Long-Range Effects on Polymer Diffusion Induced by a Bounding Interface. *Phys. Rev. Lett.* **79**, 241-244 (1997).
4. Roe, R.-J. *Methods of X-Ray and Neutron Scattering in Polymer Science* (Oxford University Press, New York, 2000).
5. Wang, C., Araki, T. & Ade, H. Soft X-ray Resonant Reflectivity of low Z Material Thin Films. *Appl. Phys. Lett.* **87**, 214109 (2005).
6. Composto, R. J. & Kramer, E. J. Mutual Diffusion Studies of Polystyrene and Poly(Xylenyl Ether) Using Rutherford Backscattering Spectrometry. *J. Mater. Sci.* **26**, 2815-2822 (1991).
7. Composto, R. J., Walters, R. M. & Genzer, J. Application of ion scattering techniques to characterize polymer surfaces and interfaces. *Mater. Sci. Eng., R* **38**, 107-180 (2002).
8. Chaturvedi, U. K. et al. Structure at Polymer Interfaces Determined by High-Resolution Nuclear Reaction Analysis. *Appl. Phys. Lett.* **56**, 1228-1230 (1990).
9. Schwarz, S. A. et al. Studies of Surface and Interface Segregation in Polymer Blends by Secondary ion Mass-Spectrometry. *Mol. Phys.* **76**, 937-950 (1992).
10. Harton, S. E., Stevie, F. A. & Ade, H. SIMS Depth Profiling of Amorphous Polymer Multilayers using O2+ and Cs+ Ion Bombardment with a Magnetic Sector Instrument. *J. Vac. Sci. Technol., A*, (in press) (2006).
11. Kim, B. J. et al. Interfacial Roughening Induced by the Reaction of End-Functionalized Polymers at a PS/P2VP Interface: Quantitative Analysis by DSIMS. *Macromolecules* **38**, 6106-6114 (2005).
12. Harton, S. E. et al. Low-Temperature Reactive Coupling at Polymer-Polymer Interfaces Facilitated by Supercritical CO2. *Polymer* **46**, 10173-10179 (2005).
13. Russell, T. P. et al. Direct Observation of Reptation at Polymer Interfaces. *Nature* **365**, 235-237 (1993).
14. Zheng, X. et al. Reptation Dynamics of a Polymer Melt near an Attractive Solid Interface. *Phys. Rev. Lett.* **74**, 407-410 (1995).
15. Hariharan, A. et al. The Effect of Finite Film Thickness on the Surface Segregation in Symmetrical Binary Polymer Mixtures. *J. Chem. Phys.* **99**, 656-663 (1993).
16. Reynolds, B. J., Ruegg, M. L., Mates, T. E., Radke, C. J. & Balsara, N. P. Experimental and Theoretical Study of the Adsorption of a Diblock Copolymer to Interfaces between Two Homopolymers. *Macromolecules* **38**, 3872-3882 (2005).
17. Coulon, G., Russell, T. P., Deline, V. R. & Green, P. F. Surface-Induced Orientation of Symmetric, Diblock Copolymers: A Secondary Ion Mass Spectrometry Study. *Macromolecules* **22**, 2581-2589 (1989).

18. Anastasiadis, S. H., Russell, T. P., Satija, S. K. & Majkrzak, C. F. The Morphology of Symmetric Diblock Copolymers as Revealed by Neutron Reflectivity. *J. Chem. Phys.* **92**, 5677-5691 (1990).
19. Russell, T. P. Changes in Polystyrene and Poly(methyl methacrylate) Interactions with Isotopic Substitution. *Macromolecules* **26**, 5819 (1993).
20. Budkowski, A., Steiner, U., Klein, J. & Schatz, G. Coexistence in a Binary Isotopic Polymer Mixture. *Europhys. Lett.* **18**, 705-710 (1992).
21. Harton, S. E., Stevie, F. A. & Ade, H. Investigation of the Effects of Isotopic Labeling at a PS/PMMA Interface using SIMS and Mean-Field Theory. *Macromolecules*, (in press) (2006).
22. Harton, S. E., Stevie, F. A. & Ade, H. Carbon-13 Labeling for Tracer Depth Profiling of Polymer Films and Multilayers using Secondary Ion Mass Spectrometry. *Appl. Phys. Lett.*, (in submission).
23. Matyjaszewski, K. & Xia, J. Atom Transfer Radical Polymerization. *Chem. Rev.* **101**, 2921-2990 (2001).
24. Xia, J. & Matyjaszewski, K. Controlled/"Living" Radical Polymerization. Atom Transfer Radical Polymerization Using Multidentate Amine Ligands. *Macromolecules* **30**, 7697-7700 (1997).
25. Matyjaszewski, K., Patten, T. E. & Xia, J. H. Controlled/"living" radical polymerization. Kinetics of the homogeneous atom transfer radical polymerization of styrene. *J. Am. Chem. Soc.* **119**, 674-680 (1997).
26. Fuchs, K., Friedrich, C. & Weese, J. Viscoelastic Properties of Narrow-Distribution Poly(methyl methacrylates). *Macromolecules* **29**, 5893-5901 (1996).
27. Frisch, H. L., Mallows, C. L. & Bovey, F. A. On Stereoregularity of Vinyl Polymer Chains. *J. Chem. Phys.* **45**, 1565-& (1966).
28. Ferguson, R. C. 220-Mhz Proton Magnetic Resonance Spectra of Polymers .I. Poly(Methyl Methacrylate). *Macromolecules* **2**, 237-& (1969).
29. Dobkowski, Z. Procedure for Evaluation of the Mark-Houwink Constants. *J. Appl. Polym. Sci.* **29**, 2683-2694 (1984).
30. Brandrup, J., Immergut, E. H. & Grulke, E. A. (eds.) *Polymer Handbook, 4th edition* (Wiley-Interscience, Hoboken, NJ, 1999).
31. Agrawal, G. et al. Interdiffusion of polymers across interfaces. *J. Polym. Sci., Part B: Polym. Phys.* **34**, 2919-2940 (1996).
32. Vanden Eynde, X., Bertrand, P. & Penelle, J. "Matrix" effects in ToF-SIMS analyses of styrene-methyl methacrylate random copolymers. *Macromolecules* **33**, 5624-5633 (2000).
33. Ziegler, J. F., Biersack, J. P. & Littmark, U. *The Stopping and Range of Ions in Solids* (Pergamon, New York, 1985).
34. Migeon, H. N., Schuhmacher, M. & Slodzian, G. Analysis of Insulating Specimens with the Cameca Ims4f. *Surf. Interface Anal.* **16**, 9-13 (1990).
35. Williams, P., Lewis, R. K., Evans, C. A. & Hanley, P. R. Evaluation of a Cesium Primary Ion Source on an Ion Microprobe Mass Spectrometer. *Anal. Chem.* **49**, 1399-1403 (1977).

36. Harton, S. E., Koga, T., Stevie, F. A., Araki, T. & Ade, H. Investigation of Blend Miscibility of a Ternary PS/PCHMA/PMMA System using SIMS and Mean-Field Theory. *Macromolecules* **38**, 10511-10515 (2005).
37. Dowsett, M. G., Barlow, R. D. & Allen, P. N. Secondary-Ion Mass-Spectrometry Analysis of Ultrathin Impurity Layers in Semiconductors and Their Use in Quantification, Instrumental Assessment, and Fundamental Measurements. *J. Vac. Sci. Technol., B* **12**, 186-198 (1994).
38. Allen, P. N. & Dowsett, M. G. Maximum-Entropy Quantification of Sims Depth Profiles - Behavior as a Function of Primary Ion Energy. *Surf. Interface Anal.* **21**, 206-209 (1994).
39. Press, W. H., Flannery, B. P., Teukolsky, S. A. & Vetterling, W. T. *Numerical Recipes in Fortran 77: The Art of Scientific Computing* (Cambridge University Press, 1992).
40. Wilson, R. G., Lux, G. E. & Kirschbaum, C. L. Depth profiling and secondary ion mass spectrometry relative sensitivity factors and systematics for polymers/organics. *J. Appl. Phys.* **73**, 2524-2529 (1993).
41. Delcorte, A., Bertrand, P. & Garrison, B. J. Collision cascade and sputtering process in a polymer. *J. Phys. Chem. B* **105**, 9474-9486 (2001).
42. Wilson, R. G., Stevie, F. A. & Magee, C. W. *Secondary Ion Mass Spectrometry: A Practical Handbook for Depth Profiling and Bulk Impurity Analysis* (John Wiley & Sons, New York, 1989).
43. Weibel, D. et al. A C60 Primary Ion Beam System for Time of Flight Secondary Ion Mass Spectrometry: Its Development and Seconedary Ion Yield Characteristics. *Anal. Chem.* **75**, 1754-1764 (2003).
44. Winograd, N. The Magic of Cluster SIMS. *Anal. Chem.* **77**, 142A-149A (2005).
45. Fuoco, E. R., Gillen, G., Wijesundara, M. B. J., Wallace, W. E. & Hanley, L. Surface Analysis Studies of Yield Enhancements in Secondary Ion Mass Spectrometry by Polyatomic Projectiles. *J. Phys. Chem. B* **105**, 3950-3956 (2001).
46. Wagner, M. S. Molecular Depth Profiling of Multilayer Polymer Films Using Time-of-Flight Secondary Ion Mass Spectrometry. *Anal. Chem.* **77**, 911-922 (2005).
47. Szakal, C., Sun, S., Wucher, A. & Winograd, N. C60 molecular depth profiling of a model polymer. *Appl. Surf. Sci.* **231-231**, 183-185 (2004).
48. Mahoney, C. M., Yu, J. & Gardella, J. A. Depth Profiling of Poly(L-lactic acid)/Triblock Copolymer Blends with Time-of-Flight Secondary Ion Mass Spectrometry. *Anal. Chem.* **77**, 3570-3578 (2005).
49. Postawa, Z., Czerwinski, B., Winograd, N. & Garrison, B. J. Microscopic insights into the sputtering of thin organic films on Ag{111} induced by C-60 and Ga bombardment. *J. Phys. Chem. B* **109**, 11973-11979 (2005).
50. Chia, V. K. F., Mount, G. R., Edgell, M. J. & Magee, C. W. Recent advances in secondary ion mass spectrometry to characterize ultralow energy ion implants. *J. Vac. Sci. Technol. B* **17**, 2345-2351 (1999).

Polymer	M_w/kDa	M_w/M_n	T_g/°C
^{13}C-PS	79.4	1.20	100
^{12}C-PS	73.7	1.19	100
PMMA	90.9	1.26	100

Table 5.1. Characteristics of polymers utilized: Polymer molecular weights and polydispersities as measured using GPC (30 °C, $CHCl_3$), and T_g's measured using DSC (10 °C/min cooling cycle).

Solution	Mass Polymer	% ^{13}C-PS (v/v)	Vol. Solvent
1	40 mg ^{13}C-PS	100	1 mL toluene
2	90 mg ^{12}C-PS	0	3 mL toluene
3	6 mg ^{13}C-PS + 111 mg ^{12}C-PS	5	3 mL 1-chloropentane
4	115 mg PMMA	0	3 mL toluene
5	15 mg ^{13}C-PS	100	2 mL benzene
6	15 mg ^{12}C-PS	0	2 mL benzene

Table 5.2. Polymer/solvent solutions used to prepare the six different sample types. Volume % ^{13}C-PS is on a solvent free basis (i.e., concentration in the cast film).

Sample	Soln.$_1$	h_1 (nm)	Method$_1$	Soln.$_2$	h_2 (nm)	Method$_2$	Soln.$_3$	h_3 (nm)	Method$_3$
A	1	180	*C*	2	125	*F*	*	0	*
B	3	175	*C*	2	125	*F*	*	0	*
C	4	145	*C*	3	175	*C*	2	125	*F*
D	4	145	*C*	3	175	*C*	4	145	*F*
E	5	70	*C*	*	0	*	*	0	*
F	6	70	*C*	*	0	*	*	0	*

Table 5.3. Six different sample types utilized, showing the solutions from Table 5.2 used for each corresponding layer (n = 1, 2, or 3), the thickness of the layer (h_n) as measured using ellipsometry, and the method used to prepare the corresponding layer (i.e., direct casting *C* or floating *F*).

	O_2^+ S_R (nm^3/ion)	O_2^+ $S_R/S_{R,Si}$	Cs^+ S_R (nm^3/ion)	Cs^+ $S_R/S_{R,Si}$
Si (100)	0.033	1.0	0.095	1.0
PS	0.046	1.1	0.11	1.4
PMMA	0.11	3.2	0.30	3.4

Table 5.4. Sputtering rates S_R, approximated using the known thicknesses of the various layers in samples A-D and the known sputtering times and raster areas. Values are also normalized using measured values for intrinsic Si (100) ($S_R/S_{R,Si}$).

	$\Delta_{84/16}$ (nm)	$\delta_{50/16}$ (nm)	$\delta_{84/50}$ (nm)	Δ_{eff} (nm)	λ_d (nm)
O_2^+	19	7	12	10	10
Cs^+	14	5	9	4	9

Table 5.5. Widths of the profiles shown in Figures 5.1c,d based on 84/16 ($\Delta_{84/16}$), 50/16 ($\delta_{50/16}$) and 84/50 ($\delta_{84/50}$) intensity crossings, and regressed parameters Δ_{eff} and λ_d (Equations 2-4).

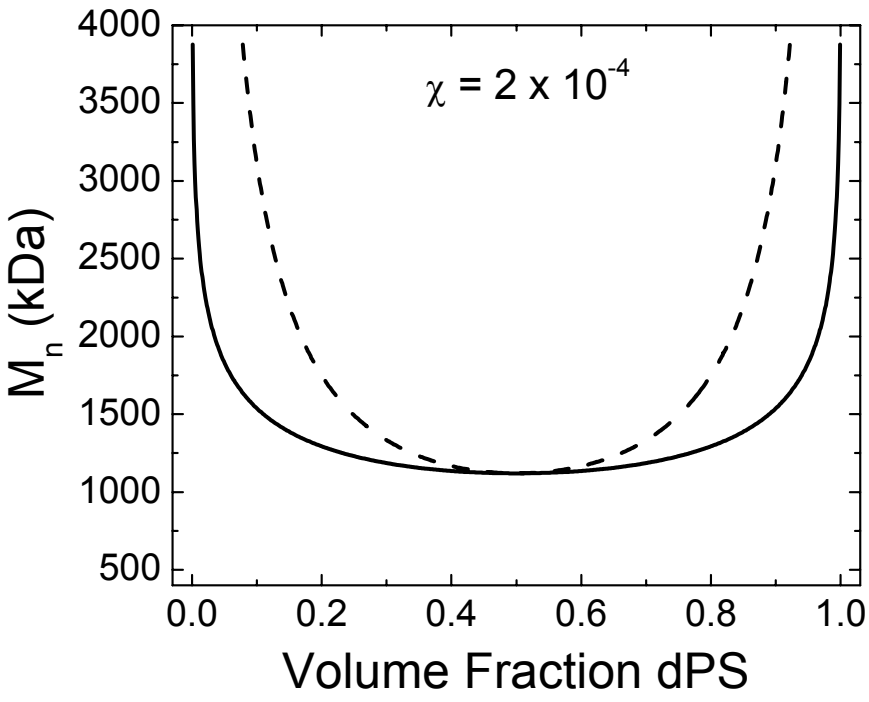

Figure 5.1. Isothermal phase diagram of a symmetric blend of 100 % deuterium substituted PS (dPS) and unlabeled PS (hPS) generated using parameters from Ref (20), assuming a concentration independent (nominal) mean-field interaction parameter $\chi = 2 \times 10^{-4}$ (*ca.* 125 °C). The solid line is the binodal (coexistence curve), while the dashed line is the spinodal. At high molecular weights, (M_n > 1100 kDa) classical phase separation, such as nucleation and growth and spinodal decomposition, can occur.

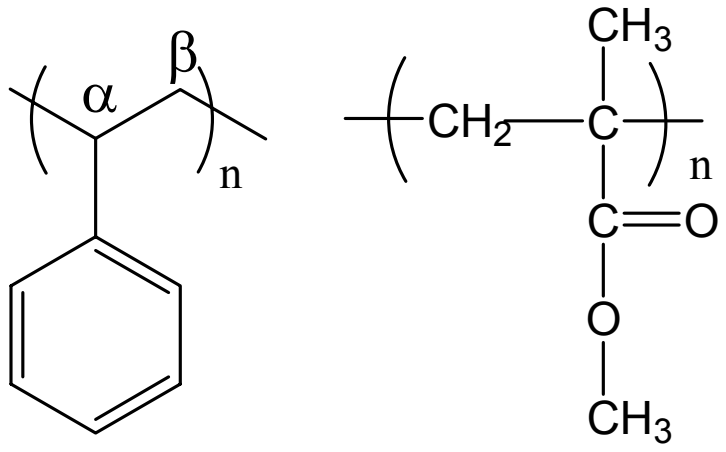

PS **PMMA**

Figure 5.2. Chemical structures for PS and PMMA. α and β are the backbone carbons in PS, both of which are ^{13}C substituted in the ^{13}C labeled styrene monomer.

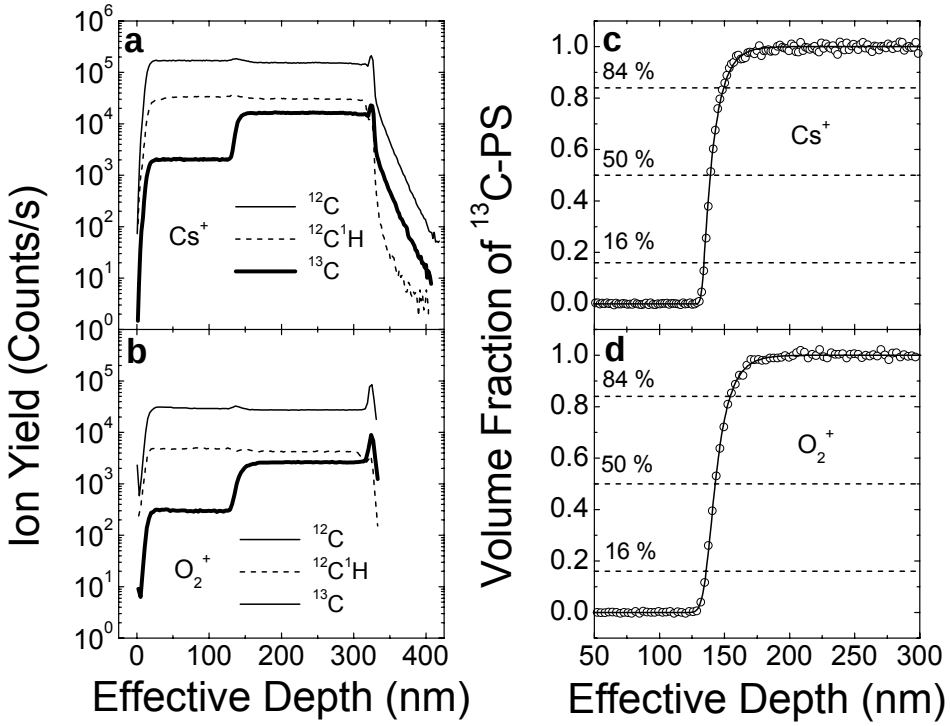

Figure 5.3. SIMS depth profiles of sample A (a, b) showing ^{12}C (solid line), $^{12}C^{1}H$ (dashed line), and ^{13}C (bold line) secondary ion yields and (c,d) volume fraction of ^{13}C-PS in the ^{12}C-PS/^{13}C-PS bilayer. Both (a, c) 6.0 keV Cs^+ and (b, c) 5.5 keV O_2^+ primary ion bombardment, with detection of negative and positive secondary ions, respectively, provide high signal-to-noise (S/N) and high detection sensitivity. $^{12}C^{1}H$ is completely mass resolved from ^{13}C for both primary ions. Shown in (c) and (d) are the midpoint (50 %) and 16 and 84 % intensity lines, which are used to semi-quantitatively describe the asymmetry of the profiles (see Table 5.5). The solid lines in (c) and (d) are a fit using a step function convoluted with a Gaussian and an exponential function (see Equations 2-4), resulting in the regression parameters summarized in Table 5.5. The effective depth was determined by assuming a constant PS sputtering rate throughout the film assembly.

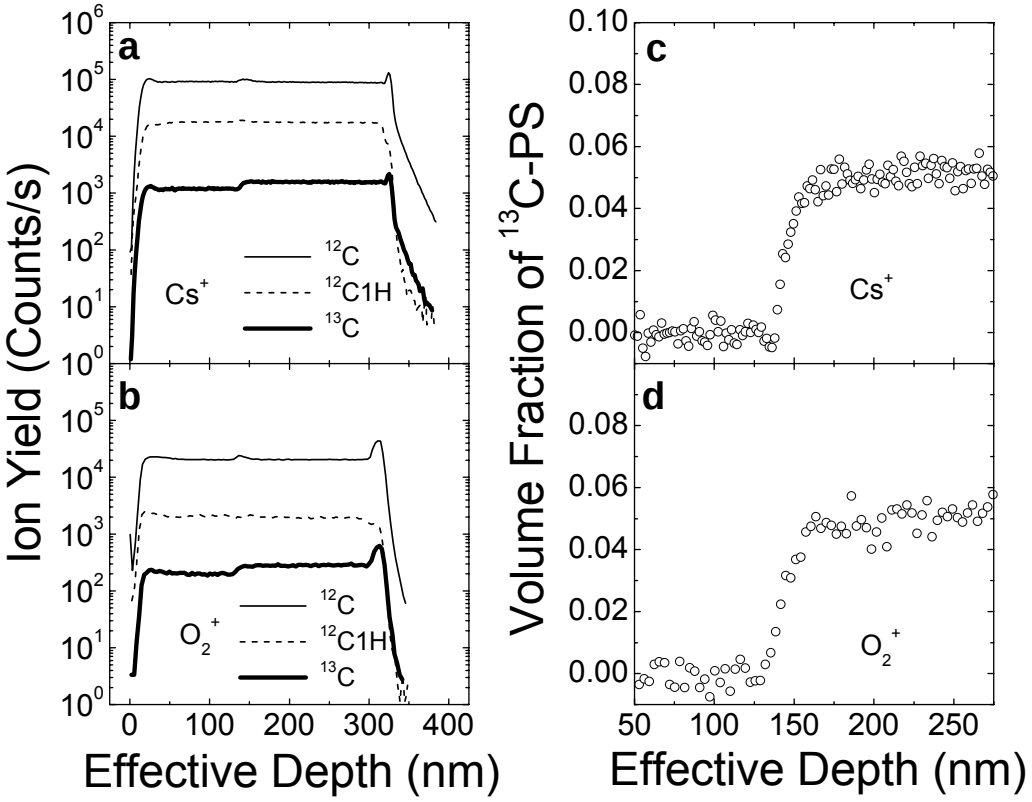

Figure 5.4. SIMS depth profiles of sample B, a bilayer consisting of ^{12}C-PS (top) and 5% (v/v) ^{13}C-PS + ^{12}C-PS, showing (a, b) ^{12}C (solid line), ^{12}C^{1}H (dashed line), and ^{13}C (bold line) secondary ion yields and (c,d) volume fraction of ^{13}C-PS as a function of effective depth. The use of (a, c) 6.0 keV (10 nA) Cs^+ primary ion bombardment provides greatly improved detection sensitivity and S/N for depth profiling of ^{13}C-PS when compared to (b, d) 5.5 keV (30 nA) O_2^+ bombardment.

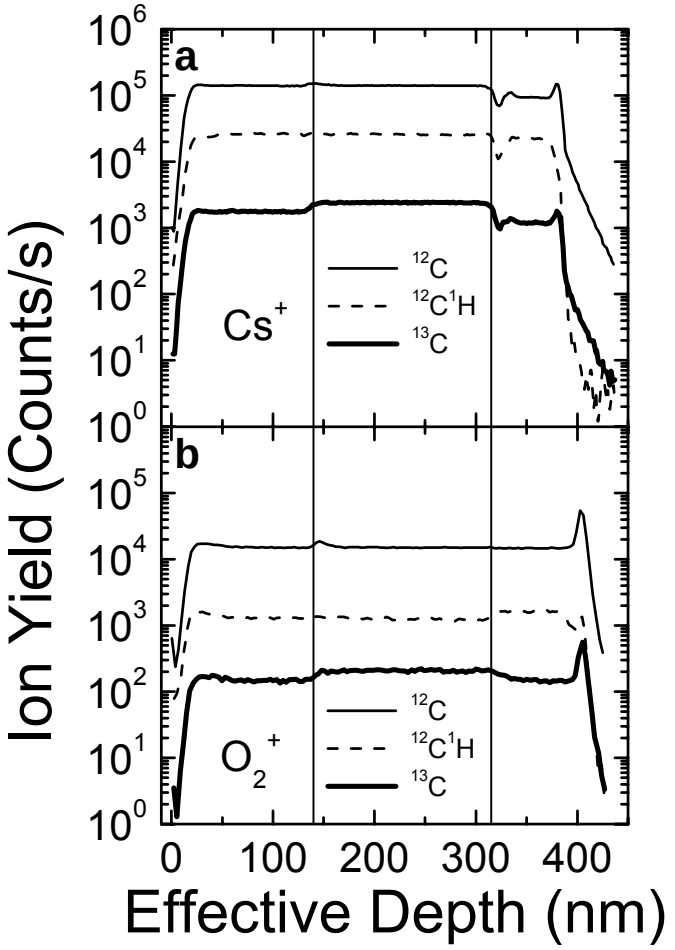

Figure 5.5. SIMS depth profiles of sample C using (a) 6.0 keV (10 nA) Cs^+, and (b) 5.5 keV (30 nA) O_2^+ primary ion bombardment. The effective depth was determined by assuming a constant PS sputtering rate throughout the film assembly. The two vertical lines show the approximate location of both the ^{12}C-PS/^{12}C-PS:^{13}C-PS (~ 135 nm) and ^{12}C-PS:^{13}C-PS/PMMA (~ 310 nm) interfaces.

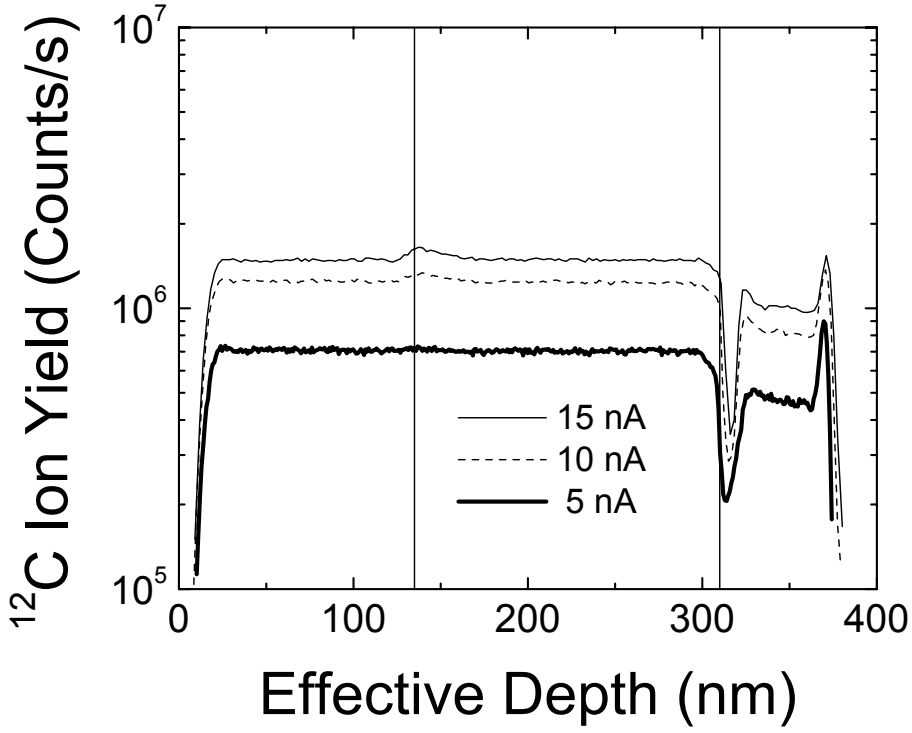

Figure 5.6. Effect of variation of 6.0 keV Cs^+ primary ion current on SIMS depth profile of sample C. The non-monotonic changes in the secondary ion yields at the ^{12}C-PS:^{13}C-PS/PMMA interface (~ 310 nm) appear to be nearly independent of primary ion current. This supports the conclusion that sample charging is not the underlying cause of the behavior observed at the heterogeneous polymer/polymer interface. The two vertical lines show the approximate location of both the ^{12}C-PS/^{12}C-PS:^{13}C-PS (~ 135 nm) and ^{12}C-PS:^{13}C-PS/PMMA (~ 310 nm) interfaces. The effective depth was determined by assuming a constant PS sputtering rate throughout the film assembly.

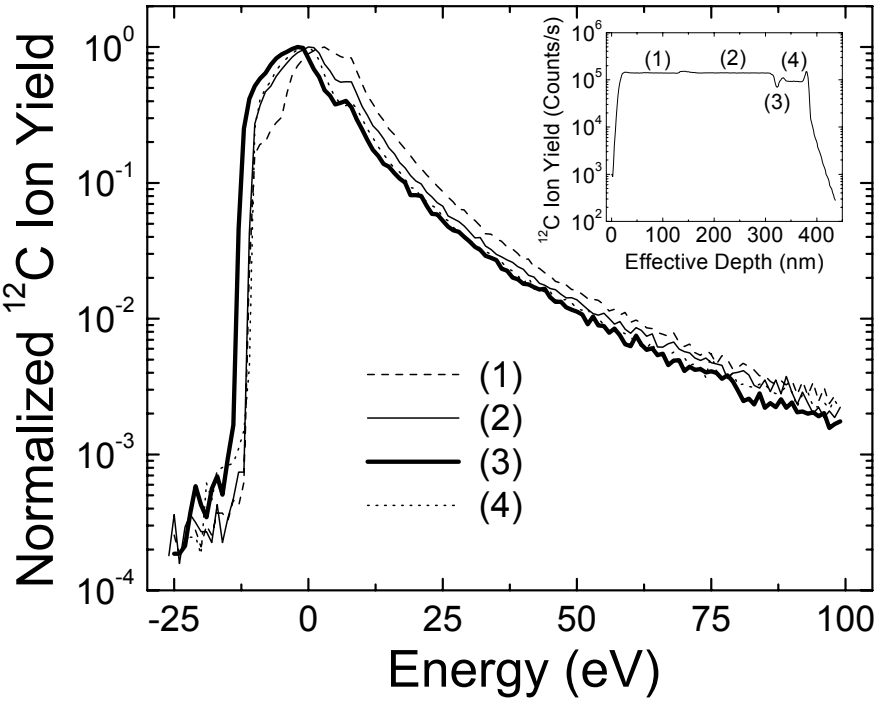

Figure 5.7. ^{12}C secondary ion energy spectra at various depths (inset) for sample C using 6.0 keV (3 nA) Cs^+ primary ion bombardment. No signs of charging are present at any depth in the sample.

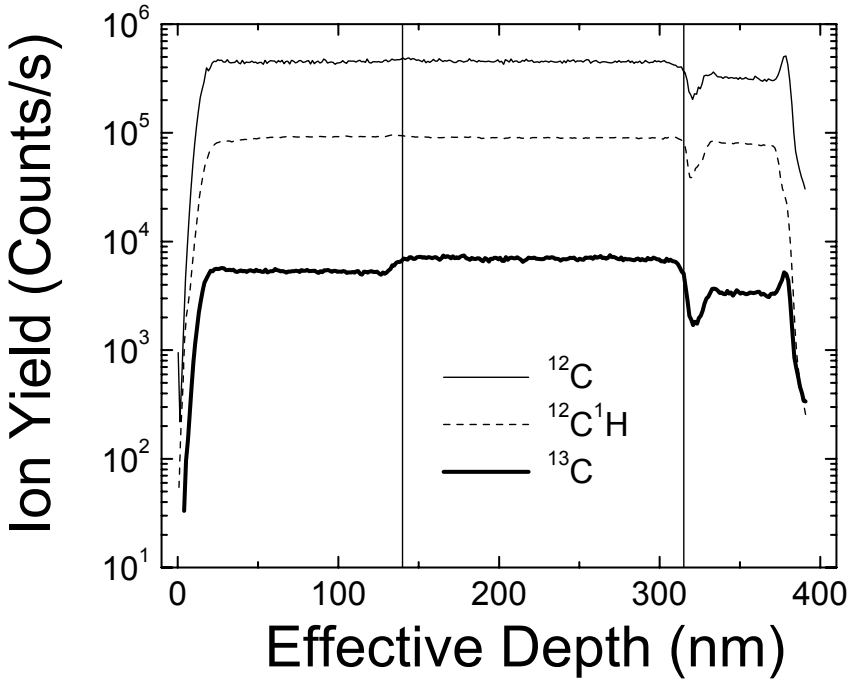

Figure 5.8. SIMS depth profile analysis of sample C using 6.0 keV Cs^+ ion bombardment (3 nA, 110 μm x 110 μm raster) and the "electron cloud" method of charge neutralization. The two vertical lines show the approximate location of both the ^{12}C-PS/^{12}C-PS:^{13}C-PS (~ 135 nm) and ^{12}C-PS:^{13}C-PS/PMMA (~ 310 nm) interfaces. The non-monotonic changes in the secondary ion yields at the ^{12}C-PS:^{13}C-PS/PMMA interface are still apparent, again proving that sample charging is not the underlying cause of this behavior. This also confirms that the "electron cloud" method of charge neutralization can be implemented without causing excess damage to the polymer film. The effective depth was determined by assuming a constant PS sputtering rate throughout the film assembly.

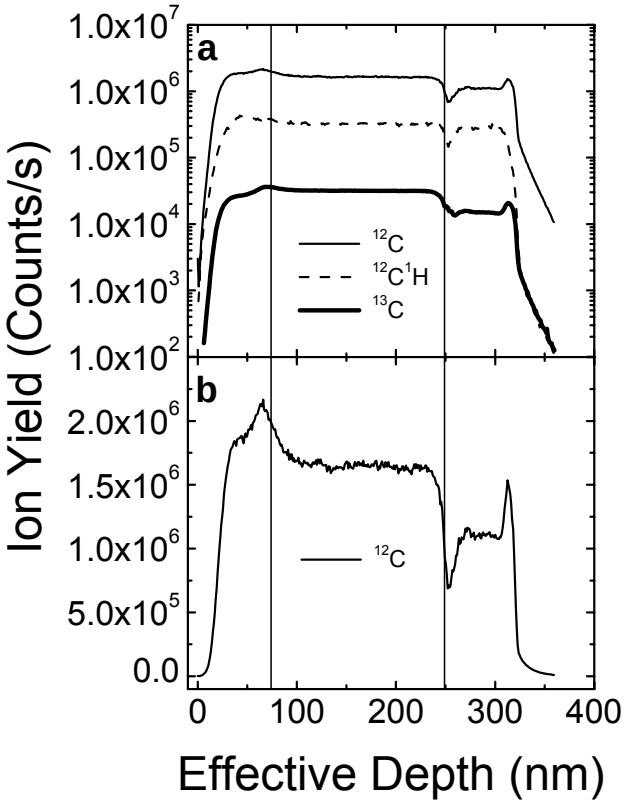

Figure 5.9. Characterization of a PMMA/^{12}C-PS:^{13}C-PS/PMMA film (sample D) using 6.0 keV (10 nA) Cs^{+} primary ion bombardment. The effective depth was determined by assuming a constant PS sputtering rate throughout the film assembly. The two vertical lines show the approximate location of both the PMMA/^{12}C-PS:^{13}C-PS (~ 75 nm) and ^{12}C-PS:^{13}C-PS/PMMA (~ 250 nm) interfaces. Changes in ^{12}C, ^{12}C^{1}H, and ^{13}C secondary ion yields are apparent through both interfaces (a), although the behavior is quite different at each interface. A plot of the ^{12}C secondary ion yield on a linear scale has also been provided (b) in order to highlight the changes in secondary ion yields at both PS/PMMA interfaces.

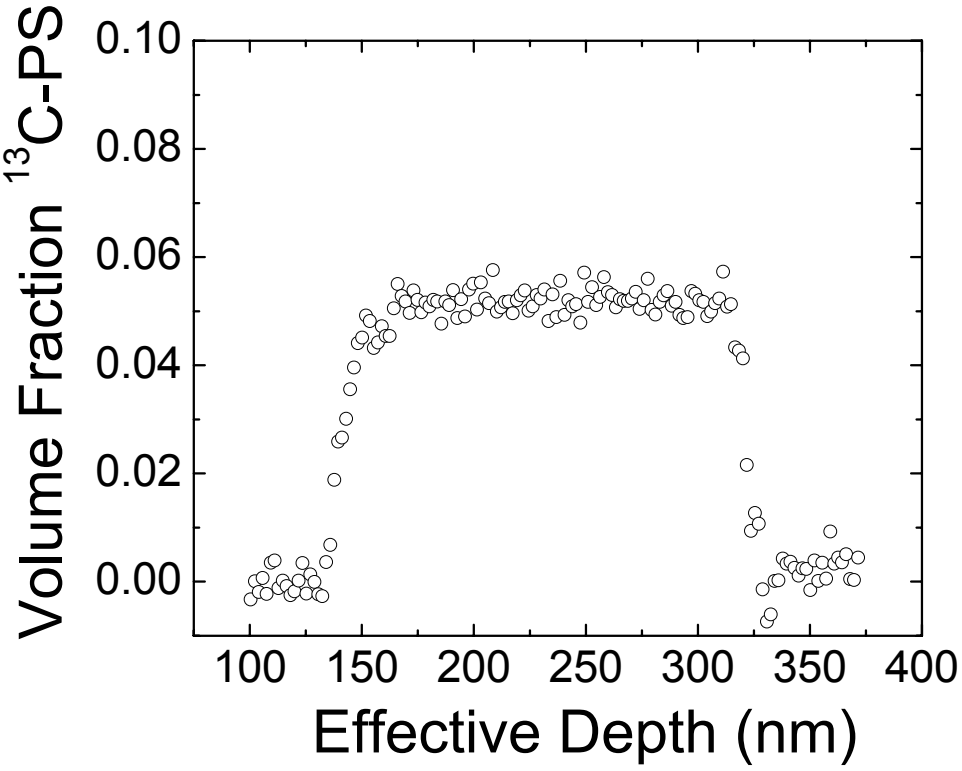

Figure 5.10. ^{13}C-PS SIMS depth profile for Sample C, showing that normalization of the ^{13}C ion yield to the total C (^{12}C + ^{13}C) ion yield (see Equation 1) can help to alleviate the non-monotonic behavior at the heterogeneous ^{12}C-PS:^{13}C-PS/PMMA interface. The ^{12}C-PS/^{12}C-PS:^{13}C-PS and ^{12}C-PS:^{13}C-PS/PMMA interfaces are located at ~ 135 and 310 nm, respectively, as shown with the vertical lines.

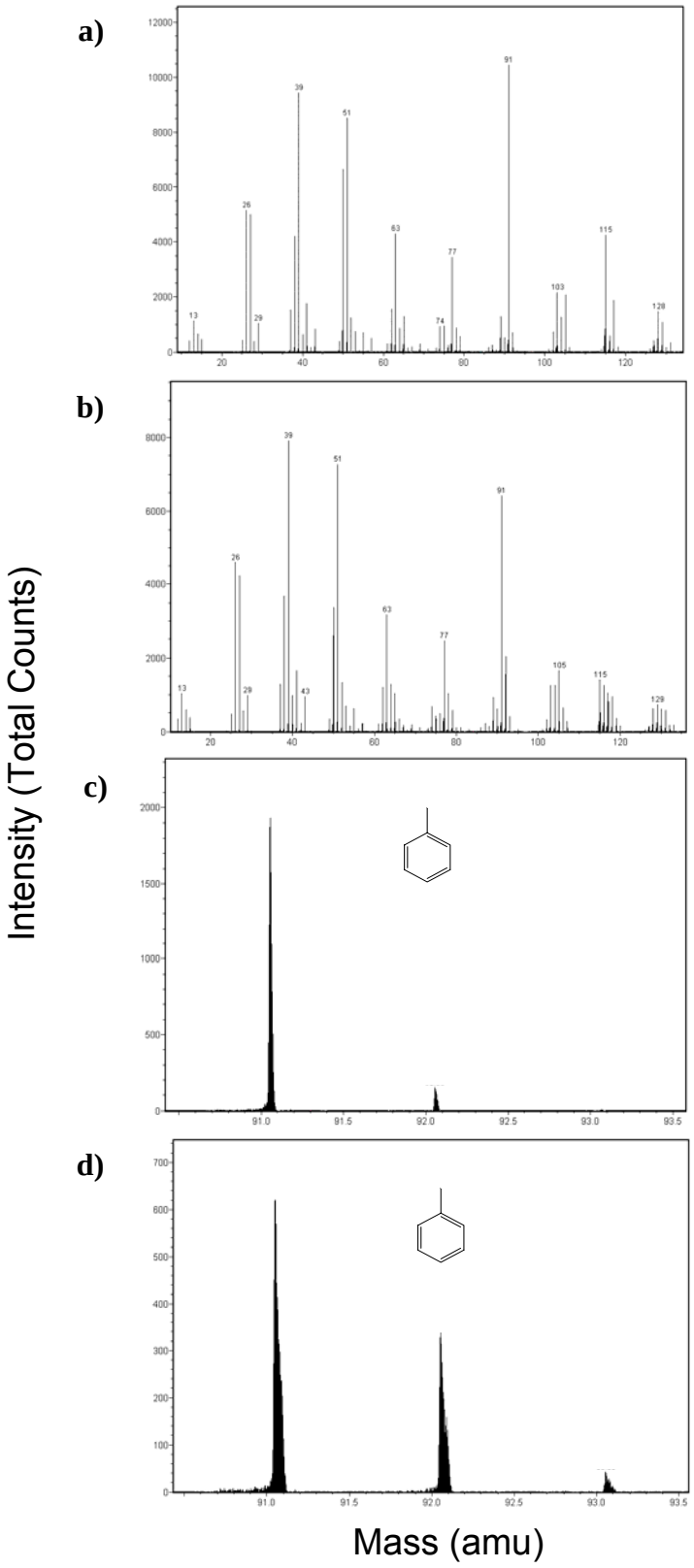
a)
b)
c)
d)
Intensity (Total Counts)
Mass (amu)

Figure 5.11. ToF SIMS (15 keV Ga^+) positive secondary ion mass spectra (total counts) for (a) ^{12}C-PS (sample E) and (b) ^{13}C-PS (sample F) from approximately 10-130 amu (0.15 amu bin) and (c) ^{12}C-PS and (d) ^{13}C-PS from approximately 91-93 amu (0.004 amu bin). Natural abundance of ^{13}C in ^{12}C-PS was verified with (c), demonstrating that there are negligible mass interferences for the C_7H_7 fragment. The peak at 93 amu (nominal) in (d) shows that the ^{13}C labeled monomer used in synthesis of the ^{13}C-PS has a slight enrichment of ^{13}C in the aromatic ring (approximately 50% over natural abundance).

6. CONCLUSIONS AND FUTURE WORK

6.1. Summary of Work

This investigation has demonstrated that thermodynamic behavior of polymers at heterogeneous polymer-polymer interfaces can be systematically investigated using SIMS. Using a model miscible blend, dPS:PCHMA, segregation to a heterogeneous dPS:PCHMA/PMMA interface was investigated as a function of dPS composition.[1] Using previously reported mean-field interaction parameters for dPS/PMMA[2] and PS/PCHMA[3] and a newly determined interaction parameter for PCHMA/PMMA using XR, SCMF was shown to be in very good agreement with the interfacial excesses of dPS determined from analysis of the SIMS profiles for 5, 10, and 20 % (v/v) dPS embedded in the PCHMA layer (see Figure 3.5). The high depth resolution of the SIMS profiles (*ca.* 7-8 nm), under the conditions implemented here (6.0 keV Cs+ primary ion bombardment), was essential in order to fully resolve the somewhat low excess observed at the dPS:PCHMA/PMMA interface (see Figures 3.2 and 3.3). This low excess is due to the high miscibility of dPS in PCHMA.[3,4] SCMF was also used to determine the change in interfacial width and interfacial tension at the dPS:PCHMA/PMMA interface as a function of dPS concentration (see Figure 3.6).[5]

Deuterium substitution has been frequently used for tracer labeling of polymers for analyses of such phenomena as reactive coupling at polymer interfaces,[6,7] polymer chain mobility near surfaces and interfaces,[8,9] and surface segregation.[10,11] It has been shown here that it cannot be considered a true tracer, particularly at an hPS:dPS/hPMMA interface, with observation of diffusion-controlled segregation of dPS to the

heterogeneous interface (see Figure 4.1). Using SCMF,[12] the enthalpic preference for dPS over hPS at the interface was quantified, and the results cannot be explained within the context of the reported values of χ (see Figure 4.7).[2] This apparent deviation from mean-field theory is also evidenced in the inability of SCMF[13] to even qualitatively describe the reported interfacial tensions for PS/PMMA[14,15] as a function of temperature (see Figure 4.8).

The use of a novel tracer ^{13}C was developed in order to provide a true tracer for SIMS analysis of polymer films and multilayers. Because of the high mass resolution required to mass resolve $^{12}C^{1}H$ from ^{13}C ($m/\Delta m \approx 3000$), a quadrupole instrument cannot be used to analyze these depth profiles (typical $m/\Delta m \sim 300$).[16] ^{13}C labeled PS and unlabeled PS and PMMA were synthesized using ATRP[17,18] and analyzed in several model multilayer systems (see Figures 5.3-5.10) using 5.5 keV impact energy O_2^+ and 6.0 keV impact energy Cs^+, with detection of positive and negative secondary ions, respectively. Because a submatrix (^{13}C) is analyzed and can be normalized to the total carbon secondary ion yield ($^{12}C + {}^{13}C$) to convert the secondary ion yield to ^{13}C-PS concentration, a reduction in matrix effects at the PS/PMMA interface was encountered using 6.0 keV impact energy Cs^+. The use of a magnetic sector SIMS instrument was shown to provide the mass resolution necessary for depth profiling of ^{13}C labeled polymers. It was also shown that the segregation that was prominent with the use of deuterium labeled PS (see Figure 4.11) was absent with the use of ^{13}C labeled PS (see Figure 5.10) at a PS/PMMA interface. Analysis of the ^{13}C labeled PS using ToF SIMS was performed to demonstrate the potential for future use of ToF SIMS for depth

profiling high molecular weight (~ 100 amu) fragments of ^{13}C labeled polymers (see Figure 5.11).

6.2. Future Work

6.2.1. Effects of Isotopic Labeling

Recent experimental results showing that the effects of deuterium labeling on polymer phase behavior near heterogeneous interfaces is somewhat of a general phenomenon and is not confined to the PS/PMMA system. Several model polymer binary systems,[2,19,20] namely PS/poly(2-vinylpyridine) (P2VP) and PS/poly(4-vinylpyridine) (P4VP) as well as PS/PMMA, have been determined to show significant segregation of dPS to the heterogeneous polymer/polymer interfaces, as shown in Figure 6.1. Therefore, further investigations will be necessary to determine exactly what types of systems are strongly affected by deuterium labeling. These investigations should extend past deuterium substituted PS to include other model polymers such as methyl substituted polystyrenes, polybutadiene, polyisoprene, poly(ethylene-*co*-propylene), and poly(ethylene-*co*-butylene). It is also hoped that the underlying mechanism can be identified. Measurements such as dielectric analysis may provide insight into the effects of dipole moment on the segregation of deuterium labeled polymers at heterogeneous interfaces, as a C-D bond is more easily polarized than a C-H bond.[21,22]

6.2.2. Diffusion Near Interfaces

The use of ^{13}C labeling can be used to create systems with true tracer polymers which can be used to re-evaluate polymer diffusion near surfaces and interfaces[9,23,24] to determine the origins of the observed phenomena, whether they are driven by the effects

of deuterium labeling or inherent slowing of polymer diffusion due to confinement effects.[25] These investigations could include diffusion at PS surfaces, and PS/P2VP, PS/P4VP, and PS/PMMA interfaces. Results could also be compared to dPS diffusion in order to reveal the effects of deuterium substitution, which could also help to re-evaluate existing data.[9,23,24]

1. Harton, S. E., Koga, T., Stevie, F. A., Araki, T. & Ade, H. Investigation of Blend Miscibility of a Ternary PS/PCHMA/PMMA System using SIMS and Mean-Field Theory. *Macromolecules* **38**, 10511-10515 (2005).
2. Russell, T. P. Changes in Polystyrene and Poly(methyl methacrylate) Interactions with Isotopic Substitution. *Macromolecules* **26**, 5819 (1993).
3. Pomposo, J. A., Mugica, A., Areizaga, J. & Cortazar, M. Modeling of phase behavior of binary and ternary blends involving copolymers of styrene, methyl methacrylate, and cyclohexyl methacrylate. *Acta Polym.* **49**, 301-311 (1998).
4. Friedrich, C., Schwarzwaelder, C. & Riemann, R.-E. Rheological and thermodynamic study of the miscible blend polystyrene/poly(cyclohexyl methacrylate). *Polymer* **37**, 2499-2507 (1996).
5. Helfand, E. Theory of the Homopolymer/Binary-Polymer-Mixture Interface. *Macromolecules* **25**, 1676-1685 (1992).
6. Kim, B. J. et al. Interfacial Roughening Induced by the Reaction of End-Functionalized Polymers at a PS/P2VP Interface: Quantitative Analysis by DSIMS. *Macromolecules* **38**, 6106-6114 (2005).
7. Harton, S. E. et al. Low-Temperature Reactive Coupling at Polymer-Polymer Interfaces Facilitated by Supercritical CO2. *Polymer* **46**, 10173-10179 (2005).
8. Russell, T. P. et al. Direct Observation of Reptation at Polymer Interfaces. *Nature* **365**, 235-237 (1993).
9. Zheng, X. et al. Reptation Dynamics of a Polymer Melt near an Attractive Solid Interface. *Phys. Rev. Lett.* **74**, 407-410 (1995).
10. Hariharan, A. et al. The Effect of Finite Film Thickness on the Surface Segregation in Symmetrical Binary Polymer Mixtures. *J. Chem. Phys.* **99**, 656-663 (1993).
11. Reynolds, B. J., Ruegg, M. L., Mates, T. E., Radke, C. J. & Balsara, N. P. Experimental and Theoretical Study of the Adsorption of a Diblock Copolymer to Interfaces between Two Homopolymers. *Macromolecules* **38**, 3872-3882 (2005).
12. Hariharan, A., Kumar, S. K. & Russell, T. P. Surface Segregation in Binary Polymer Mixtures - a Lattice Model. *Macromolecules* **24**, 4909-4917 (1991).
13. Helfand, E. & Tagami, Y. Theory of the Interface Between Immiscible Polymers. *J. Polym. Sci., Part B: Polym. Phys.* **9**, 741 (1971).
14. Wu, S. Surface and Interfacial Tensions of Polymer Melts. II. Poly(methyl methacrylate), Poly(n-butyl methacrylate), and Polystyrene. *J. Phys. Chem* **74**, 632-638 (1970).
15. Carriere, C. J., Biresaw, G. & Sammler, R. L. Temperature dependence of the interfacial tension of PS/PMMA, PS/PE, and PMMA/PE blends. *Rheol. Acta* **39**, 476-482 (2000).

16. Chia, V. K. F., Mount, G. R., Edgell, M. J. & Magee, C. W. Recent advances in secondary ion mass spectrometry to characterize ultralow energy ion implants. *J. Vac. Sci. Technol. B* **17**, 2345-2351 (1999).
17. Matyjaszewski, K. & Xia, J. Atom Transfer Radical Polymerization. *Chem. Rev.* **101**, 2921-2990 (2001).
18. Xia, J. & Matyjaszewski, K. Controlled/"Living" Radical Polymerization. Atom Transfer Radical Polymerization Using Multidentate Amine Ligands. *Macromolecules* **30**, 7697-7700 (1997).
19. Dai, K. H. & Kramer, E. J. Determining the Temperature-dependent Flory Interaction Parameter for Strongly Immiscible Polymers from Block-Copolymer Segregation Measurements. *Polymer* **35**, 157-161 (1994).
20. Clarke, C. J. et al. Measurements of the Flory-Huggins interaction parameter for polystyrene-poly(4-vinylpyridine) blends. *Macromolecules* **30**, 4184-4188 (1997).
21. Bates, F. S. & Wignall, G. D. Isotope-Induced Quantum-Phase Transitions in the Liquid State. *Phys. Rev. Lett.* **57**, 1429-1432 (1986).
22. Jones, R. A. L., Kramer, E. J., Rafailovich, M. H., Sokolov, J. & Schwarz, S. A. Surface Enrichment in an Isotopic Polymer Blend. *Phys. Rev. Lett.* **62**, 280-283 (1989).
23. Zheng, X. et al. Long-Range Effects on Polymer Diffusion Induced by a Bounding Interface. *Phys. Rev. Lett.* **79**, 241-244 (1997).
24. Pu, Y. et al. Mobility of Polymer Chains Confined at a Free Surface. *Phys. Rev. Lett.* **87**, Art. # 206101 (2001).
25. Ellison, C. J. & Torkelson, J. M. The distribution of glass-transition temperatures in nanoscopically confined glass formers. *Nat. Mater.* **2**, 695-700 (2003).

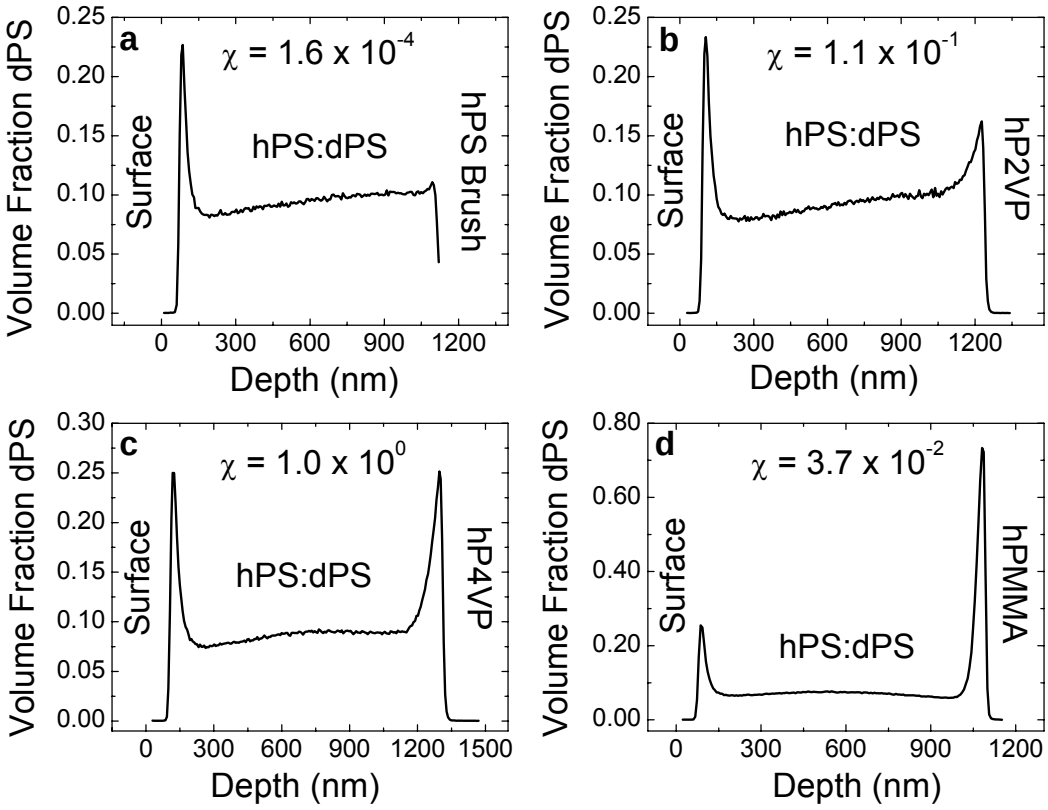

Figure 6.1. Segregation of high molecular weight (ca. 1500 kDa) dPS to a) hPS:dPS/hPS brush, b) hPS:dPS/P2VP, c) hPS:dPS/P4VP, and d) hPS:dPS/PMMA interfaces as determined using SIMS with 5.5 keV O_2^+ primary ion bombardment with detection of positive secondary ions. The values of χ for dPS and the substrate polymer are shown in each SIMS profile. All samples were annealed at 176 °C for 64 days.

7. BIBLIOGRAPHY OF ALL WORKS CITED

Ade, H. & Hsiao, B. X-ray Linear Dichroism Microscopy. *Science* **262**, 1427-1429 (1993).

Ade, H., Kilcoyne, A. L. D., Tyliszczak, T., Hitchcock, P., Anderson, E., Harteneck, B., Rightor, E. G., Mitchell, G. E., Hitchock, A. P. & Warwick, T. Scanning Transmission X-Ray Microscopy at a Bending Magnet Beamline at the Advanced Light Source. *J. Phys. IV* **104**, 3-8 (2003).

Ade, H., Zhang, X., Cameron, S., Costello, C., Kirz, J. & Williams, S. Chemical Contrast in X-ray Microscopy and Spatially Resolved XANES Spectroscopy of Organic Specimens. *Science* **258**, 972 (1992).

Agrawal, G., Wool, R. P., Dozier, W. D., Felcher, G. P., Zhou, J., Pispas, S., Mays, J. W. & Russell, T. P. Interdiffusion of polymers across interfaces. *J. Polym. Sci., Part B: Polym. Phys.* **34**, 2919-2940 (1996).

Allen, P. N. & Dowsett, M. G. Maximum-Entropy Quantification of Sims Depth Profiles - Behavior as a Function of Primary Ion Energy. *Surf. Interface Anal.* **21**, 206-209 (1994).

Amashta, I. A. K. & Sanchez, G. Estimation of Unperturbed Dimensions of Poly(cyclohexyl methacrylate) from light scattering, osmometry and viscosity data. *Eur. Polym. J.* **11**, 223-223 (1975).

Anastasiadis, S. H., Russell, T. P., Satija, S. K. & Majkrzak, C. F. The Morphology of Symmetric Diblock Copolymers as Revealed by Neutron Reflectivity. *J. Chem. Phys.* **92**, 5677-5691 (1990).

Antonietti, M., Coutandin, J. & Sillescu, H. Chainlength and temperature dependence of self-diffusion coefficients in polystyrene. *Makromol. Chem., Rapid Commun.* **5**, 525-528 (1984).

Bates, F. S. & Fredrickson, G. H. Block copolymers - Designer soft materials. *Phys. Today* **52**, 32-38 (1999).

Bates, F. S., Muthukumar, M., Wignall, G. D. & Fetters, L. J. Thermodynamics of Isotopic Polymer Mixtures - Significance of Local Structural Symmetry. *J. Chem. Phys.* **89**, 535-544 (1988).

Bates, F. S. & Wignall, G. D. Isotope-Induced Quantum-Phase Transitions in the Liquid State. *Phys. Rev. Lett.* **57**, 1429-1432 (1986).

Bates, F. S. & Wignall, G. D. Nonideal Mixing in Binary Blends of Perdeuterated and Protonated Polystyrenes. *Macromolecules* **19**, 932-934 (1986).

Bates, F. S., Wignall, G. D. & Koehler, W. C. Critical-Behavior of Binary-Liquid Mixtures of Deuterated and Protonated Polymers. *Phys. Rev. Lett.* **55**, 2425-2428 (1985).

Binder, K. *Monte Carlo and Moecular Dynamics Simulations in Polymer Science* (Oxford University Press, Oxford, 1995).

Brandrup, J., Immergut, E. H. & Grulke, E. A. (eds.) *Polymer Handbook, 4th edition* (Wiley-Interscience, Hoboken, NJ, 1999).

Brochard, F., Jouffroy, J. & Levinson, P. Polymer-Polymer Diffusion in Melts. *Macromolecules* **16**, 1638-1641 (1983).

Brochard, F., Jouffroy, J. & Levinson, P. Polymer Diffusion in Blends: Effects of Mutual Friction. *Macromolecules* **17**, 2925-2927 (1984).

Broseta, D., Fredrickson, G. H., Helfand, E. & Leibler, L. Molecular Weight and Polydispersity Effects at Polymer-Polymer Interfaces. *Macromolecules* **23**, 132-139 (1990).

Budkowski, A., Steiner, U., Klein, J. & Schatz, G. Coexistence in a Binary Isotopic Polymer Mixture. *Europhys. Lett.* **18**, 705-710 (1992).

Callaghan, T. A. & Paul, D. R. Interaction Energies for Blends of Poly(methyl methacrylate), Polystyrene, and Poly(a-methylstyrene) by the Critical Molecular Weight Method. *Macromolecules* **26**, 2439-2450 (1993).

Carriere, C. J., Biresaw, G. & Sammler, R. L. Temperature dependence of the interfacial tension of PS/PMMA, PS/PE, and PMMA/PE blends. *Rheol. Acta* **39**, 476-482 (2000).

Castner, D. G. View from the edge. *Nature* **422**, 129-130 (2003).

Chaturvedi, U. K., Steiner, U., Zak, O., Krausch, G., Schatz, G. & Klein, J. Structure at Polymer Interfaces Determined by High-Resolution Nuclear Reaction Analysis. *Appl. Phys. Lett.* **56**, 1228-1230 (1990).

Chia, V. K. F., Mount, G. R., Edgell, M. J. & Magee, C. W. Recent advances in secondary ion mass spectrometry to characterize ultralow energy ion implants. *J. Vac. Sci. Technol. B* **17**, 2345-2351 (1999).

Clarke, C. J., Eisenberg, A., LaScala, J., Rafailovich, M. H., Sokolov, J., Li, Z., Qu, S., Nguyen, D., Schwarz, S. A., Strzhemechny, Y. & Sauer, B. B. Measurements of the Flory-Huggins interaction parameter for polystyrene-poly(4-vinylpyridine) blends. *Macromolecules* **30**, 4184-4188 (1997).

Coleman, M. M., Graf, J. F. & Painter, P. C. *Specific Interactions and the Miscibility of Polymer Blends* (Technomic, Lancaster, PA, 1991).

Coleman, M. M., Narvett, L. A. & Painter, P. C. A counterintuitive observation concerning hydrogen bonding in polymer blends. *Polymer* **39**, 5867-5869 (1998).

Composto, R. J. & Kramer, E. J. Mutual Diffusion Studies of Polystyrene and Poly(Xylenyl Ether) Using Rutherford Backscattering Spectrometry. *J. Mater. Sci.* **26**, 2815-2822 (1991).

Composto, R. J., Kramer, E. J. & White, D. M. Reptation in Polymer Blends. *Polymer* **31**, 2320-2328 (1990).

Composto, R. J., Mayer, J. W., Kramer, E. J. & White, D. M. Fast Mutual Diffusion in Polymer Blends. *Phys. Rev. Lett.* **57**, 1312-1315 (1986).

Composto, R. J., Walters, R. M. & Genzer, J. Application of ion scattering techniques to characterize polymer surfaces and interfaces. *Mater. Sci. Eng., R* **38**, 107-180 (2002).

Coulon, G., Russell, T. P., Deline, V. R. & Green, P. F. Surface-Induced Orientation of Symmetric, Diblock Copolymers: A Secondary Ion Mass Spectrometry Study. *Macromolecules* **22**, 2581-2589 (1989).

Crank, J. *The Mathematics of Diffusion* (Oxford University Press, New York, 1975).

Dai, K. H. & Kramer, E. J. Determining the Temperature-dependent Flory Interaction Parameter for Strongly Immiscible Polymers from Block-Copolymer Segregation Measurements. *Polymer* **35**, 157-161 (1994).
Delcorte, A., Bertrand, P. & Garrison, B. J. Collision cascade and sputtering process in a polymer. *J. Phys. Chem. B* **105**, 9474-9486 (2001).
Deline, V. R., Evans, C. A. & Williams, P. Unified Explanation for Secondary Ion Yields. *Appl. Phys. Lett.* **33**, 578-580 (1978).
Deline, V. R., Katz, W., Evans, C. A. & Williams, P. Mechanism of Sims Matrix Effect. *Appl. Phys. Lett.* **33**, 832-835 (1978).
Dobkowski, Z. Procedure for Evaluation of the Mark-Houwink Constants. *J. Appl. Polym. Sci.* **29**, 2683-2694 (1984).
Dowsett, M. G., Barlow, R. D. & Allen, P. N. Secondary-Ion Mass-Spectrometry Analysis of Ultrathin Impurity Layers in Semiconductors and Their Use in Quantification, Instrumental Assessment, and Fundamental Measurements. *J. Vac. Sci. Technol., B* **12**, 186-198 (1994).
Dudowicz, J., Freed, K. F. & Lifschitz, M. Towards a Molecular-Basis for Understanding the Behavior of Isotopic Polymer Blends - Lattice Cluster Theory Computations for Psd Psh Blends. *Macromolecules* **27**, 5387-5398 (1994).
Edwards, S. F. The statistical mechanics of polymers with excluded volume. *Proc. Phys. Soc. London* **85**, 613-624 (1965).
Ellison, C. J. & Torkelson, J. M. The distribution of glass-transition temperatures in nanoscopically confined glass formers. *Nat. Mater.* **2**, 695-700 (2003).
Faldi, A., Genzer, J., Composto, R. J. & Dozier, W. D. Segregation at the Interface between a Homopolymer and a Binary Polymer Blend. *Phys. Rev. Lett.* **74**, 3388-3391 (1995).
Ferguson, R. C. 220-Mhz Proton Magnetic Resonance Spectra of Polymers .I. Poly(Methyl Methacrylate). *Macromolecules* **2**, 237-& (1969).
Fetters, L. J., Lohse, D. J., Milner, S. T. & Graessley, W. W. Packing length influence in linear polymer melts on the entanglement, critical, and reptation molecular weights. *Macromolecules* **32**, 6847-6851 (1999).
Fleer, G. J., Stuart, M. A. C., Scheutjens, J. M. H. M., Cosgrove, T. & Vincent, B. *Polymers at Interfaces* (Chapman & Hall, New York, 1993).
Flory, P. J. Thermodynamics of High Polymer Solutions. *J. Chem. Phys.* **9**, 660 (1941).
Flory, P. J. *Principles of Polymer Chemistry* (Cornell University Press, Ithaca, NY, 1953).
Forrey, C., Koberstein, J. T. & Pan, D. H. Surface segregation in miscible blends of polystyrene and poly(vinylmethyl ether): Comparison of theory and experiment. *Interface Sci.* **11**, 211-223 (2003).
Fredrickson, G. H. & Sides, S. W. Theory of polydisperse inhomogeneous polymers. *Macromolecules* **36**, 5415-5423 (2003).
Friedrich, C., Schwarzwaelder, C. & Riemann, R.-E. Rheological and thermodynamic study of the miscible blend polystyrene/poly(cyclohexyl methacrylate). *Polymer* **37**, 2499-2507 (1996).

Frisch, H. L., Mallows, C. L. & Bovey, F. A. On Stereoregularity of Vinyl Polymer Chains. *J. Chem. Phys.* **45**, 1565-& (1966).

Fuchs, K., Friedrich, C. & Weese, J. Viscoelastic Properties of Narrow-Distribution Poly(methyl methacrylates). *Macromolecules* **29**, 5893-5901 (1996).

Fuoco, E. R., Gillen, G., Wijesundara, M. B. J., Wallace, W. E. & Hanley, L. Surface Analysis Studies of Yield Enhancements in Secondary Ion Mass Spectrometry by Polyatomic Projectiles. *J. Phys. Chem. B* **105**, 3950-3956 (2001).

Ge, S., Pu, Y., Zhang, W., Rafailovich, M., Sokolov, J., Buenviaje, C., Buckmaster, R. & Overney, R. M. Shear Modulation Force Microscopy Study of Near Surface Glass Transition Temperatures. *Phys. Rev. Lett.* **85**, 2340-2343 (2000).

Genzer, J. Copolymer adsorption on planar substrates with a random distribution of chemical heterogeneities. *J. Chem. Phys.* **115**, 4873-4882 (2001).

Genzer, J. & Composto, R. Effect of Molecular Weight on the Interfacial Excess, Tension, and Width in a Homopolymer Binary Polymer Blend System. *Macromolecules* **31**, 870-878 (1998).

Genzer, J. & Composto, R. J. The Interface Between Immiscible Polymers Studied by Low-Energy Forward Recoil Spectrometry and Neutron Reflectivity. *Polymer* **40**, 4223-4228 (1999).

Genzer, J., Faldi, A. & Composto, R. J. Mean-field theory of the interface between a homopolymer and a binary-polymer mixture. *J. Chem. Phys.* **105**, 10134-10144 (1996).

Genzer, J., Rothman, J. B. & Composto, R. J. Improved Hydrogen and Deuterium Depth Profiling in Polymers Using Low-Energy Forward Recoil Spectrometry. *Nucl. Instrum. Methods Phys. Res., B* **86**, 345-354 (1994).

Geoghegan, M., Nicolai, T., Penfold, J. & Jones, R. A. L. Kinetics of Surface Segregation and the Approach to Wetting in an Isotopic Polymer Blend. *Macromolecules* **30**, 4220-4227 (1997).

Granick, S., Kumar, S. K., Amis, E. J., Antonietti, M., Balazs, A. C., Chakraborty, A. K., Grest, G. S., Hawker, C., Janmey, P., Kramer, E. J., Nuzzo, R., Russell, T. P. & Safinya, C. R. Macromolecules at surfaces: Research challenges and opportunities from tribology to biology. *J. Polym. Sci., Part B: Polym. Phys.* **41**, 2755-2793 (2003).

Haley, J. C. & Lodge, T. P. Failure of time-temperature superposition in dilute miscible polymer blends. *Colloid Polym. Sci.* **282**, 793-801 (2004).

Haley, J. C. & Lodge, T. P. A framework for predicting the viscosity of miscible polymer blends. *J. Rheol.* **48**, 463-486 (2004).

Hariharan, A., Kumar, S. K., Rafailovich, M. H., Sokolov, J., Zheng, X., Duong, D. H., Schwarz, S. A. & Russell, T. P. The Effect of Finite Film Thickness on the Surface Segregation in Symmetrical Binary Polymer Mixtures. *J. Chem. Phys.* **99**, 656-663 (1993).

Hariharan, A., Kumar, S. K. & Russell, T. P. A Lattice Model for the Surface Segregation of Polymer-Chains Due to Molecular-Weight Effects. *Macromolecules* **23**, 3584-3592 (1990).

Hariharan, A., Kumar, S. K. & Russell, T. P. Surface Segregation in Binary Polymer Mixtures - a Lattice Model. *Macromolecules* **24**, 4909-4917 (1991).
Hariharan, A., Kumar, S. K. & Russell, T. P. Free Surfaces of Polymer Blends .1. Theoretical Framework and Application to Symmetrical Polymer Blends. *J. Chem. Phys.* **98**, 6516-6525 (1993).
Hariharan, A., Kumar, S. K. & Russell, T. P. Free Surfaces of Polymer Blends .2. Effects of Molecular-Weight and Applications to Asymmetric Polymer Blends. *J. Chem. Phys.* **99**, 4041-4050 (1993).
Hariharan, A., Kumar, S. K. & Russell, T. P. Reversal of the Isotopic Effect in the Surface Behavior of Binary Polymer Blends. *J. Chem. Phys.* **98**, 4163-4173 (1993).
Harrison, C., Park, M., Chaikin, P. M., Register, R. A., Adamson, D. H. & Yao, N. Layer by layer imaging of diblock copolymer films with a scanning electron microscope. *Polymer* **39**, 2733-2744 (1998).
Harton, S. E., Koga, T., Stevie, F. A., Araki, T. & Ade, H. Investigation of Blend Miscibility of a Ternary PS/PCHMA/PMMA System using SIMS and Mean-Field Theory. *Macromolecules* **38**, 10511-10515 (2005).
Harton, S. E., Stevie, F. A. & Ade, H. Carbon-13 Labeling for Tracer Depth Profiling of Polymer Films and Multilayers using Secondary Ion Mass Spectrometry. *Appl. Phys. Lett.*, (in submission).
Harton, S. E., Stevie, F. A. & Ade, H. Diffusion-Controlled Reactive Coupling at Polymer-Polymer Interfaces. *Macromolecules* **38**, 3543-3546 (2005).
Harton, S. E., Stevie, F. A. & Ade, H. SIMS Depth Profiling of Amorphous Polymer Multilayers using O2+ and Cs+ Ion Bombardment with a Magnetic Sector Instrument. *J. Vac. Sci. Technol., B* **(in submission)** (2005).
Harton, S. E., Stevie, F. A. & Ade, H. Investigation of the Effects of Isotopic Labeling at a PS/PMMA Interface using SIMS and Mean-Field Theory. *Macromolecules*, (in press) (2006).
Harton, S. E., Stevie, F. A. & Ade, H. SIMS Depth Profiling of Amorphous Polymer Multilayers using O2+ and Cs+ Ion Bombardment with a Magnetic Sector Instrument. *J. Vac. Sci. Technol., A*, (in press) (2006).
Harton, S. E., Stevie, F. A. & Ade, H. SIMS Depth Profiling of Deuterium Labeled Polymers in Polymer Multilayers. *Appl. Surf. Sci.*, (in press) (2006).
Harton, S. E., Stevie, F. A., Spontak, R. J., Koga, T., Rafailovich, M. H., Sokolov, J. C. & Ade, H. Low-Temperature Reactive Coupling at Polymer-Polymer Interfaces Facilitated by Supercritical CO2. *Polymer* **46**, 10173-10179 (2005).
Helfand, E. Theory of the Homopolymer/Binary-Polymer-Mixture Interface. *Macromolecules* **25**, 1676-1685 (1992).
Helfand, E. & Sapse, A. M. Theory of Unsymmetric Polymer-Polymer Interfaces. *J. Chem. Phys.* **62**, 1327-1331 (1975).
Helfand, E. & Tagami, Y. Theory of the Interface Between Immiscible Polymers. *J. Polym. Sci., Part B: Polym. Phys.* **9**, 741 (1971).
Helfand, E. & Tagami, Y. Theory of the Interface between Immiscible Polymers. II. *J. Chem. Phys.* **56**, 3592-3601 (1972).

Hino, T., Song, Y. H. & Prausnitz, J. M. Equation-of-State Analysis of Binary Copolymer Systems .2. Homopolymer and Copolymer Mixtures. *Macromolecules* **28**, 5717-5724 (1995).

Honig, R. E. Sputtering of Surfaces by Positive Ion Beams of Low Energy. *J. Appl. Phys.* **29**, 549-555 (1958).

Hu, X., Zhang, W., Si, M., Gelfer, M., Hsiao, B., Rafailovich, M., Sokolov, J., Zaitsev, V. & Schwarz, S. Dynamics of Polymers in Organosilicate Nanocomposites. *Macromolecules* **36**, 823-829 (2003).

Huggins, M. L. Solutions of Long Chain Compounds. *J. Chem. Phys.* **9**, 440 (1941).

Indrakanti, A., Jones, R. L. & Kumar, S. K. Do "nonequilibrium" effects control strong surface segregation from polymer blends? *Macromolecules* **37**, 9-12 (2004).

Indrakanti, A., Ramesh, N., Duda, J. L. & Kumar, S. K. Modeling diffusion in miscible polymer blend films. *J. Chem. Phys.* **121**, 546-553 (2004).

Jerome, J., Zhu, S., Seo, Y. S., Ho, M., Pernodet, N., Gambino, R., Sokolov, J., Rafailovich, M. H., Zaitsev, V., Schwarz, S. & DiNardo, R. Phase segregation of thin film polymer blends on Au nanopatterned Si substrates. *Macromolecules* **37**, 6504-6510 (2004).

Jones, R. A. L. *Polymers at Surfaces and Interfaces* (Cambridge University Press, New York, 1999).

Jones, R. A. L., Kramer, E. J., Rafailovich, M. H., Sokolov, J. & Schwarz, S. A. Surface Enrichment in an Isotopic Polymer Blend. *Phys. Rev. Lett.* **62**, 280-283 (1989).

Jones, R. A. L., Norton, L. J., Kramer, E. J., Bates, F. S. & Wiltzius, P. Surface-Directed Spinodal Decompositon. *Phys. Rev. Lett.* **66**, 1326-1329 (1991).

Kilcoyne, A. L. D., Tyliszczak, T., Steele, W. F., Fakra, S., Hitchcock, P., Franck, K., Anderson, E., Harteneck, B., Rightor, E. G., Mitchell, G. E., Hitchcock, A. P., Yang, L., Warwick, T. & Ade, H. Interferometer Controlled Scanning Transmission X-Ray Microscopes at the Advanced Light Source. *J. Synchr. Rad.* **10**, 125-136 part 2 (2003).

Kim, B. J., Kang, H., Char, K., Katsov, K., Fredrickson, G. H. & Kramer, E. J. Interfacial Roughening Induced by the Reaction of End-Functionalized Polymers at a PS/P2VP Interface: Quantitative Analysis by DSIMS. *Macromolecules* **38**, 6106-6114 (2005).

Kim, E., Kramer, E. J., Garrett, P. D., Mendelson, R. A. & Wu, W. C. Surface Segregation in Blends of Styrene-Acrylonitrile Copolymers. *Polymer* **36**, 2427-2433 (1995).

Kim, E., Kramer, E. J. & Osby, J. O. Tracer Diffusion in the Blends of Polystyrene and Tetramethylbisphenol-a Polycarbonate. *Macromolecules* **28**, 1979-1989 (1995).

Kim, E., Kramer, E. J., Osby, J. O. & Walsh, D. J. Mutual Diffusion and Thermodynamics in the Blends of Polystyrene and Tetramethylbisphenol-a Polycarbonate. *J. Polym. Sci., Part B: Polym. Phys.* **33**, 467-478 (1995).

Kramer, E. J. Depth profiling methods that provide information complementary to neutron reflectivity. *Physica B* **173**, 189-198 (1991).

Lodge, T. P. & McLeish, T. C. B. Self-concentrations and effective glass transition temperatures in polymer blends. *Macromolecules* **33**, 5278-5284 (2000).

Magee, C. W., Jacobson, D. & Gossmann, H.-J. Accuracy of secondary ion mass spectrometry in determining ion implanted B doses as confirmed by nuclear reaction analysis. *J. Vac. Sci. Technol. B* **18**, 489-492 (2000).

Mahoney, C. M., Yu, J. & Gardella, J. A. Depth Profiling of Poly(L-lactic acid)/Triblock Copolymer Blends with Time-of-Flight Secondary Ion Mass Spectrometry. *Anal. Chem.* **77**, 3570-3578 (2005).

Mansky, P., Liu, Y., Huang, E., Russell, T. P. & Hawker, C. Controlling Polymer-Surface Interactions with Random Copolymer Brushes. *Science* **275**, 1458-1460 (1997).

Matsen, M. W. & Schick, M. Stable and Unstable Phases of a Diblock Copolymer Melt. *Phys. Rev. Lett.* **72**, 2660-2663 (1994).

Matsen, M. W. & Schick, M. Self-assembly of block copolymers. *Curr. Opin. Colloid Interface Sci.* **1**, 329-336 (1996).

Matyjaszewski, K., Patten, T. E. & Xia, J. H. Controlled/"living" radical polymerization. Kinetics of the homogeneous atom transfer radical polymerization of styrene. *J. Am. Chem. Soc.* **119**, 674-680 (1997).

Matyjaszewski, K. & Xia, J. Atom Transfer Radical Polymerization. *Chem. Rev.* **101**, 2921-2990 (2001).

McKinley, J. M., Stevie, F. A., Granger, C. N. & Renard, D. Analysis of alkali elements in insulators using a CAMECA IMS-6f. *J. Vac. Sci. Technol. A* **18**, 273-277 (2000).

Mezzenga, R., Ruokolainen, J., Fredrickson, G. H., Kramer, E. J., Moses, D., Heeger, A. J. & Ikkala, O. Templating Organic Semi-conductors via Self-Assembly of Polymer Colloids. *Science* **299**, 1872-1874 (2003).

Migeon, H. N., Schuhmacher, M. & Slodzian, G. Analysis of Insulating Specimens with the Cameca Ims4f. *Surf. Interface Anal.* **16**, 9-13 (1990).

Miwa, Y., Tanabe, T., Yamamoto, K., Sugino, Y., Sakaguchi, M., Sakai, M. & Shimada, S. Segmental dynamics and self-concentration around chain ends in miscible blend of poly(cyclohexyl methacrylate) and poly(cyclohexyl acrylate) as studied by the spin-label technique. *Macromolecules* **37**, 8612-8617 (2004).

Munoz-Bonilla, A., Madruga, E. L. & Fernandez-Garcia, M. Atom transfer radical polymerization of cyclohexyl methacrylate at a low temperature. *J. Polym. Sci., Part A: Polym. Chem.* **43**, 71-77 (2005).

Novak, B. M., Risse, W. & Grubbs, R. H. The Development of Well-Defined Catalysts for Ring-Opening Olefin Metathesis Polymerizations (Romp). *Adv. Polym. Sci.* **102**, 47-72 (1992).

Odian, G. *Principles of Polymerization* (John Wiley & Sons, Inc., Hoboken, NJ, 2004).

Painter, P. C. & Coleman, M. M. *Fundamentals of Polymer Science: An Introductory Text* (Technomic Publishing Co., Inc., Lancaster, PA, 1997).

Paul, D. R. & Bucknall, C. B. (eds.) *Polymer Blends, Vols. I and II* (Wiley, New York, 2000).

Pavlinec, J. & Lazar, M. Cross-linking of poly(methyl methacrylate) by aminolysis of ester functions with diamines. *J. Appl. Polym. Sci.* **55**, 39-45 (1995).

Pivovarov, A. L., Stevie, F. A. & Griffis, D. P. Improved charge neutralization method for depth profiling of bulk insulators using O2+ primary beam on a magnetic sector SIMS instrument. *Appl. Surf. Sci.* **231-232**, 786-790 (2004).

Pomposo, J. A., Mugica, A., Areizaga, J. & Cortazar, M. Modeling of phase behavior of binary and ternary blends involving copolymers of styrene, methyl methacrylate, and cyclohexyl methacrylate. *Acta Polym.* **49**, 301-311 (1998).

Postawa, Z., Czerwinski, B., Winograd, N. & Garrison, B. J. Microscopic insights into the sputtering of thin organic films on Ag{111} induced by C-60 and Ga bombardment. *J. Phys. Chem. B* **109**, 11973-11979 (2005).

Prausnitz, J. M., Lichtenhaler, R. N. & de Azevedo, E. G. *Molecular Thermodynamics of Fluid-Phase Equilibria* (Prentice Hall, Englewood Cliffs, NJ, 1986).

Press, W. H., Flannery, B. P., Teukolsky, S. A. & Vetterling, W. T. *Numerical Recipes in Fortran 77: The Art of Scientific Computing* (Cambridge University Press, 1992).

Pu, Y., Rafailovich, M. H., Sokolov, J., Gersappe, D., Peterson, T., Wu, W.-L. & Schwarz, S. A. Mobility of Polymer Chains Confined at a Free Surface. *Phys. Rev. Lett.* **87**, Art. # 206101 (2001).

Quirk, R. P., Yin, J. & Fetters, L. J. Carbonation and Related Reactions of Poly(Styryl)Lithium. *Macromolecules* **22**, 85-90 (1989).

Reynolds, B. J., Ruegg, M. L., Mates, T. E., Radke, C. J. & Balsara, N. P. Experimental and Theoretical Study of the Adsorption of a Diblock Copolymer to Interfaces between Two Homopolymers. *Macromolecules* **38**, 3872-3882 (2005).

Roe, R.-J. *Methods of X-Ray and Neutron Scattering in Polymer Science* (Oxford University Press, New York, 2000).

Russell, T. P. Changes in Polystyrene and Poly(methyl methacrylate) Interactions with Isotopic Substitution. *Macromolecules* **26**, 5819 (1993).

Russell, T. P., Deline, V. R., Dozier, W. D., Felcher, G. P., Agrawal, G., Wool, R. P. & Mays, J. W. Direct Observation of Reptation at Polymer Interfaces. *Nature* **365**, 235-237 (1993).

Russell, T. P., Hjelm, R. P. & Seeger, P. A. Temperature-Dependence of the Interaction Parameter of Polystyrene and Poly(Methyl Methacrylate). *Macromolecules* **23**, 890-893 (1990).

Russell, T. P., Karim, A., Mansour, A. & Felcher, G. P. Specular Reflectivity of Neutrons by Thin Polymer-Films. *Macromolecules* **21**, 1890-1893 (1988).

Ruzette, A. V. & Leibler, L. Block copolymers in tomorrow's plastics. *Nature Mater.* **4**, 19-31 (2005).

Ryan, A. J. Polymer science - designer polymer blends. *Nature Mater.* **1**, 8-10 (2002).

Sanchez, I. C. & Lacombe, R. H. Statistical Thermodynamics of Polymer Solutions. *Macromolecules* **11**, 1145-1156 (1978).

Schwarz, S. A., Wilkens, B. J., Pudensi, M. A. A., Rafailovich, M. H., Sokolov, J., Zhao, X., Zhao, W., Zheng, X., Russell, T. P. & Jones, R. A. L. Studies of Surface and Interface Segregation in Polymer Blends by Secondary ion Mass-Spectrometry. *Mol. Phys.* **76**, 937-950 (1992).

Seeck, O. H., Kaendler, I. D., Tolan, M., Shin, M., Rafailovich, M. H., Sokolov, J. & Kolb, R. Analysis of X-Ray Reflectivity Data from Low-Contrast Polymer Bilayer Systems using a Fourier Method. *Appl. Phys. Lett.* **76**, 2713-2715 (2000).

Sferrazza, M., Jones, R. A. L. & Bucknall, D. G. Thermally driven collapse of a polymer brush in a polymer matrix. *Phys. Rev. E* **59**, 4434-4440 (1999).

Sferrazza, M., Xiao, C., Jones, R. A. L., Bucknall, D. G., Webster, J. & Penfold, J. Evidence for Capillary Waves at Immiscible Polymer/Polymer Interfaces. *Phys. Rev. Lett.* **78**, 3693-3696 (1997).

Shin, K., Hu, X., Zheng, X., Rafailovich, M. H., Sokolov, J., Zaitsev, V. & Schwarz, S. A. Silicon Oxide Surface as a Substrate of Polymer Thin Films. *Macromolecules* **34**, 4993-4998 (2001).

Shull, K. R. & Kramer, E. J. Mean-Field Theory of Polymer Interfaces in the Presence of Block Copolymers. *Macromolecules* **23**, 4769-4779 (1990).

Sokolov, J., Rafailovich, M. H., Jones, R. A. L. & Kramer, E. J. Enrichment Depth Profiles in Polymer Blends Measured by Forward Recoil Spectrometry. *Appl. Phys. Lett.* **54**, 590-592 (1989).

Sostarecz, A. G., Sun, S., Szakal, C., Wucher, A. & Winograd, N. Depth profiling studies of multilayer films with a C60+ ion source. *Appl. Surf. Sci.* **231-232**, 179-182 (2004).

Stamm, M., Reiter, G. & Kunz, K. The use of X-Ray and Neutron Reflectometry for the Investigation of Polymeric Thin-Films. *Physica B* **173**, 35-42 (1991).

Strzhemechny, Y. M., Schwarz, S. A., Schacter, J., Rafailovich, M. H. & Sokolov, J. Secondary ion mass spectrometry study of silicon surface preparation and the polystyrene/silicon interface. *J. Vac. Sci. Technol. A* **15**, 894-898 (1997).

Szakal, C., Sun, S., Wucher, A. & Winograd, N. C60 molecular depth profiling of a model polymer. *Appl. Surf. Sci.* **231-231**, 183-185 (2004).

Szwarc, M. Living Polymers. *Nature* **178**, 1168-1169 (1956).

Szwarc, M., Levy, M. & Milkovich, R. Polymerization Initiated by Electron Transfer to Monomer - a New Method of Formation of Block Polymers. *J. Am. Chem. Soc.* **78**, 2656-2657 (1956).

Vanden Eynde, X., Bertrand, P. & Penelle, J. "Matrix" effects in ToF-SIMS analyses of styrene-methyl methacrylate random copolymers. *Macromolecules* **33**, 5624-5633 (2000).

Wagner, M. S. Molecular Depth Profiling of Multilayer Polymer Films Using Time-of-Flight Secondary Ion Mass Spectrometry. *Anal. Chem.* **77**, 911-922 (2005).

Wang, C., Araki, T. & Ade, H. Soft X-ray Resonant Reflectivity of low Z Material Thin Films. *Appl. Phys. Lett.* **87**, 214109 (2005).

Weibel, D., Wong, S., Lockyer, N., Blenkinsopp, P., Hill, R. & Vickerman, J. C. A C60 Primary Ion Beam System for Time of Flight Secondary Ion Mass Spectrometry: Its Development and Seconedary Ion Yield Characteristics. *Anal. Chem.* **75**, 1754-1764 (2003).

Werner, A., Schmid, F. & Müller, M. Monte Carlo simulations of copolymers at homopolymer interfaces: Interfacial structure as a function of the copolymer density. *J. Chem. Phys.* **110**, 5370-5379 (1999).

White, D. M. & Nye, S. A. Preparation of Deuterated Poly(2,6-Dimethyl-1,4-Phenylene Oxide). *Macromolecules* **17**, 2643-2645 (1984).

Williams, P., Lewis, R. K., Evans, C. A. & Hanley, P. R. Evaluation of a Cesium Primary Ion Source on an Ion Microprobe Mass Spectrometer. *Anal. Chem.* **49**, 1399-1403 (1977).

Wilson, R. G., Lux, G. E. & Kirschbaum, C. L. Depth profiling and secondary ion mass spectrometry relative sensitivity factors and systematics for polymers/organics. *J. Appl. Phys.* **73**, 2524-2529 (1993).

Wilson, R. G., Stevie, F. A. & Magee, C. W. *Secondary Ion Mass Spectrometry: A Practical Handbook for Depth Profiling and Bulk Impurity Analysis* (John Wiley & Sons, New York, 1989).

Winograd, N. The Magic of Cluster SIMS. *Anal. Chem.* **77**, 142A-149A (2005).

Wu, S. Surface and Interfacial Tensions of Polymer Melts. II. Poly(methyl methacrylate), Poly(n-butyl methacrylate), and Polystyrene. *J. Phys. Chem* **74**, 632-638 (1970).

Xia, J. & Matyjaszewski, K. Controlled/"Living" Radical Polymerization. Atom Transfer Radical Polymerization Using Multidentate Amine Ligands. *Macromolecules* **30**, 7697-7700 (1997).

Xu, J., Ostrowski, S., Szakal, C., Ewing, A. G. & Winograd, N. ToF-SIMS imaging with cluster ion beams. *Appl. Surf. Sci.* **231-232**, 159-163 (2004).

Zhao, W., Zhao, X., Rafailovich, M. H., Sokolov, J., Mansfield, T., Stein, R. S., Composto, R. C., Kramer, E. J., Jones, R. A. L., Sansone, M. & Nelson, M. Neutron and x-ray reflectivity measurements of polystyrene/poly(bromostyrene) (PS/PBrS) interfaces. *Physica B* **173**, 43-46 (1991).

Zhao, X., Zhao, W., Sokolov, J., Rafailovich, M. H., Schwarz, S. A., Wildens, B. J., Jones, R. A. L. & Kramer, E. J. Determination of the Concentration Profile at the Surface of d-PS/ h-PS Blends Using High-Resolution Ion-Scattering. *Macromolecules* **24**, 5991-5996 (1991).

Zheng, X., Rafailovich, M. H., Sokolov, J., Y, S., Schwarz, S. A., Sauer, B. B. & Rubinstein, M. Long-Range Effects on Polymer Diffusion Induced by a Bounding Interface. *Phys. Rev. Lett.* **79**, 241-244 (1997).

Zheng, X., Sauer, B. B., Alsten, J. G. V., Schwarz, S. A., Rafailovich, M. H., Sokolov, J. & Rubinstein, M. Reptation Dynamics of a Polymer Melt near an Attractive Solid Interface. *Phys. Rev. Lett.* **74**, 407-410 (1995).

Zhu, S., Liu, Y., Rafailovich, M. H., Sokolov, J., Gersappe, D., Winesett, D. A. & Ade, H. Confinement Induced Miscibility in Polymer Blends. *Nature* **400**, 49-51 (1999).

Ziegler, J. F., Biersack, J. P. & Littmark, U. *The Stopping and Range of Ions in Solids* (Pergamon, New York, 1985).